LATERAL BEHAVIOR OF PILES ON SLOPES IN COHESIVE SOILS UNDER DRAINED CONDITIONS

A THESIS SUBMITTED TO
THE GRADUATE SCHOOL OF NATURAL AND APPLIED SCIENCES
OF
MIDDLE EAST TECHNICAL UNIVERSITY

BY

OZAN KANGAL

IN PARTIAL FULFILLMENT OF THE REQUIREMENTS
FOR
THE DEGREE OF MASTER OF SCIENCE
IN
CIVIL ENGINEERING

JANUARY 2025

Approval of the thesis:

LATERAL BEHAVIOR OF PILES ON SLOPES IN COHESIVE SOILS UNDER DRAINED CONDITIONS

submitted by **OZAN KANGAL** in partial fulfillment of the requirements for the degree of **Master of Science** i**n Civil Engineering, Middle East Technical University** by,

Prof. Dr. Naci Emre Altun
Dean, Graduate School of Natural and Applied Sciences _____

Prof. Dr. Erdem Canbay
Head of the Department, Civil Engineering _____

Prof. Dr. Erdal Çokça
Supervisor, Civil Engineering, METU _____

Assoc. Prof. Dr. Mustafa Abdullah Sandıkkaya
Co-Supervisor, Civil Engineering, Hacettepe University _____

Examining Committee Members:

Prof. Dr. Berna Unutmaz
Civil Engineering, Hacettepe University _____

Prof. Dr. Erdal Çokça
Civil Engineering, METU _____

Assoc. Prof. Dr. Mustafa Abdullah Sandıkkaya
Civil Engineering, Hacettepe University _____

Assoc. Prof. Dr. Nejan Huvaj Sarıhan
Civil Engineering, METU. _____

Assoc. Prof. Dr. Mustafa Tolga Yılmaz
Engineering Sciences, METU _____

Date: 02.01.2025

I hereby declare that all information in this document has been obtained and presented in accordance with academic rules and ethical conduct. I also declare that, as required by these rules and conduct, I have fully cited and referenced all material and results that are not original to this work.

Name Last name: Ozan Kangal

Signature:

ABSTRACT

LATERAL BEHAVIOR OF PILES ON SLOPES IN COHESIVE SOILS UNDER DRAINED CONDITIONS

Kangal, Ozan
Master of Science, Civil Engineering
Supervisor: Prof. Dr. Erdal Çokça
Co-Supervisor: Assoc. Prof. Dr. Mustafa Abdullah Sandıkkaya

January 2025, 106 pages

A series of finite element analyses was conducted to investigate the influence of several parameters on p-y curve properties for cohesive soils under drained conditions. Soil conditions include strength and deformation properties relating to plasticity index (PI) and SPT-N_{60} values. Geometric conditions include slope angle, pile-to-crest distance, and slope height. The analyses focus on the variation of the p-y curve properties, especially concerning the distance from the crest, under various conditions. The general trend observed is that PI, slope angle, and slope height are negatively correlated with ultimate lateral earth pressure (P_u) of the p-y curve, while SPT-N_{60} exhibits a positive correlation with P_u and initial slope (K_i) of the p-y curve. Overall, while specific results may be different under varying conditions, one general trend exists: piles located on the slopes display similar lateral behavior as the piles at the crest for a distance ratio (pile distance to crest/slope length) of 0.9 or less.

Keywords: Piles, Lateral Loading, p-y Curves, Finite Element Analysis, Soil Slope

ÖZ

EĞİM ÜZERİNDEKİ KAZIKLARIN DRENAJLI KOŞULLARDA KOHEZYONLU ZEMİNLERDE YATAY DAVRANIŞI

Kangal, Ozan
Yüksek Lisans, İnşaat Mühendisliği
Tez Yöneticisi: Prof. Dr. Erdal Çokça
Ortak Tez Yöneticisi: Assoc. Prof. Dr. Mustafa Abdullah Sandıkkaya

Ocak 2025, 106 sayfa

Drenajlı kohezyonlu zeminlerde çeşitli parametrelerin p-y eğrisi özellikleri üzerindeki etkisini araştırmak amacıyla sonlu eleman analizleri yapılmıştır. Zemin koşulları, plastisite indeksi (PI) ve SPT-N_{60} değerleri ile değişen mukavemet ve deformasyon özelliklerini; geometrik koşullar ise şev açısı, kazık-tepe mesafesi ve şev yüksekliğini içermektedir. Analizler, p-y eğrisi özelliklerinin kazığın şev tepesine olan uzaklığına göre değişimine odaklanmıştır. Genel olarak PI, şev açısı ve şev yüksekliğinin nihai yanal zemin basıncı (P_u) ile negatif; SPT-N_{60}'ın ise Pu ve başlangıç eğimi (K_i) ile pozitif korelasyon gösterdiği gözlemlenmiştir. Farklı koşullar altında değişiklikler olabilse de, yamaçlardaki kazıkların 0.9 veya daha az bir mesafe oranında (kazığın şev tepesine olan uzaklığı/şev uzunluğu) tepedeki kazıklarla benzer yanal davranış sergilediği belirlenmiştir.

Anahtar Kelimeler: Kazıklar, Yanal Yükleme, p-y Eğrileri, Sonlu Elemanlar Analizi, Şevli Zemin

To my beloved family and to my brothers and sisters by heart,

ACKNOWLEDGMENTS

The author wishes to express his deepest gratitude to his supervisor Prof. Dr. Erdal Çokça and co-supervisor Assoc. Prof. Dr. Mustafa Abdullah Sandıkkaya for their guidance, advice, criticism, encouragements and insight throughout the research.

Special thanks should be given to my colleagues, and my brothers and sisters by heart. Their advice and suggestions have been very helpful in my thesis and career.

I would like to thank The Scientific and Technological Research Council of Turkey (TÜBİTAK) for their financial support during my graduate study within the scope of the 2210-A scholarship

And last but not least, I would like to thank my father, Serdar Kangal, my mother, Nihal Kangal, and my cat, Zeytin, for their unconditional trust and endless support. I am also deeply grateful to my sister, Ezgi Kangal, who has consistently supported me throughout my education. Knowing that they stand by me in every decision I make has given me immense courage in life.

TABLE OF CONTENTS

LIST OF TABLES

TABLES

LIST OF FIGURES

FIGURES

LIST OF ABBREVIATIONS

ABBREVIATIONS

2D : Two Dimensional

3D : Three Dimensional

FD : Finite Difference

FDA : Finite Difference Analysis

FDM : Finite Difference Method

FE : Finite Element

FEA : Finite Element Analysis

FEM : Finite Element Method

H : Horizontal

HS : Hardening Soil

V : Vertical

LIST OF SYMBOLS

SYMBOLS

c : Cohesion

c' : Effective cohesion

c_u : Undrained shear strength

D : Diameter

E : Modulus of elasticity

EA : Pile's axial rigidity

E'_s : Long term/drained deformation modulus

E_{50}^{ref} : Triaxial loading stiffness

EI : Pile's bending stiffness

E_{oed}^{ref} : Oedometer loading stiffness

E_u : Short term/undrained deformation modulus

E_{ur}^{ref} : Triaxial unloading stiffness

H : Height

H_o : Pile head load

J : Dimensionless empirical constant (0.5 for soft clays and 0.25 for medium clay)

K_i : Initial slope

$K_{i\theta}$: Initial stiffness of the p-y curve for slope

K_{io}= : Initial stiffness of the p-y curve for level ground

L : Length

m : power law

N_{60} : SPT value corrected for 60% energy ratio

p : Lateral soil resistance

PI : Plasticity index

P_p : Rankine's passive pressure

P_u : Ultimate lateral earth pressure

Q : Shear force

S : Slope angle in radians

U : Translational degree of freedom

y : Lateral displacement

z : Depth

γ' : Effective unit weight

θ : Angle of slope

ϕ : Angle of friction

φ : Rotational degree of freedom

ϕ' : Effective angle of friction

CHAPTER 1

INTRODUCTION

1.1 Slope Stabilizing Piles and p-y Curves

The stability of the slope is one of the most essential issues in geotechnical engineering especially in areas prone to landslides or where construction might disturb the natural ground. The failure of a slope can result in potentially disastrous situations with loss of life, structural damage, and a number of other economical burdens. One of the most effective stabilization methods is using slope stabilizing piles. These piles act as deep foundations, driven or drilled into the ground, resisting lateral soil movements and enhancing overall slope stability.

Slope stabilizing piles work by blocking potential slip surfaces and transferring the load from moving soil to deeper, more stable layers or bedrock. This redistribution of forces minimizes the likelihood of slope failure and enhances overall slope stability. Success of this type of piles largely depends on type of soil, slope shape, and pile characteristics like length, diameter, and strength of material.

An essential aspect of designing slope-stabilizing piles is accurately predicting their response to lateral forces. This prediction ensures that the piles can effectively stabilize the slope without experiencing excessive bending or failure. Understanding this behavior has allowed engineers to optimize pile design in such a way that adequate support is developed without compromising the integrity and safety of the slope. In general, p-y curves are utilized in engineering analyses to describe the interaction between piles and the surrounding soil. These curves graphically portray the relationship between soil lateral resistance (p) and pile lateral displacement (y) over their depths. By using p-y curves, engineers can better understand how piles will behave under lateral loads, which is crucial for designing stable foundations that

can withstand the forces exerted by the soil, especially in slope stabilization scenarios.

The developed P-y curves are based on field tests, laboratory studies, and research conducted to understand how piles would laterally respond to wind, waves, seismic activity, or soil movements.These curves define, for any given depth, the relationship between p and y. The p-y curves allow engineers to map this relation in predicting capacity development of piles due to lateral loading and check for possible bending, deflection, and shear forces along a pile's full length for the stability and safety of pile-supported structures against lateral stress.

Creating p-y curves usually involves adjusting test data to fit mathematical models that reflect the complex behavior of soil under lateral loads. These models vary based on factors such as soil type, pile depth, and the nature of the applied load. Examples of this would be the development of various p-y curves of non-cohesive and cohesive soils. For each type, they are specially fitted to the properties and failure behaviors of the unique soil. Using these types of specific curves, soil-specific traits like stiffness or resistance to lateral movement can accurately be represented in the analysis, so that more accurate predictions can be made about performance of piles under lateral loads.

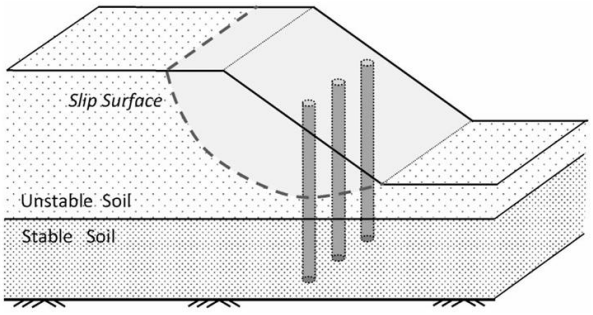

Figure 1.1 Illustration of Slope Stabilizing Piles (Kourkoulis et al., 2012)

1.2 Scope of this Study

The basic components of the analysis in geotechnical engineering on the lateral load capacity of piles are the p-y curves. Nonetheless, the majority of established models rely on installations on level terrain, consistent loading, and uniform soil layer conditions. Therefore, the usually referred p-y models from Matlock (1970), Reese et al. (1975), and Welch & Reese (1972) often show deviations when applied to the lateral loads of slope-stabilizing piles. These models are incapable of representing the actual complexity of the pile-soil interaction in sloped environments and cannot predict the actual outcome.

It is established through a number of studies that the angle of slope is an important parameter affecting the performance of piles installed in sloping ground in terms of its load-deflection behaviour (Georgiadis & Georgiadis, 2010; Mezazigh and Levacher 1998; Muthukkumaran et al., 2008; Nimityongskul et al., 2018; Sharafi et al., 2015). However, a thorough review of the literature on this subject reveals that comprehensive studies addressing all the relevant soil and geometric parameters for cohesive soils in drained condition are totally lacking. Most of the previous studies focused on piles located at the crest of slopes or investigated the influence of distance from the crest in the case of piles installed on flat ground. Indeed, the studies that have directly explored the behavior of piles placed on the slope itself are so limited. This gap leaves an incomplete understanding of how pile performance varies under different conditions in sloped environments. It highlights the need for more in-depth research that considers the effects of both soil characteristics and geometric variations when piles are placed directly on slopes.

The future studies are suggested to be directed at comprehensive analysis of various parameters that influence the propetries of p-y curve, as the ultimate lateral earth pressure (P_u) and the initial slope (K_i) in cohesive soils in drained condition. This would include an exhaustive investigation into the interaction of these parameters with pile behavior to provide better understanding of their influence. Thus, by studying the variations in characteristics of the p-y curve from these factors, future

studies can more accurately develop the model on piles in complicated soil conditions. These parameters are divided into two as soil conditions and geometric conditions. Soil conditions encompass the deformation and strength parameters of cohesive soil, such as drained deformation modulus (E'_s), effective angle of friction (ϕ'), and effective cohesion (c') which are influenced by the plasticity index (PI) and SPT-N_{60} values. Geometric conditions include slope height (directly related to the length of the pile) and slope angle, both of which significantly impact the stability and performance of piles in sloped environments. Understanding these factors is crucial for accurately predicting pile behavior under lateral loads. Besides this, as mentioned before, since there is no detailed study conducted on the examination of p-y properties in piles directly on the slope itself, this subject should be focused on. Previous studies were conducted for piles located in the crest of the slope or have focused solely on the effect of pile's distance to the crest for piles placed on flat terrain. In this study, how the distance from the crest changes the p-y properties under different conditions in piles located on the slope far from the crest should be examined.

The format of this thesis is as follows: Chapter 2 examines pertinent literature, while Chapter 3 describes the methodology, including the selection of parameters for comparing and evaluating p-y curves. Chapter 4 presents the analysis results and discusses how p-y curve behavior varies with different parameters. Chapter 5 summarizes the study's main conclusions, provides a comparison of p-y curves obtained from finite element analysis on level ground with those derived using the p-y models in the literature by using RSPile software, and provides a comparison of p-y curves for the piles located on flat and sloped terrains.. Finally, the chapter offers important remarks and recommendations for future research.

CHAPTER 2

LITERATURE REVIEW

In most parts of the world, slope stability problems pose a great danger to infrastructure, property, and human life. Slope stability problems may be mitigated using various methods. These include ensuring stability through the use of stabilizing piles.

Piles utilized for slope stabilization are exposed to lateral forces resulting from the horizontal movement of the surrounding soil and are, therefore, classified as passive piles by researchers. (Ashour & Ardalan, 2012; Chen & Martin, 2002; He et al., 2015; Poulos, 1995; Viggiani, 1981).

The conventional overall factor of safety for a slope or landslide has been defined as the ratio of the shear strength available along the failure surface to the shear stress imposed by the moving soil. According to this definition, stability of slopes can be effectively improved through: a) reduction of the driving-equilibrium shear stress b) increase of shear strength. Extensive applications of vertical piles in the slope/drilled shaft system increase the safety factor by reducing the driving shear load and diminishing the potential slope failure within the sliding soil mass (Yamin & Liang, 2010). They are typically designed to reduce soil displacement rates before any potential failure mechanisms occur (Galli & di Prisco, 2013).

Designing slope-stabilizing piles is a complex challenge because it has to be performed considering lateral forces exerted on the pile system by both the sliding materials and the sliding zone. The three-dimensional nature of pile-soil interaction requires deep insight based on the deformation and strength properties in both the soil and the pile (Ashour & Ardalan, 2012). This adds up to the complexity since soil behavior in itself is inherently anisotropic, heterogeneous, and non-linear, which

need to be incorporated during analysis to ensure effective pile performance in stabilizing slopes (Dutta and Roy 2002).

The soil pressure on a section of the pile due to surrounding soil displacement depends mainly on the strength parameters of the soil, overburden pressure, and spacing between piles. If the pile is assumed to be rigid and infinitely long, the pressure would be independent of the stiffness of the pile. The force exerted by the soil mass along the pile segment above the slip surface is transmitted to the stable soil layers below, as shown in Figure 2.1. (Ashour & Ardalan, 2012).

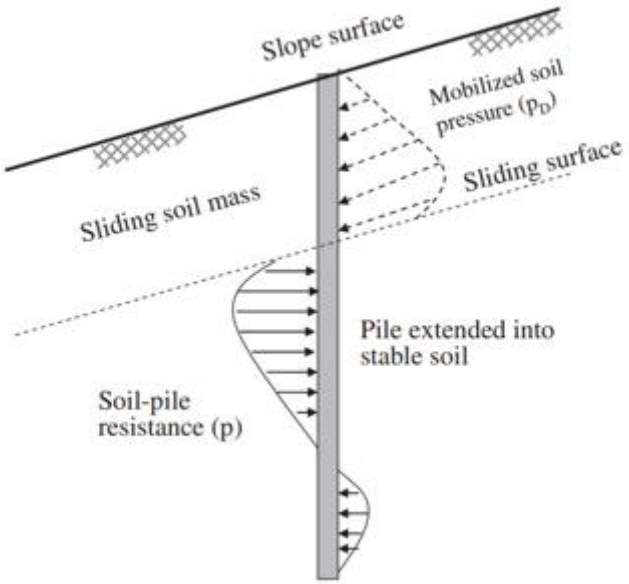

Figure 2.1 Driving Force Generated by the Shifted Soil Mass Above the Sliding Surface (Ashour & Ardalan, 2012)

Lateral loading of a single pile is equilibrated by lateral soil resistance, and it induces bending moment and shear force in a pile cross section. One of the important design issues is to determine these forces developed in the piles caused by unstable slope movements (Chow, 1996).

Various methods, including empirical, analytical, and numerical approaches, are utilized for designing stabilizing piles. These methods can generally be categorized into two types: (1) pressure or displacement-based methods (Broms, 1964; Hassiotis

et al., 1997; Ito & Matsui, 1975; Lee et al., 1995; Poulos, 1995; Viggiani, 1981), and (2) numerical methods, such as finite differences and finite elements (Chow, 1996; Jeong et al., 2003; Kourkoulis et al., 2012; R. Y. Liang & Yamin, 2010; R. Liang & Zeng, 2002).

Moreover, it is obvious from the modern body of research that innovated methodologies have been created for stabilizing pile design. Some of them are hybrid method of analysis (Chow, 1996; Kourkoulis et al., 2012), coupled method of analysis (Ashour & Ardalan, 2012) and uncoupled method of analysis (Jeong et al., 2003).

2.1 Pressure or Displacement Methods

In such models, the pile is considered a beam connected to the surrounding soil through nonlinear springs. In this model, the displacement of either slope or load has been imposed on the supports of the springs. By this method, solutions for two differential equations can be applied to calculate the lateral capacity of the pile interacting with the soil in terms of the lateral reaction:

1. For the segment of the pile located above the sliding surface

$$EI\left(\frac{d^4y_1}{dz^4}\right) = q(z)\ for\ z < 0 \tag{2.1}$$

where y_1 represents the pile's displacement above the sliding surface, assumed to be at z=0. The plastic deformation principle is used to calculate the force intensity, q(z).

2. For the segment of the pile located below the sliding surface:

$$EI\left(\frac{d^4y_2}{dz^4}\right) = -Ky_2\ for\ z \geq 0 \tag{2.2}$$

Where K is associated with the soil's modulus of subgrade reaction and y_2 is pile deflection beneath the sliding surface.

Although it is relatively straightforward, this approach does require detailed information, including the deformation pattern of the slope, the lateral soil modulus distribution (which often requires intensive field investigations), and the maximum soil pressure applied on the pile laterally at variable depths. All these factors are crucial for accurately modeling the interaction between the soil and the pile and for predicting the pile's lateral behavior (Kourkoulis et al., 2012).

2.1.1 Pressure-Based Methods

The pressure-based approaches, as outlined by Broms (1964), Viggiani (1981), (Hassiotis et al., 1997), and Ito and Matsui (1975), revolve around examining passive piles under lateral soil pressure. Nevertheless, a major drawback of such approaches is that they only consider the ultimate limit state to provide some indication of the maximum value of soil pressure, ignoring how resistance develops as the soil moves and mobilizes soil-pile pressure.

However, most of those methods are only addressing the final state and can't provide insight into the maximum soil-pile pressure without capturing the formation of resistance with advancing soil movement (activated soil-pile interaction pressure). Apart from this, the simplicity of assumptions in those approaches is far from the reality of the interaction between soil and pile.

In their analytical study, Ito and Matsui (1975) estimated the soil pressures caused by soil displacement on piles located in a single row. Their approach relied on the basic assumption that the soil is soft and deforms plastically around the piles. Ito and Matsui's plasticity theory allows the derivation of a rational procedure for estimating the magnitude of lateral force imposed by the soil layer on stabilizing piles per unit thickness during soil compacted between piles. (Figure 2.2).

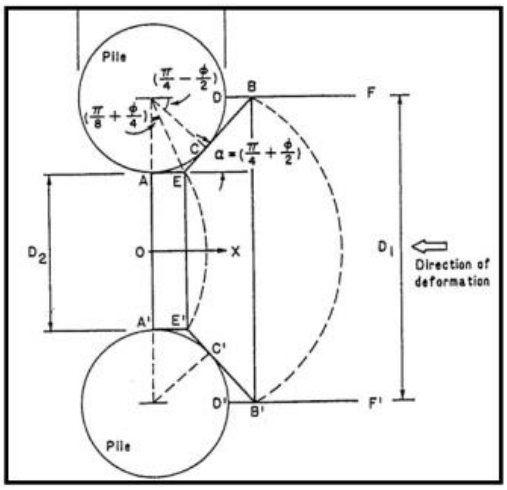

Figure 2.2. Plastic Deformation Status of the Soil Near Piles (Ito and Matsui, 1975)

Ito et al. (1981) presented a method for estimating slope stability when supported by a single line of piles, considering additional support provided by these piles to the available natural stabilizing forces resisting the slope. In general, in such a method, the safety factor is calculated by an ordinary slice method as the ratio of total driving forces to the total resisting forces. Applying Ito and Matsui's (1975) theory of plasticity, additional resistance provided by the piles is estimated considering the piles to be rigid and the soil around it at plastic equilibrium condition, neglecting the effect of frictional forces.

A method that took into account the additional resistance from the piles added to the in situ forces acting on the slope was presented by Hassiotis et al. (1997). In this method, the slope stability is expressed in terms of a factor of safety where the ratio of total resisting forces over the total driving forces is calculated using the standard method of slices. The authors, in the present study, estimate the lateral resistance contributed by the piles using the plasticity theory developed by Ito and Matsui (1975). The mentioned theory assumes the surrounding soil to be in a condition of plastic equilibrium and the piles to be rigid, neglecting the frictional forces acting between the piles and the soil. The method does focus on the spacing of piles, and where the theoretical basis tends to work best is when the spacing is two times larger than the diameter of the piles. Moreover, it points out the need for consideration of

the properties of soil deformations coupled with the potential for plastic deformation around the piles. The findings provide a realistic approach to the design of slope stabilization systems supported by piles by affirming the very important role that piles play in maintaining slope stability. The study fuses theoretical and analytical insight, hence serving as a useful framework for improving slope stability using pile systems.

2.1.2 Displacement-Based Methods

Lateral reaction analyses based on the methods developed by Poulos (1995) and Lee et al. (1995) make use of the criterion for soil displacement above the sliding surface. One of the strong points of these displacement-based methods is their capability to consider soil displacement resistance acting against the pile-a feature which is not accounted for in pressure-based approaches. Moreover, it better captures the kind of fundamental dynamics which the interaction between soil and pile essentially possesses. For the same reason, displacement-based methods tend to be more accurate than pressure-based methods in describing soil-pile interaction within the shearing soil mass. Moreover, their results tend to be in better agreement with empirical evidence.

Poulos (1995) and Lee et al. (1995) applied a simplified boundary element method to analyze the behavior of piles in sequential rows. The methodology accounts for the passive response of piles in rows through the incorporation of limit equilibrium solutions for slope stability. Originally proposed by Poulos (1973), this method presents one of the basic concepts for analyzing pile performance in slope stability. In this approach, the soil is considered as an elastic continuum and the piles are modeled using a simple elastic beam, as indicated in Figure 2.3. The method assumes free-field soil movement and calculates the maximum shear force that each pile can develop and the corresponding lateral response of the pile.

Thus, by predefining the soil movement, this type of analysis enables more realistic estimation of the lateral resistance capacity of stabilization piles.

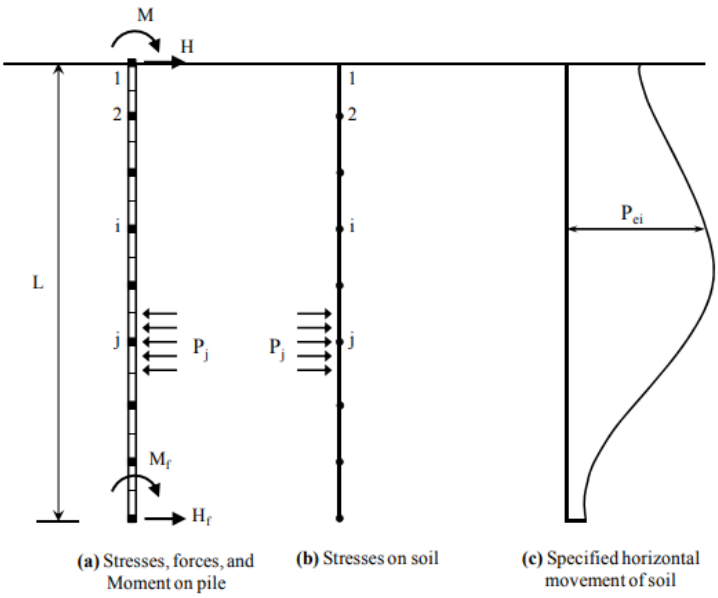

Figure 2.3 Model for Lateral Movement of Piles in Soil (Poulos, 1995)

2.2 Numerical Methods

With the help of major progress in computer and software technologies, finite element and finite difference methods have gained much popularity recently. Such approaches allow the taking into account of complex geometries and the modeling of soil-structure interaction, like arching phenomena and pile group effects. Among other things, numerical techniques also provide high accuracy and deliver detailed results for analysis of soil stability and structural safety (Kourkoulis et al., 2012).

Over the last few years, a number of researchers have employed numerical approaches (Chow, 1996; Jeong et al., 2003; Kourkoulis et al., 2011, 2012; R. Liang & Zeng, 2002; Yamin & Liang, 2010) to look into the relationship between soil and piles in slopes that have been stabilized by piles.

Zeng and Liang (2002) developed a design method based on the stabilization mechanism of piles with a particular focus on the arching mechanism. This approach

provides a basic interpretation of the ground-stabilizing effect due to drilled piles. Figure 2.4 shows the two-dimensional finite element approach that was used to model the arching behavior. In the analyses, it was assumed that the soil is represented by an elasto-perfectly plastic material, and the Mohr-Coulomb criterion was implemented for the finite element analysis. The model took into consideration conditions of rigid shaft behavior with variations in plane-strain, soil parameters, and pile dimensions. The results have shown that the properties of the drilled piles, the movements of observed soils, and the soil parameters, all together, are critical in influencing soil arching behavior. Load transfer curves were generated from 2D finite element simulations with systematic parameter analysis. Unlike the traditional stabilization piles, which use a slicing method, this approach reduces the interfacial forces transmitted to the slice of soil behind the piles. Therefore, the load reduction factor serves to provide a positive effect on stabilization.

The study by Yamin and Liang (2010) used a three-dimensional FE approach to investigate the interaction between slopes and drilled piles, at the same time understanding the arching behavior crucial for slope stabilization. Using three-dimensional finite element modeling, this study simulates soil-structure interaction within a pile system placed on a slope. In particular, it investigates how drilled piles increase slope stability by redistributing soil pressure. The model in detail shows the piles affecting the load distribution on the soils to ensure stability in the sloping soils. These simulations incorporate different soil properties and pile dimensions under various slope conditions. The soil in the simulations exhibits elasto-perfectly plastic behavior with failure criterion combined with the Mohr-Coulomb failure criterion. The results indicate that soil arching behavior is significantly influenced by soil movement and properties, as well as the characteristics of drilled piles.

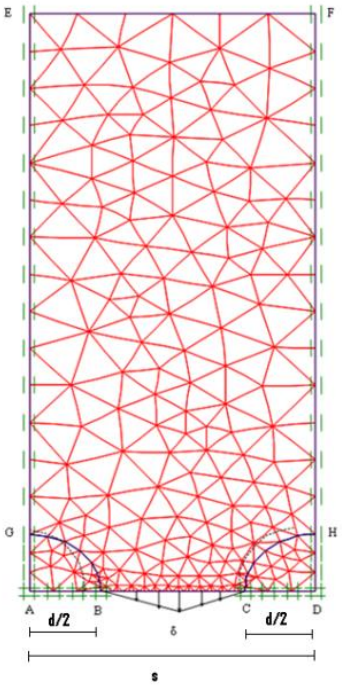

Figure 2.4 Slope/Shaft System Finite Element Model (Zeng and Liang, 2002)

Kourkoulis et al. (2011) investigated how slopes prone to seismic activity can be stabilized using piles. The study includes a parametric analysis to assess the influence of piles in these conditions and evaluate the potential contribution of piles on stability in different situations. This analysis provides a valuable perspective on engineering design by clarifying the impact of piles in seismic zones. The study employs numerical modeling to simulate the behavior of piles in seismically unstable slopes, examining various parameters such as diameter, pile spacing, length, and soil properties The main results indicate that more frequent pile spacing, and increased pile length significantly enhance stability. Larger diameter piles also have a positive effect on stability, although this effect is much less than that of factors like spacing and length. These findings show the important parameters needed to be considered in the sizing and placing of piles in order to stabilize the slope. Also, the soil's properties, particularly its stiffness and strength, are essential to the stabilizing system's overall functionality.

2.3 Hybrid Method of Analysis

The hybrid approach is, in a broader sense, a way of getting results by mixing different approaches so as to cut down the computational effort expended by the user. Several researchers coupled several methodologies, which are numerical or analytical.

Because the hybrid approach analysis can effectively connect the ease of commonly used analytical tools with the accuracy of 3D FE simulations, it is gaining widespread appeal.

Chow (1996) developed a numerical model using beam elements to represent piles as linear elastic materials, while the soil properties were represented by the modulus of subgrade reaction. A hybrid analytical model was developed to analyze the behavior of single piles, incorporating pile-soil-pile interaction within the framework of elasticity theory. Ultimate soil pressure values for piles in cohesive and cohesionless soils were determined using the equations proposed by Viggiani (1981) and Broms (1964), respectively. The analysis also accounted for the relationship between the soil's lateral stiffness and its Young's modulus.

More recently, Kourkoulis et al. (2012) introduced a new methodology, based on the "hybrid" approach, which tries to simplify the slope-stabilizing pile design process in order to reduce the computational effort usually required by three-dimensional analyses of soil-structure interaction. The hybrid approach presented in this work combines the precision of detailed three-dimensional FE simulations using the straightforwardness of commonly used analytical methods. The approach consists of two main steps. First, the required lateral resistance force per unit length for raising an unstable slope to an acceptable safety factor is determined by a conventional slope stability analysis method. In the second step, through a detailed 3D finite element analysis, the optimal pile arrangement providing the required lateral resistance force for achieving the desired deformation level will be determined. This is particularly the recommended approach for the second phase, since it separates the slope

geometry from the computation of lateral pile resistance and enables the numerical analysis to focus on a localized zone of the soil surrounding the piles, as indicated schematically in Figure 2.5a. The final resistance is then computed by imposing a uniform displacement profile along the model boundary, modeling only a representative slice of the soil adjacent to the pile, as schematically shown in Figure 2.5b. This has the effect of greatly reducing computational complexity without any serious loss of accuracy. Case studies are presented illustrating the hybrid approach in optimizing pile design for slope stabilization projects.

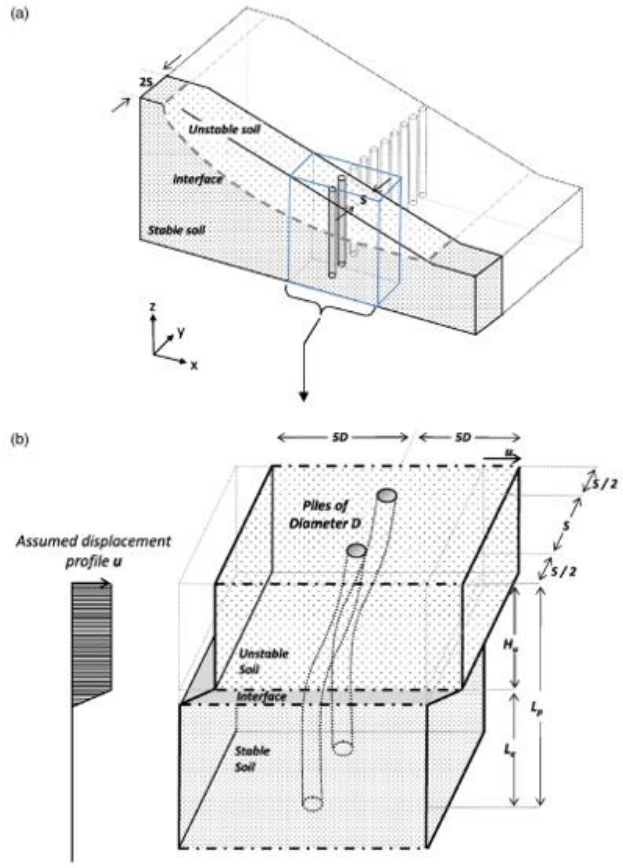

Figure 2.5 Schematic Display of the Simplified "Hybrid" Approach (Kourkoulis et al., 2012)

2.4 Uncoupled Method

The uncoupled approach to analyzing piles for slope stabilization involves separately evaluating the pile response (bending moment, displacement, and shear force) and the overall slope stability. The method treats pile performance and slope stability independently of each other, based on the principle that each is analyzed according to a specific method of analysis.

Jeong et al. (2003) propose, on the contrary, a simplified numerical approach in order to assess the response of slope-pile systems subjected to lateral soil movements. This approach analyzes the behavior of one single row of piles situated above and below the critical surface using the load transfer technique. This involves a two-step approach where, in step one, pressure-displacement curves for the subsoil are developed based on experimental data or finite element analysis. These curves are then used to simulate soil-pile interaction in a nonlinear analysis using hyperbolic load transfer relationships derived from the pressure-displacement data as shown in Figure 2.6. In the second step, these pressure-displacement curves are used to analyze the piles modeled as beams with nonlinear soil spring supports. The approach is particularly suited for scenarios where the sliding soil masses along a slip surface are stabilized by rows of piles which restrain movement and transfer loads to the underlying stable soil layers.

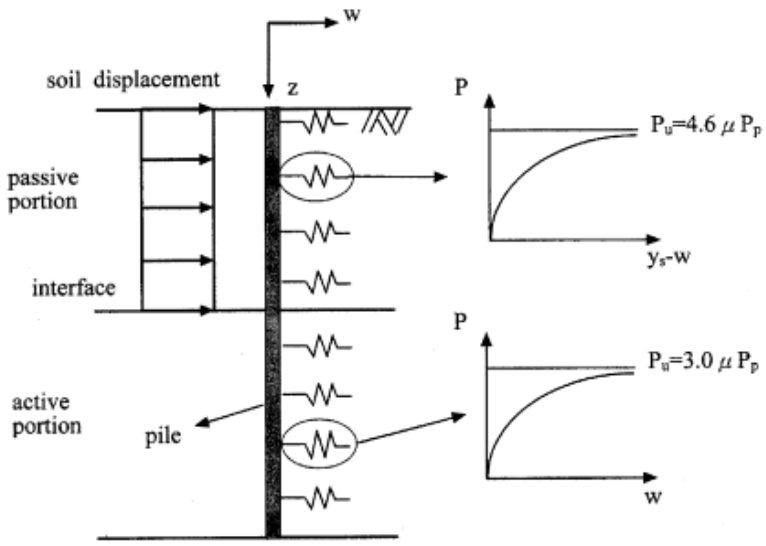

Figure 2.6 A Pile Affected by Lateral Soil Displacement (Jeong et al., 2003)

2.5 Pressure-Displacement (p-y) Curves

The most commonly used conceptual models for pile systems under horizontal loads are those that discretize the pile into a series of beam elements and then connect the soil to the pile with nonlinear springs. In fact, the Winkler soil model simplifies the behavior of the soil by representing it as a series of independent, closely spaced linear or nonlinear springs. Each spring responds independently to the applied load, which represents the soil's resistance to deformation. The soil deforms only around the loaded areas and does not interact with neighboring springs according to this model. Figure 2.7.shows the Winkler soil model using a p-y curve for piles operating under horizontal loads.

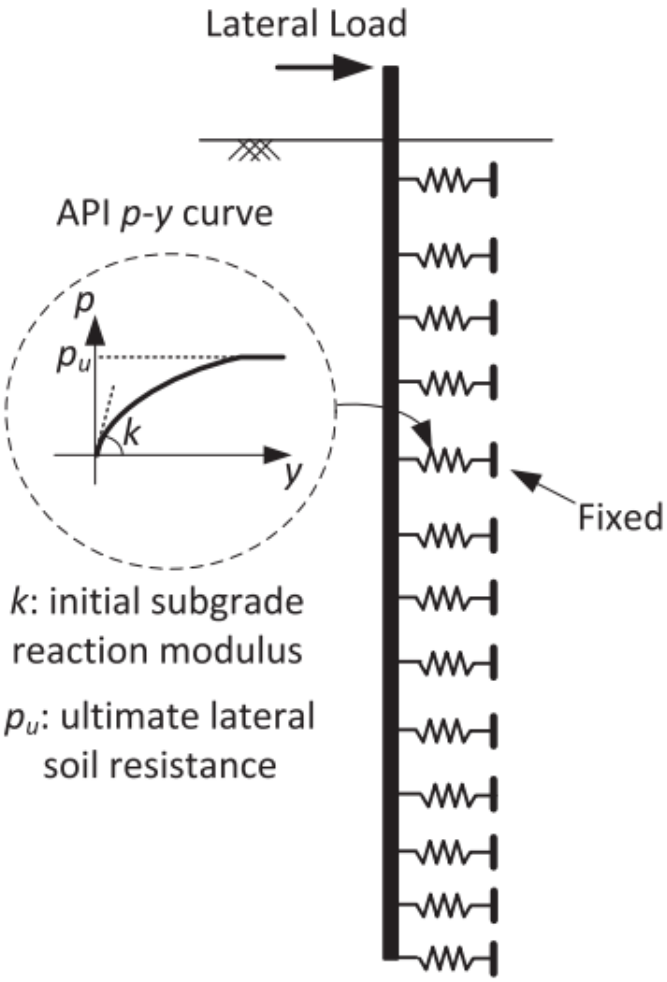

Figure 2.7 Schematic of the Static Analysis of Laterally Loaded Single Piles Using the Spring Method in Practice (Rahmani et al., 2018)

One of the important factors when horizontal large loads are applied is the need for accurate modeling of mechanical interaction that occurs owing to the presence of soil around a pile. The practitioners usually apply the subgrade reaction approach for the analysis of the interaction of soil-pile problems. In addition, empirical equations are usually employed for lateral subgrade reaction values. Nevertheless, this interaction is complicated since the soil is anisotropic, heterogeneous, and non-linear; therefore, these aspects must be incorporated in the modeling process for it to be effective (Dutta and Roy 2002).

In modeling piles subjected to horizontal loads, the p-y curve is a critical component as it defines the relationship between the horizontal soil pressure and the pile's displacement. The curves enable the simulation of nonlinear soil behavior and its resistance to different displacements of the pile for more precise analysis of the interaction that occurs between the soil and the pile.

The concept of modeling soil with p-y curves originated from an analogy with soil behavior in triaxial tests. Meymand (1998) noted that McClelland and Focht introduced this idea in 1958. The authors suggested associating the triaxial stress–strain characteristics with pile load curves at certain depths. Within this method, the anticipated modulus of subgrade reaction for every distinct soil level is utilized to evaluate soil behavior. This method helps in translating soil behavior observed in lab tests to practical pile design applications (Folić et al., 2018).

In a study carried out by Matlock (1970), laterally loaded single piles are examined in soft clay, and relationships between different variables that affect lateral behavior of single piles are given. These are mainly soil characteristics, pile size and applied load. The work of Matlock shows how these variables relate to the deflection of piles embedded in soft clays. In addition to this, the methodology of Matlock embraces all the aspects of field tests, laboratory experiments, analysis of results and theoretical modeling providing a clear picture of lateral behavior of piles in soft cohesive soils. The study evaluates the applicability of existing theoretical models, specifically p-y curves, in predicting the lateral behavior of piles embedded in soft cohesive soils.

Matlock (1970) presented a parabolic p-y curve shape as shown in Figure 2.8 with a theoretical infinite initial tangent modulus at zero deflection. Soil strain (ε) is utilized to determine the initial tangent stiffness of the p-y curve. The pile's diameter and depth significantly influence the ultimate capacity (P_u) of the p-y curve.

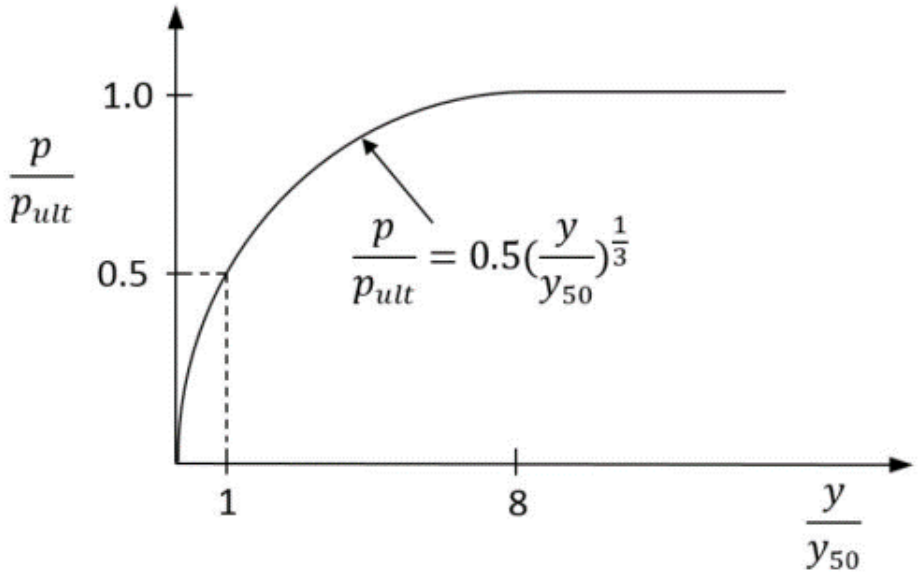

Figure 2.8 p-y Curve of Soft Cohesive Soil Under Static Load (Matlock, 1970)

For soft clays in the presence of free water, the following formulation is recommended, utilizing the smaller value obtained from the provided equations to calculate P_u.

$$P_u = c_u D(3 + \frac{\gamma'}{c_u} z + J\frac{z}{D}) \quad (2.3)$$

$$P_u = 9c_u D \quad (2.4)$$

The following formula determines the reference displacement (y_{50}):

$$y_{50} = 2.5\varepsilon_{50}\, D \quad (2.5)$$

where ε_{50} is the strain for an undrained tri-axial compression test at half the maximum load.

The study by Welch and Reese (1972), titled "Laterally Loaded Behavior of Drilled Shafts," examines the lateral response of drilled shafts embedded in cohesive soils,

with a particular focus on dry, stiff clay. The research aims to understand how this type of soil interacts with piles when subjected to lateral forces.

Welch and Reese performed full-scale field tests of drilled piles under various horizontal loads. These tests evaluated the deformation of the piles against different load magnitudes and measured the respective horizontal response of the surrounding soil. These tests were quite useful in the development of p-y curves for dry stiff clays. This information has been used to enhance models of soil-pile interaction and to develop more realistic pile designs for the conditions described.

The p-y curves developed in this research showed a bilinear shape, as depicted in Figure 2.9, similar to the p-y curves for soft clay suggested by Matlock (1970). For the development of the p-y curve, initial tangent stiffness was determined from the soil strain (ε). In addition, the ultimate horizontal capacity, P_u of the p-y curve was found to be closely related to pile diameter and soil depth. This relationship has particular significance for the accurate performance prediction of piles under horizontal loading in stiff clay conditions. A detailed review of these parameters is necessary to optimize pile design and give correct estimates of soil resistance.

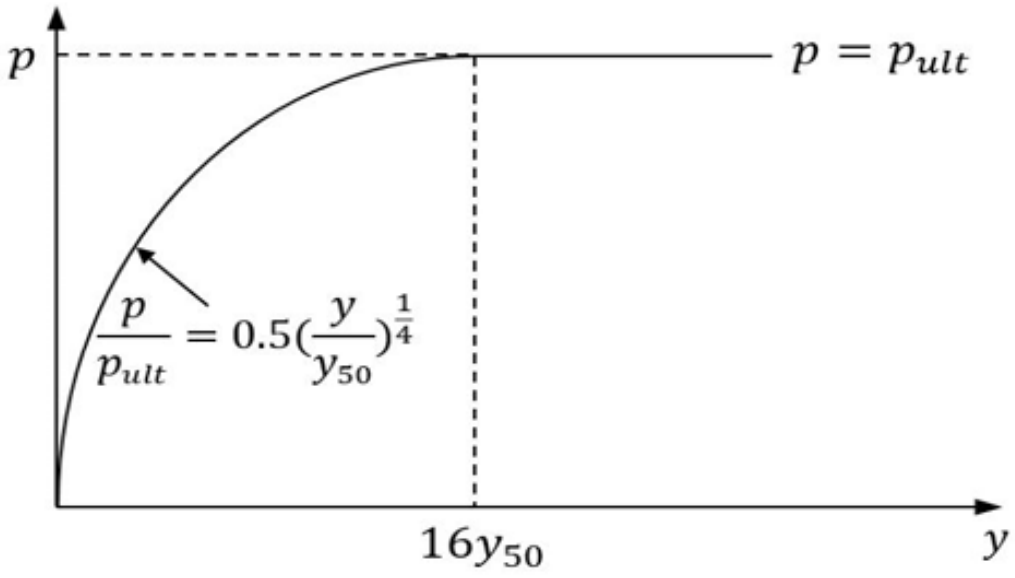

Figure 2.9 p-y Curve of Stiff Cohesive Soil Under Static Load Welch and Reese (1972)

For stiff clays in the presence of free water, the following formulation is recommended, utilizing the smaller value obtained from the provided equations to calculate $P_{u.}$

$$P_u = c_u D(3 + \frac{\gamma'}{c_u} z + J\frac{z}{D}) \tag{2.6}$$

$$P_u = 9c_u D \tag{2.7}$$

The following formula determines the reference displacement (y_{50}):

$$y_{50} = 2.5\varepsilon_{50}\, D \tag{2.8}$$

where ε_{50} is the strain for an undrained tri-axial compression test at half the maximum load.

Reese et al. (1975) carried out a comprehensive study of the response of piles subjected to lateral loads in submerged stiff clay soils. This study places special emphasis on the use and validation of the p-y curve methodology. Piles of different sizes were tested under lateral loads, pile rotations at depths were measured and soil samples were collected, and their mechanical properties were analyzed. The research establishes the relationship between soil parameters and pile properties with respect to stiff clay soils under water, pointing out that p-y curves are effective in predictions. Further verification of this methodology is presented by comparing field observations with analytical predictions for the validity of the methodology in design and analysis.

Reese et al. (1975) developed a formulation for p-y curves to describe the response of stiff cohesive soils under conditions involving free water. The form of the proposed curve is made up of five portions and Figure 2.10 shows its shape.

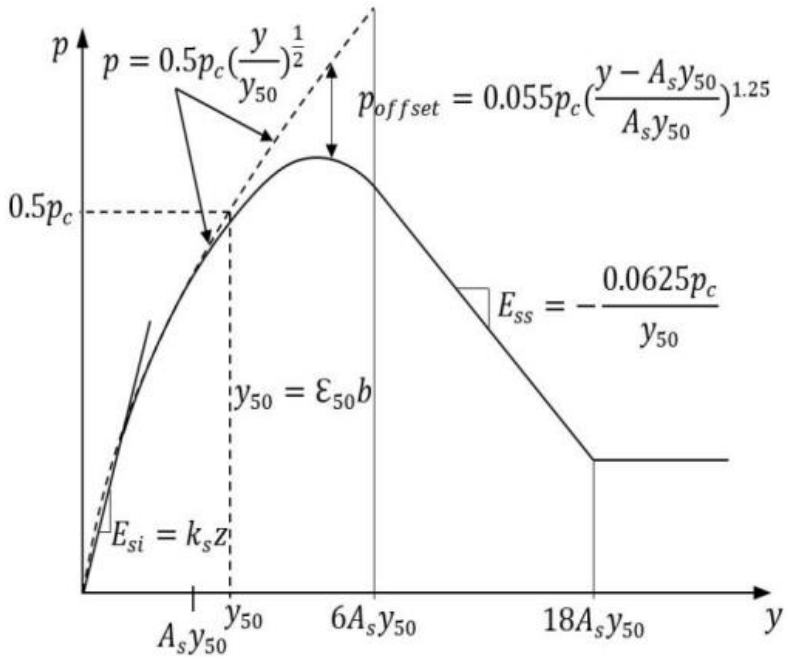

Figure 2.10 p-y Curve for Stiff Cohesive Soil with Water (Reese et al., 1975)

The smaller numbers provided by the following equations is used to compute P_u.

$$P_u = 2c_a D + \gamma' Dz + 2.83c_a z \quad (2.9)$$

$$P_u = 11c_u D \quad (2.10)$$

Figure 2.11 shows A_s coefficient that is dependent on the depth to diameter ratio.

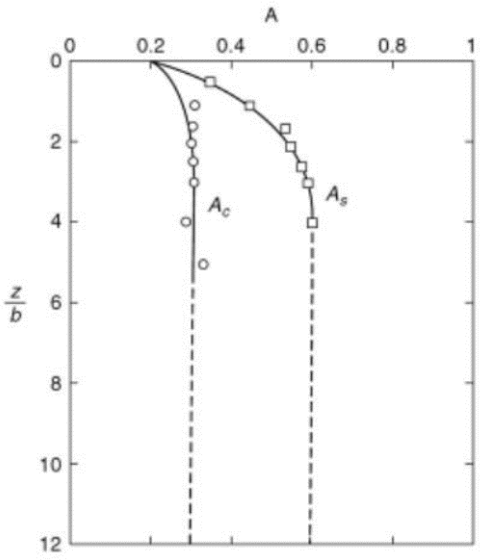

Figure 2.11 Values of Constants As and Ac (Reese & Van Impe, 2011)

2.5.1 Slope Effect on Pressure-Displacement (p-y) Curves

The conventional p-y models are typically applicable to piles installed in level ground (Matlock, 1970; Reese et al., 1975; Welch & Reese, 1972). A number of studies have revealed that the angle of the slope has considerable influence on the load-deflection behavior of piles installed in sloping ground (Georgiadis & Georgiadis, 2010; Mezazigh and Levacher, 1998; Muthukkumaran et al., 2008; Nimityongskul et al., 2018; Sharafi et al., 2015).

In the study of Georgiadis and Georgiadis (2010), a three-dimensional numerical model is developed and used to fully analyze the behavior of piles subjected to horizontal loading at undrained clay slopes. For this purpose, the authors investigate the pile shaft interaction with the surrounding soil for different slope geometries. In addition, it proposes a reduction factor to account for slope angle and pile dimensions on the lateral capacity of piles. This factor helps in addressing pile performance on sloping ground more effectively.

The following formula can be used to approximate the reduction, which depends on the slope angle:

$$\mu = \frac{K_{i\theta}}{K_{io}} = cos\theta + \frac{z}{6D}(1 - cos\theta) \tag{2.11}$$

Where:

At depths exceeding of z= 6D the initial stiffness $K_{i\theta}$ becomes equal to K_{io}.

For piles positioned near the slope, this factor is applied to modify the initial stiffness of the p-y curves, enabling a more accurate prediction of pile response. Research indicated that the horizontal resistance is diminished significantly for more steeper slopes. This emphasizes why such considerations should be included within the design stage for the pile-supported structures in sloping areas in order to maintain their functionality and safety. However, long piles placed at a distance from the slope crest are outside the scope of this study. The FEM adopted in the study was developed only for piles lying on top of the slope as it will be shown in Figure 2.12.

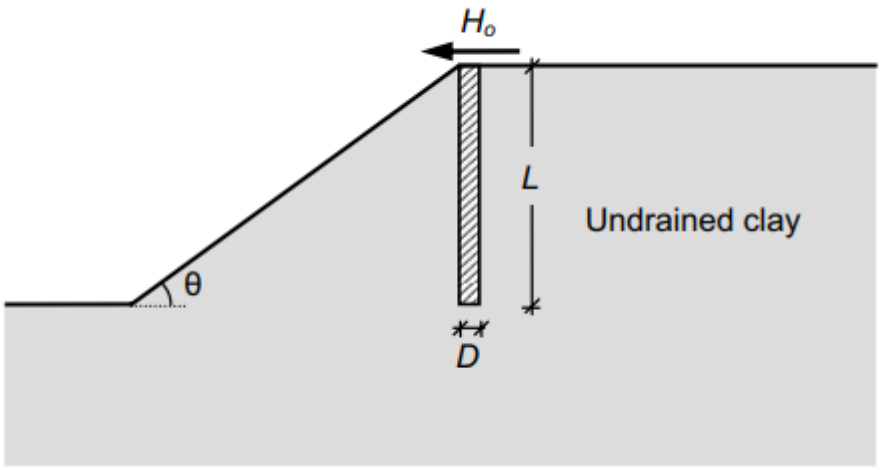

Figure 2.12 Definition of the Issue in the Undrained Lateral Pile Response Research in Sloping Ground (Georgiadis & Georgiadis, 2010)

In an experimental study, Mezazigh and Levacher (1998) studied the effects of slopes on the lateral behavior of piles in sandy soils. The slope geometry and the distance between the pile and the slope crest had been at the center of the research findings because of their influences on lateral load capacity. Their research revealed that, because of reduced passive resistance, a pile located near the slope has reduced lateral load capacity. The study addresses this by proposing a modification to the p-y curves with a reduction coefficient, in this case named the p-multiplier. The results also show that beyond a certain distance, which is about 8D for the 1V:2H slope and 12D for the 1V:1.5H slope, where "D" is for pile diameter, "V" for vertical component, and "H" for horizontal component, the slope effect becomes negligible. These findings indicated the critical importance of accounting for slope conditions when designing pile foundations.

Muthukkumaran et al. (2008) performed laboratory model tests in dry sand with the aim of establishing p-y curves for sandy soils when supporting a structure located under different slope angles. The tests consisted of a series of long pile tests to investigate slope angles on the lateral load capacity and bending moment of a pile located at the crest of a slope. In fact, the study focuses on slope angle and relative density effects on bending moment, horizontal soil resistance, and lateral displacement. The results refine the methodology presented in API RP 2A (2000) by introducing a reduction factor R, which enables the development of more precise dimensionless p-y curves for piles in sloping soils. The values of p/P_u obtained from the experiments are used to predict R by multiple regression analysis, and the reduction factor is given in the form of following equation:

$$R = 0.74 + 0.0378\left(\frac{Z}{D}\right) - 0.6315 * S\,; R \leq 1 \qquad (2.12)$$

Where:

S = slope angle expressed in radians (valid within the range of 0.66 to 0.50).

This reduction factor is supposed to be crucial for enhancing the reliability of pile design in sloped terrains.

Nimityongskul et al. (2018) performed full-scale lateral load tests on fully instrumented piles in cohesive soils for the investigation of their lateral behavior under free-field conditions and near slopes. Instead of placing the piles directly on the slope, they installed them on flat ground at different distances from the crest of the slope, applying lateral loads to them. The present study primarily focused on the performance of piles in terms of their lateral capacity with respect to the distance from the crest of the slope. It was observed that the piles up to a distance of 4D from the slope crest showed, in general, a reduction in the lateral load capacity, essentially because of the passive resistance in front of the pile, which was insufficiently mobilized under lateral loading. Besides, it was noted that the initial stiffness of the p-y curve for the same pile remained practically unchanged by changes in the pile's distance from the crest, as shown in Figure 2.13.

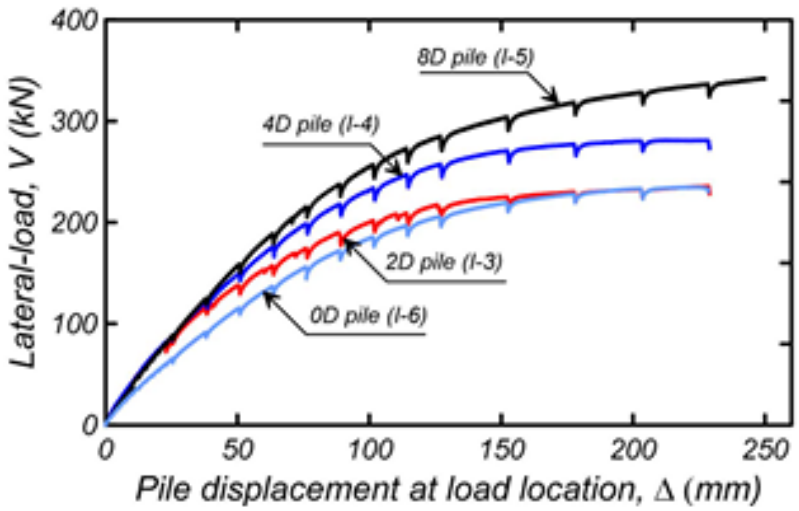

Figure 2.13 Load-Displacement Curves for Piles at Various Locations (Nimityongskul et al., 2018)

It was further found in the study that proximity to the slope significantly affects the initial stiffness of the load-displacement curve and the maximum lateral load

capacity of piles. This effect diminishes at a distance of 8D or more from the slope crest and can be considered negligible beyond that point. Considering the slope effect, p-multipliers were developed taking into account variations in the distance between the pile and the crest. Furthermore, it was realized that these p-multipliers depend not only on the pile's distance from the slope but also on the magnitude of soil displacement.

Slope effects on the p-y curves by 3D FDA were studied by Sharafi et al. (2015). In the current study, the performance of vertical individual piles under static horizontal load in flat and sloping terrains for c-ϕ soils-that is, soils exhibiting both cohesive and frictional properties-is developed. In the study presented here, various slope inclinations are being examined and different distances between the pile center and the crest of the slope. Both interface normal and shear stiffness are considered for pile-soil interaction analysis. Sharafi et al. (2015) observed that the ultimate horizontal resistance of soils increases with a decrease in the slope angle and an increase in the pile center-to-slope crest distance. This indicates that flatter slopes and piles located further away from the crest are more capable of providing greater horizontal load resistance. The frictional component of c-ϕ soils then becomes more prominent under such conditions to enhance lateral load capacity. This paper has underlined the importance of slope geometry and position of the pile, which makes it worthy for developing p-y curves in sloped terrains.

Reese et al. (2006) presented a p-multiplier for the ultimate soil resistance near the ground surface in saturated clay as a function of slope angle for piles located at the slope crest. The variation of the p-multiplier with slope angle from their study may be approximated by the following equation.

$$p - multiplier = \frac{1}{1 + \tan(\theta)} \tag{2.13}$$

CHAPTER 3

METHODOLOGY

This study presents a series of 2D, drained, nonlinear FE analyses to examine the piles behavior in both level and sloped ground. Additionally, the study aims to investigate the impact of the pile's proximity to the slope crest on essential p-y curve properties, specifically the initial slope (K_i) and the ultimate horizontal earth pressure (P_u), under drained loading conditions on sloped terrain. In the analysis, the effects of the groundwater table are not considered. Also, as slope stability in long-term conditions and the principle of effective stresses are considered, soil can be assumed to be drained soil.

The results of this research show that the general shape of p-y curves for c-ϕ cohesive soils. The analysis results were used to figure out how the K_i and P_u values change according to the spacing between the pile and the crest of the slope. For this purpose, the pile to crest distance parameter was analyzed under different soil and geometric conditions. Thus, the changes in the ultimate lateral earth pressure (P_u) and initial slope (K_i) with varying soil and geometric parameters were observed.

3.1 Finite Element Analyses

The finite element method (FEM) provides advantages with better modeling of slopes featuring complicated geometry, different conditions of loading, reinforcing materials, water flow, and advanced assumptions about soil behavior. It also gives a more distinct view on soil deformations. Another significant advantage is that no prior assumptions about the location or shape of the sliding surface are necessary. Instead, weak zones will naturally appear in areas within the soil where the shear strength cannot resist the applied shear forces, and thus these weak zones are spontaneously exposed.

Numerous analyses were carried out using the Plaxis 2D FE program. In these analyses, geometric properties such as slope angle, slope height, pile to crest distance and soil properties such as plasticity index (PI) and SPT-N_{60} values were varied.

The example geometry of the problem analyzed is illustrated in Figure 3.1.

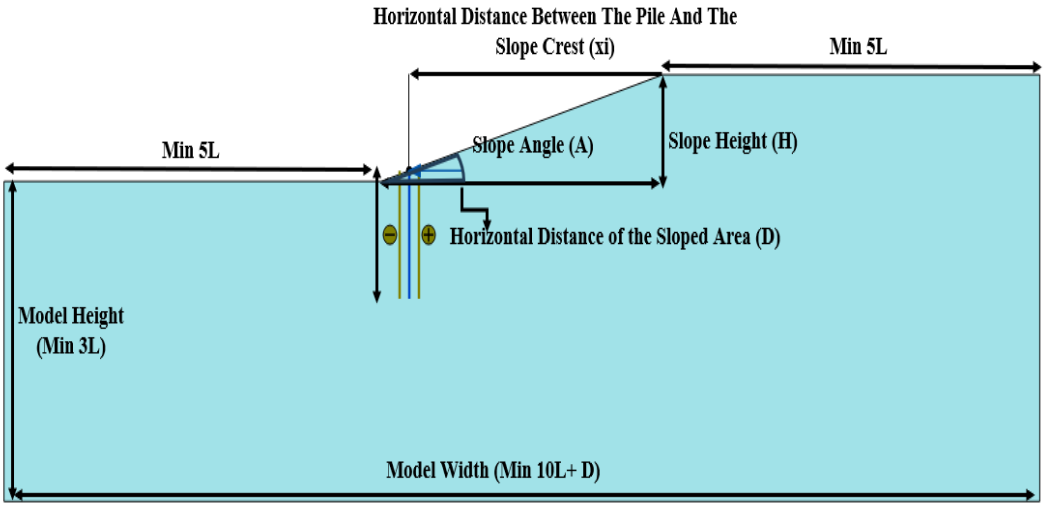

Figure 3.1 The Example Geometry of the Problem

In PLAXIS 2D finite element analysis, soil formations were represented using 15-node triangular mesh elements, which allows for ninth-degree integration. Cylindrical piles, on the other hand, are modeled using plate elements. In the 2D models, these plate elements have three degrees of freedom at each node: two translational (U_x, U_y) and one rotational, which is around the out-of-plane axis (φ_z) and within the x-y plane. The construction phases are simulated by activating or removing the elements of soil cluster and plate. At each step, the software iteratively renews the calculations until a new equilibrium is reached. The deformations of the piles and the variation of the bending moments, shear, and axial forces developed at each load stage will be obtained from the analysis. The results will also present the node deformations of the soil clusters in detail, total and effective stresses, and plastic points within the soil mass.

The deformed mesh geometries resulting from the final loading condition in the finite element analyses for the cases represented by the notations H15A15X00N15PI10, H15A15X09N15PI10, and H15A15X10N15PI10 are shown in Figure 3.2, Figure 3.3 and Figure 3.4 respectively.

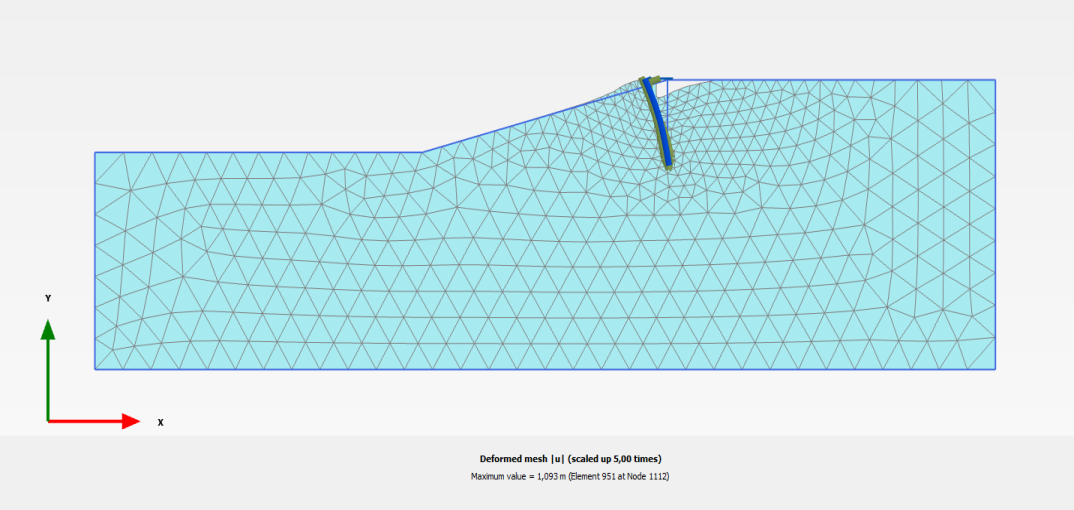

Figure 3.2 Deformed Mesh Geometry for the Case Represented by H15A15X00N15PI10 Notation

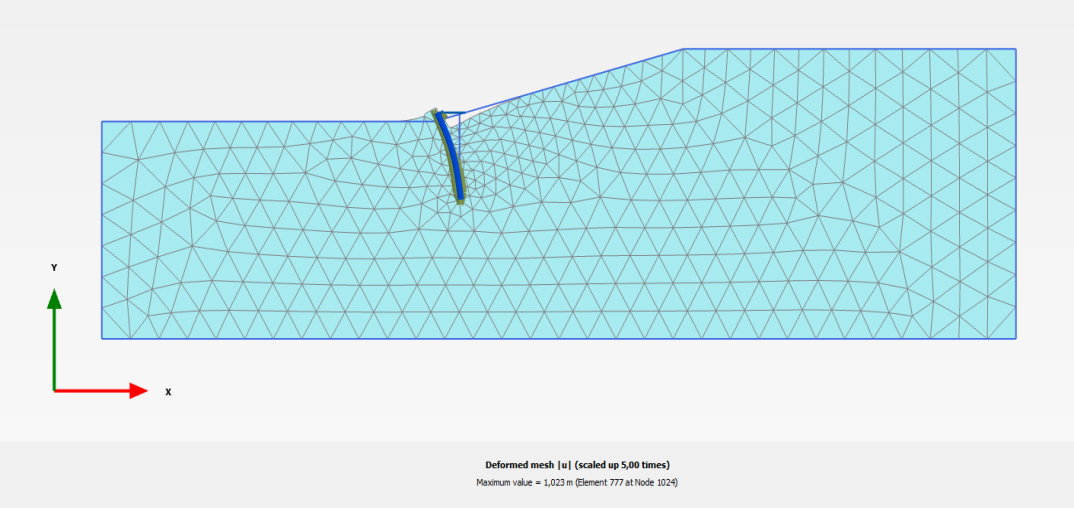

Figure 3.3 Deformed Mesh Geometry for the Case Represented by H15A15X09N15PI10 Notation

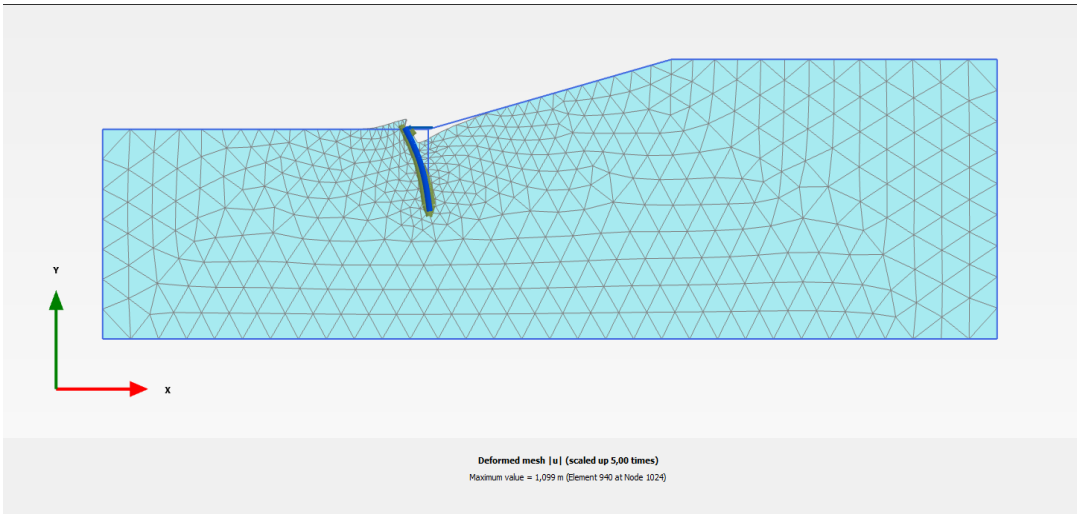

Figure 3.4 Deformed Mesh Geometry for the Case Represented by H15A15X10N15PI10 Notation

The simulation used the method of plane strain. The model is two-dimensional, in which displacements and strains in the direction perpendicular to the plane are assumed as zero, therefore reducing the analysis into in-plane behavior.

The impacts of the ground water table have not been taken into account in this study, which assumes that the soil is drained by considering the principles of effective stresses and long-term slope stability.

In the analyses "Hardening Soil (HS)" material model was chosen to reflect the plastic behavior of clay units. This material model uses effective unit weight (γ'), effective internal friction angle (ϕ'), effective cohesion (c') and soil stiffness parameters as inputs. These parameters were determined using the SPT-N_{60} and PI values with the help of the related correlations given in the Section 3.3. In the material model used, soil stiffness parameters were defined based on plastic straining due to shearing (E_{50}^{ref}), plastic straining due to primary compression (E_{oed}^{ref}), reloading stiffness (E_{ur}^{ref}), and the power law (m). In this study, it is assumed that E_{50}^{ref} is equal to the drained deformation modulus (E'_s), while the E_{ur}^{ref} value is set to three times the value of E_{50}^{ref}, the E_{oed}^{ref} value is taken as equal to E_{50}^{ref}, and the power law parameter (m) is assigned a value of 0.50, as recommended in the PLAXIS manual.

In the Plaxis 2D model, the model height was defined as three times the pile length, measured downward from the base of the slope. Similarly, the model width was set to five times the pile length, extending beyond the boundaries of the slope. This configuration aims to minimize end effects and ensure accurate simulation results. The mesh was constrained in all directions on the bottom boundary, while being vertically fixed in the normal direction on the vertical boundaries. Subsequently, the pile was modeled by activating plate and interface elements, and a horizontal load was applied to its top.

The following steps were followed when obtaining the p-y curve for specific conditions using the FE program:

1- The first step in each analysis was to develop initial stresses by applying gravity loading of soil self-weight.
2- Continue the pile construction by activating plate and interface elements.
3- Defining a horizontal pile head load in the sliding direction.
4- To obtain the p-y behavior of the soil continuously, the load was increased at each step until the soil body collapsed. As a result, the loads along the pile are a consequence of the applied pile head load and the horizontal load exerted on the pile due to the slope. In the next stage, the obtained p-y curves are generated as a result of these loads.
5- The p-y curves were obtained by differentiating the Q-z (shear force-depth) diagrams in order to obtain p-z (lateral soil pressure- depth) diagrams for a range of pile head loads H_o. A computational program was utilized to perform this task by optimally fitting the Q-z (shear force-depth) data to a curve that best fitted the data set, before calculating the first derivatives at chosen points. Corresponding p-z diagrams were consequently matched together with the lateral deflection-depth diagrams, y-z diagrams to develop the load-displacement or p-y curves as shown in Figure 3.5. The details of this process are given in Appendix A.

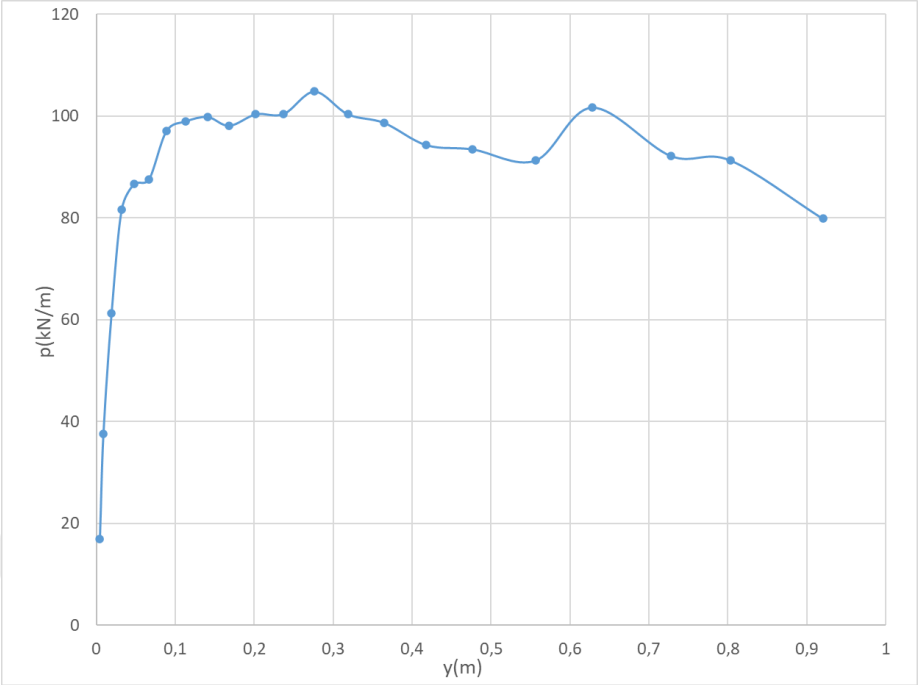

Figure 3.5 The p-y Diagram for An Example Case

3.2 Parametric Study

For each factor that has an influence on the ultimate lateral earth pressure (P_u) and initial slope (K_i), finite element analysis was performed with all other parameters held constant. In this way, the effect of each variable parameter on the p-y curve behavior can be clearly observed.

3.2.1 Soil Conditions

The analyses were performed on drained clay soils for which strength and deformation parameters were defined based on the plasticity index (PI) and SPT-N_{60} values of cohesive soils. How the strength and deformation parameters were determined based on these values will be explained in the Section 3.3.

- Plasticity Index (PI)

Two different plasticity index values are chosen as PI=10% and PI=20%.

- SPT-N_{60} Values

Three different SPT-N_{60} values are chosen as 8,15 and 30 to reflect the behavior of clays with medium, stiff and very stiff consistency respectively, following the criteria outlined in Table 3.1, as proposed by Terzaghi and Peck (1967).

Table 3.1 Classification of Clay Soil Using SPT (Terzaghi and Peck, 1967)

SPT Value	Type
0-2	Very Soft
2-4	Soft
4-8	Medium
8-15	Stiff
15-30	Very Stiff

3.2.2 Geometric Conditions

- Slope Angle

Two slope angles, 5° and 15°, were selected for analysis. In addition to analyses conducted on piles located on slopes, studies were also performed for piles situated on level ground.

- Slope Height (Also Pile Length)

Two different slope heights are chosen as 10 m and 15 meters. For those slope heights, piles with length 12 m and 18 m were studied respectively.

- Pile's Distance to Crest

A geometry parameter, Xx notation, is defined to indicate the distance between the pile and the crest of the slope. In this respect, x is defined as xi/D, where xi represents the horizontal distance between the pile and the slope crest, and D represents the horizontal distance of the sloped area. The definitions of the lengths involved are indicated in Figure 3.6.

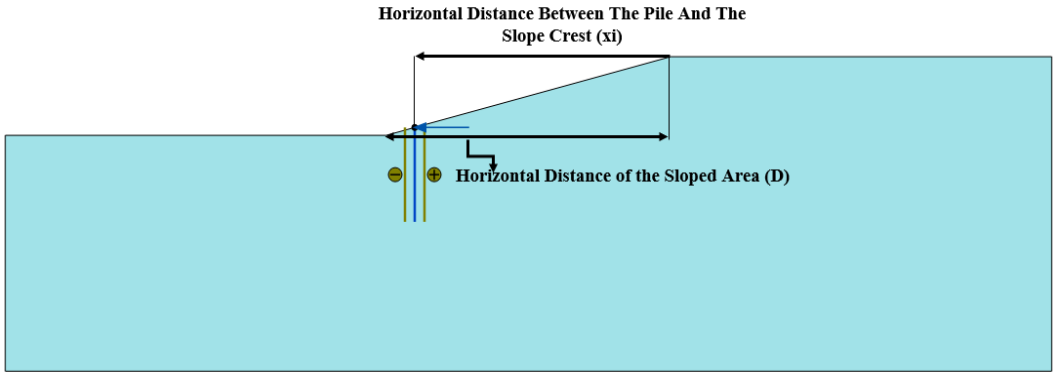

Figure 3.6 Distances for the Defination of Xx Notation

Parameter Xx defines the location of the pile inside a slope geometry. For instance, the value of x in the X09 parameter is 0.9. This contains detailed information on the location of the pile in the corresponding case: the ratio of the horizontal distance between the crest of the slope and the pile to the horizontal length of the sloping

ground is 0.9. For each of the variable parameters, three scenarios were examined with respect to the distances between the pile and the slope crest, represented by the parameters X00, X09, and X10. The distances have been chosen in such a way that horizontal behavior could be examined for the pile at the slope crest (X00) and at the base of the slope (X10). The choice of Distance X09 was based on preliminary research, which has shown that at least up to this distance, the pile's behavior closely resembles that observed at the crest of the slope; beyond this point, it aligns more closely with the behavior of the pile at the toe of the slope.

However, considering the different geometric and soil conditions this behavior was not always achieved. For this reason, for some cases X08 and X095 situations were also studied.

In order to examine the scenarios generated by all of these parameters, 114 different analyses were performed. For all the analyses piles with 1.00 m diameter were used. The pile series having constant spacing, equal to the pile's diameter, is simulated in the PLAXIS 2D program as a continuous wall of an equivalent thickness extended in the longitudinal direction. Considering the dimensions of the piles assumed to be constructed with C20 concrete (E=28000 MPa), the finite element program was configured with an axial rigidity (EA) value of 219911 kN/m and a flexural rigidity (EI) value of 13744 kN·m²/m.

The p-y curves have different shapes at various depths and do not reach their ultimate value, P_u, for some specified displacement on the pile head. Nevertheless, from the actual curves developed based on results of static lateral load tests, the p-y curves reach their ultimate value, P_u, at shallow depths (Sharafi et al., 2015).

Since continuous p-y curves could not be obtained at all depths until the collapse of the soil mass, p-y curves were generated at a depth of 3 meters where regular data could be collected to ensure consistency in the study.

The series of analyses performed, and the geometric and soil properties are shown in Table 3.2

Table 3.2 Parametric Properties of Numeric Analyses

Scenario No	Pile Properties		Geometrical Properties			Cohesive Soil Parameters Properties		Notation
	L (m)	D (m)	Slope Height (m)	Slope Angle (Deg)	Distance from Crest (x/L)	PI (%)	SPT N_{60}	
1	12	1.0	NA	0	NA	10	8	H10A00X--N08PI10
2	12	1.0	NA	0	NA	10	15	H10A00X--N15PI10
3	12	1.0	NA	0	NA	10	30	H10A00X--N30PI10
4	12	1.0	NA	0	NA	20	8	H10A00X--N08PI20
5	12	1.0	NA	0	NA	20	15	H10A00X--N15PI20
6	12	1.0	NA	0	NA	20	30	H10A00X--N30PI20
7	18	1.0	NA	0	NA	10	8	H15A00X--N08PI10
8	18	1.0	NA	0	NA	10	15	H15A00X--N15PI10

Table 3.2 Parametric Properties of Numeric Analyses (continued)

Scenario No	Pile Properties		Geometrical Properties			Cohesive Soil Parameters Properties		Notation
	L (m)	D (m)	Slope Height (m)	Slope Angle (Deg)	Distance from Crest (x/L)	PI (%)	SPT N_{60}	
9	18	1.0	NA	0	NA	10	30	H15A00X--N30PI10
10	18	1.0	NA	0	NA	20	8	H15A00X--N08PI20
11	18	1.0	NA	0	NA	20	15	H15A00X--N15PI20
12	18	1.0	NA	0	NA	20	30	H15A00X--N30PI20
13	12	1.0	10	5	0	10	8	H10A05X00N08PI10
14	12	1.0	10	5	0	10	15	H10A05X00N15PI10
15	12	1.0	10	5	0	10	30	H10A05X00N30PI10
16	12	1.0	10	5	0	20	8	H10A05X00N08PI20

Table 3.2 Parametric Properties of Numeric Analyses (continued)

Scenario No	Pile Properties		Geometrical Properties			Cohesive Soil Parameters Properties		Notation
	L (m)	D (m)	Slope Height (m)	Slope Angle (Deg)	Distance from Crest (x/L)	PI (%)	SPT N_{60}	
17	12	1.0	10	5	0	20	15	H10A05X00N15PI20
18	12	1.0	10	5	0	20	30	H10A05X00N30PI20
19	12	1.0	10	5	0.9	10	8	H10A05X09N08PI10
20	12	1.0	10	5	0.9	10	15	H10A05X09N15PI10
21	12	1.0	10	5	0.9	10	30	H10A05X09N30PI10
22	12	1.0	10	5	0.9	20	8	H10A05X09N08PI20
23	12	1.0	10	5	0.9	20	15	H10A05X09N15PI20
24	12	1.0	10	5	0.9	20	30	H10A05X09N30PI20

Table 3.2 Parametric Properties of Numeric Analyses (continued)

Scenario No	Pile Properties		Geometrical Properties			Cohesive Soil Parameters Properties		Notation
	L (m)	D (m)	Slope Height (m)	Slope Angle (Deg)	Distance from Crest (x/L)	PI (%)	SPT N_{60}	
25	12	1.0	10	5	1.0	10	8	H10A05X10N08PI10
26	12	1.0	10	5	1.0	10	15	H10A05X10N15PI10
27	12	1.0	10	5	1.0	10	30	H10A05X10N30PI10
28	12	1.0	10	5	1.0	20	8	H10A05X10N08PI20
29	12	1.0	10	5	1.0	20	15	H10A05X10N15PI20
30	12	1.0	10	5	1.0	20	30	H10A05X10N30PI20
31	12	1.0	10	15	0	10	8	H10A15X00N08PI10
32	12	1.0	10	15	0	10	15	H10A15X00N15PI10

Table 3.2 Parametric Properties of Numeric Analyses (continued)

Scenario No	Pile Properties		Geometrical Properties			Cohesive Soil Parameters Properties		Notation
	L (m)	D (m)	Slope Height (m)	Slope Angle (Deg)	Distance from Crest (x/L)	PI (%)	SPT N_{60}	
33	12	1.0	10	15	0	10	30	H10A15X00N30PI10
34	12	1.0	10	15	0	20	8	H10A15X00N08PI20
35	12	1.0	10	15	0	20	15	H10A15X00N15PI20
36	12	1.0	10	15	0	20	30	H10A15X00N30PI20
37	12	1.0	10	15	0.9	10	8	H10A15X09N08PI10
38	12	1.0	10	15	0.9	10	15	H10A15X09N15PI10
39	12	1.0	10	15	0.9	10	30	H10A15X09N30PI10
40	12	1.0	10	15	0.9	20	8	H10A15X09N08PI20

Table 3.2 Parametric Properties of Numeric Analyses (continued)

Scenario No	Pile Properties		Geometrical Properties			Cohesive Soil Parameters Properties		Notation
	L (m)	D (m)	Slope Height (m)	Slope Angle (Deg)	Distance from Crest (x/L)	PI (%)	SPT N_{60}	
41	12	1.0	10	15	0.9	20	15	H10A15X09N15PI20
42	12	1.0	10	15	0.9	20	30	H10A15X09N30PI20
43	12	1.0	10	15	1.0	10	8	H10A15X10N08PI10
44	12	1.0	10	15	1.0	10	15	H10A15X10N15PI10
45	12	1.0	10	15	1.0	10	30	H10A15X10N30PI10
46	12	1.0	10	15	1.0	20	8	H10A15X10N08PI20
47	12	1.0	10	15	1.0	20	15	H10A15X10N15PI20
48	12	1.0	10	15	1.0	20	30	H10A15X10N30PI20

Table 3.2 Parametric Properties of Numeric Analyses (continued)

Scenario No	Pile Properties		Geometrical Properties			Cohesive Soil Parameters Properties		Notation
	L (m)	D (m)	Slope Height (m)	Slope Angle (Deg)	Distance from Crest (x/L)	PI (%)	SPT N_{60}	
49	18	1.0	15	5	0	10	8	H15A05X00N08PI10
50	18	1.0	15	5	0	10	15	H15A05X00N15PI10
51	18	1.0	15	5	0	10	30	H15A05X00N30PI10
52	18	1.0	15	5	0	20	8	H15A05X00N08PI20
53	18	1.0	15	5	0	20	15	H15A05X00N15PI20
54	18	1.0	15	5	0	20	30	H15A05X00N30PI20
55	18	1.0	15	5	0.9	10	8	H15A05X09N08PI10
56	18	1.0	15	5	0.9	10	15	H15A05X09N15PI10

Table 3.2 Parametric Properties of Numeric Analyses (continued)

Scenario No	Pile Properties		Geometrical Properties			Cohesive Soil Parameters Properties		Notation
	L (m)	D (m)	Slope Height (m)	Slope Angle (Deg)	Distance from Crest (x/L)	PI (%)	SPT N_{60}	
57	18	1.0	15	5	0.9	10	30	H15A05X09N30PI10
58	18	1.0	15	5	0.9	20	8	H15A05X09N08PI20
59	18	1.0	15	5	0.9	20	15	H15A05X09N15PI20
60	18	1.0	15	5	0.9	20	30	H15A05X09N30PI20
61	18	1.0	15	5	1.0	10	8	H15A05X10N08PI10
62	18	1.0	15	5	1.0	10	15	H15A05X10N15PI10
63	18	1.0	15	5	1.0	10	30	H15A05X10N30PI10
64	18	1.0	15	5	1.0	20	8	H15A05X10N08PI20

Table 3.2 Parametric Properties of Numeric Analyses (continued)

Scenario No	Pile Properties		Geometrical Properties			Cohesive Soil Parameters Properties		Notation
	L (m)	D (m)	Slope Height (m)	Slope Angle (Deg)	Distance from Crest (x/L)	PI (%)	SPT N_{60}	
65	18	1.0	15	5	1.0	20	15	H15A05X10N15PI20
66	18	1.0	15	5	1.0	20	30	H15A05X10N30PI20
67	18	1.0	15	15	0	10	8	H15A15X00N08PI10
68	18	1.0	15	15	0	10	15	H15A15X00N15PI10
69	18	1.0	15	15	0	10	30	H15A15X00N30PI10
70	18	1.0	15	15	0	20	8	H15A15X00N08PI20
71	18	1.0	15	15	0	20	15	H15A15X00N15PI20
72	18	1.0	15	15	0	20	30	H15A15X00N30PI20

Table 3.2 Parametric Properties of Numeric Analyses (continued)

Scenario No	Pile Properties		Geometrical Properties			Cohesive Soil Parameters Properties		Notation
	L (m)	D (m)	Slope Height (m)	Slope Angle (Deg)	Distance from Crest (x/L)	PI (%)	SPT N_{60}	
73	18	1.0	15	15	0.9	10	8	H15A15X09N08PI10
74	18	1.0	15	15	0.9	10	15	H15A15X09N15PI10
75	18	1.0	15	15	0.9	10	30	H15A15X09N30PI10
76	18	1.0	15	15	0.9	20	8	H15A15X09N08PI20
77	18	1.0	15	15	0.9	20	15	H15A15X09N15PI20
78	18	1.0	15	15	0.9	20	30	H15A15X09N30PI20
79	18	1.0	15	15	1.0	10	8	H15A15X10N08PI10
80	18	1.0	15	15	1.0	10	15	H15A15X10N15PI10

Table 3.2 Parametric Properties of Numeric Analyses (continued)

Scenario No	Pile Properties		Geometrical Properties			Cohesive Soil Parameters Properties		Notation
	L (m)	D (m)	Slope Height (m)	Slope Angle (Deg)	Distance from Crest (x/L)	PI (%)	SPT N_{60}	
81	18	1.0	15	15	1.0	10	30	H15A15X10N30PI10
82	18	1.0	15	15	1.0	20	8	H15A15X10N08PI20
83	18	1.0	15	15	1.0	20	15	H15A15X10N15PI20
84	18	1.0	15	15	1.0	20	30	H15A15X10N30PI20
85	12	1.0	10	5	0.8	10	15	H10A05X08N15PI10
86	12	1.0	10	5	0.8	10	30	H10A05X08N30PI10
87	12	1.0	10	5	0.8	20	30	H10A05X08N30PI20
88	12	1.0	10	5	0.95	10	15	H10A05X095N15PI10

Table 3.2 Parametric Properties of Numeric Analyses (continued)

Scenario No	Pile Properties		Geometrical Properties			Cohesive Soil Parameters Properties		Notation
	L (m)	D (m)	Slope Height (m)	Slope Angle (Deg)	Distance from Crest (x/L)	PI (%)	SPT N_{60}	
89	12	1.0	10	5	0.95	10	30	H10A05X095N30PI10
90	12	1.0	10	5	0.95	20	30	H10A05X095N30PI20
91	12	1.0	10	15	0.8	10	8	H10A15X08N08PI10
92	12	1.0	10	15	0.8	10	15	H10A15X08N15PI10
93	12	1.0	10	15	0.8	10	30	H10A15X08N30PI10
94	12	1.0	10	15	0.8	20	8	H10A15X08N08PI20
95	12	1.0	10	15	0.8	20	15	H10A15X08N15PI20
96	12	1.0	10	15	0.8	20	30	H10A15X08N30PI20

Table 3.2 Parametric Properties of Numeric Analyses (continued)

Scenario No	Pile Properties		Geometrical Properties			Cohesive Soil Parameters Properties		Notation
	L (m)	D (m)	Slope Height (m)	Slope Angle (Deg)	Distance from Crest (x/L)	PI (%)	SPT N_{60}	
97	12	1.0	10	15	0.95	10	8	H10A15X095N08PI10
98	12	1.0	10	15	0.95	10	15	H10A15X095N15PI10
99	12	1.0	10	15	0.95	10	30	H10A15X095N30PI10
100	12	1.0	10	15	0.95	20	8	H10A15X095N08PI20
101	12	1.0	10	15	0.95	20	15	H10A15X095N15PI20
102	12	1.0	10	15	0.95	20	30	H10A15X095N30PI20
103	18	1.0	15	15	0.8	10	8	H15A15X08N08PI10
104	18	1.0	15	15	0.8	10	15	H15A15X08N15PI10

Table 3.2 Parametric Properties of Numeric Analyses (continued)

Scenario No	Pile Properties		Geometrical Properties			Cohesive Soil Parameters Properties		Notation
	L (m)	D (m)	Slope Height (m)	Slope Angle (Deg)	Distance from Crest (x/L)	PI (%)	SPT N_{60}	
105	18	1.0	15	15	0.8	10	30	H15A15X08N30PI10
106	18	1.0	15	15	0.8	20	8	H15A15X08N08PI20
107	18	1.0	15	15	0.8	20	15	H15A15X08N15PI20
108	18	1.0	15	15	0.8	20	30	H15A15X08N30PI20
109	18	1.0	15	15	0.95	10	8	H15A15X095N08PI10
110	18	1.0	15	15	0.95	10	15	H15A15X095N15PI10
111	18	1.0	15	15	0.95	10	30	H15A15X095N30PI10
112	18	1.0	15	15	0.95	20	8	H15A15X095N08PI20

Table 3.2 Parametric Properties of Numeric Analyses (continued)

Scenario No	Pile Properties		Geometrical Properties			Cohesive Soil Parameters Properties		Notation
	L (m)	D (m)	Slope Height (m)	Slope Angle (Deg)	Distance from Crest (x/L)	PI (%)	SPT N_{60}	
113	18	1.0	15	15	0.95	20	15	H15A15X095N15PI20
114	18	1.0	15	15	0.95	20	30	H15A15X095N30PI20

3.2.3 Notation Explanation

In this study, HxAxXxNxPIx notation was used to indicate parametric variables in each graph (the last column in Table 3.2). The variables in the notation are explained as follows:

- Hx: Slope Height
- Ax: Slope Angle
- Xx: Pile's distance to the crest ratio, as explained in detail in previous sections.
- Nx: SPT-N_{60} Value of the Soil
- PIx: The Soil's Plasticity Index Value

For example, the notation H15A15X09N15PI10 indicates that the p-y curve graph at a depth of 3 meters is given for a model with a slope height of 15 meters, a slope angle of 15 degrees, a pile-to-peak distance ratio of 0.9, a soil SPT-N_{60} value of 15 and a plasticity index of 10.

3.3 Determination of Deformation and Strength Parameters

As mentioned earlier, in this study soils having two variable parameters plasticity index (PI) and SPT-N_{60} values are investigated. In the study, two different plasticity index values which were 10% and 20%, and three different SPT-N_{60} values which were 8, 15, and 30, are chosen. Under this condition, 6 different soil combinations are obtained regarding strength and deformation parameters. For each combination, the corresponding strength parameters (effective cohesion, effective friction angle, undrained shear strength) and deformation parameters as drained deformation modulus-were calculated as described below.

3.3.1 Effective Internal Friction Angle (ϕ')

To determine the effective angle of internal friction (ϕ') for cohesive soils, the relationship proposed by Terzaghi, Peck and Mesri (1996), shown in Figure 3.7, was used.

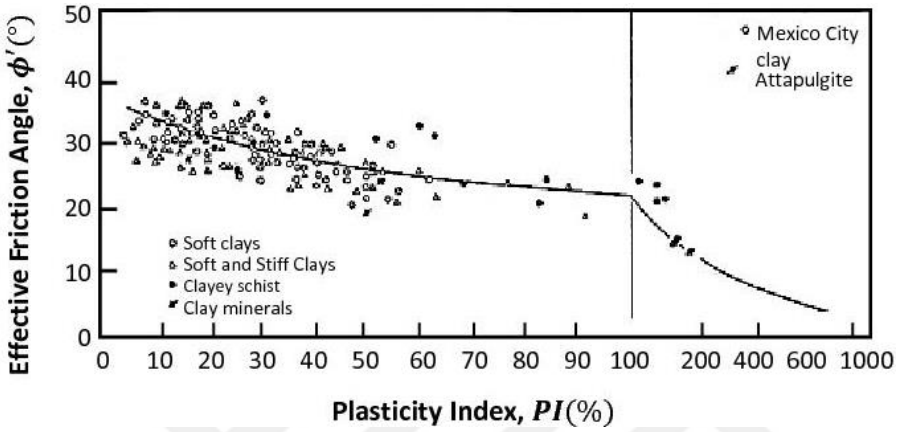

Figure 3.7 Effective Friction Angle and Plasticity Index Relationship (Terzaghi, Peck & Mesri, 1996)

3.3.2 Effective Cohesion (c')

Effective cohesion value of the cohesive soils was selected by using the relationship proposed by Lunne et al. (1997) as follows,

$$c' = \alpha^* \ tan\,\phi' \tag{3.1}$$

Here, ϕ' represents the effective angle of internal friction, and α^* values can be referenced from Table 3.3.

Table 3.3 Value Ranges of α^* Coefficient for Different Types of Soils (Lunne et al., 1997)

Soil Type	α^*	$tan\,\phi'$
Soft Clays	5 – 10	0.35 – 0.45
Medium clays	10 – 20	0.40 – 0.55
Hard clays	20 – 50	0.50 – 0.60
Soft silts	0 – 5	0.50 – 0.60
Medium silts	5 – 15	0.55 – 0.65
Hard silts	15 – 30	– 0.70

3.3.3 Undrained Shear Strength (c_u)

Additionally, undrained shear strength values were calculated for each soil type to facilitate the application of p-y curves from the literature for cohesive soils and to determine the E's value for each soil type.

Undrained shear strength (c_u) of cohesive units was determined from empirical relationships suggested by Stroud (1974) using SPT N_{60} values is used follows,

$$c_u = f_1 \, N_{60} \tag{3.2}$$

Here, N_{60} represents the SPT-N_{60} value, f_1 is a factor that changes with the plasticity index (PI) as shown in Figure 3.8

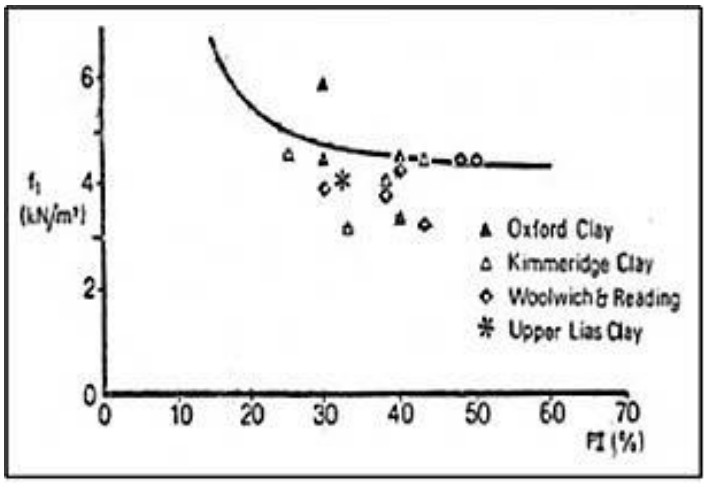

Figure 3.8 Coefficient f_1 Variation Using the Plasticity Index (PI) (Stroud, 1974)

3.3.4 Drained Deformation Modulus (E'$_s$)

Short-term/undrained deformation modulus (E_u) values were determined from empirical relationships suggested by Bowles (1996) using undrained shear strength (c_u) values as follows:

$$E_u = (100 - 500)\, c_u \tag{3.3}$$

The relationship between the long-term/drained deformation modulus, E'$_s$, and the short-term/undrained deformation modulus, E_u in cohesive soils from empirical relationships suggested by Poulos and Small (2000) is as follows:

$$E'_s = \beta' E_u \tag{3.4}$$

Where β' is a factor that varies with the soil type as given in Table 3.4.

Table 3.4 Recommended β' factors for different soil types (Poulos and Small, 2000)

Soil Type	$\beta' Factor$
Gravel	0.9
Sand	0.8
Silt, Silty Clay	0.7
Hard Clay	0.6
Soft Clay	0.4

3.3.5 Soil Types Used in the Analyses

After having information about how to find the parameters required in the analysis for cohesive soils in drained condition, as an example, strength and deformation parameters of the soil type having 20% PI and 30 SPT-N_{60} values were obtained as follows.

Effective Internal Friction Angle (ϕ')

PI= 20% → ϕ'=30˚ (Terzaghi, Peck & Mesri, 1996)

Effective Cohesion (c')

Given ϕ' = 30˚, tan 30˚ is calculated as 0.58. For hard clays, this places α^* within the range of 10 to 50, resulting in an expected effective cohesion (c') range of 11 to 28 kPa. Based on this interval, c' is selected as 17 kPa.

Undrained Shear Strength

PI= 20% → f_1 = 5.6 (Stroud, 1974)

$c_u = f_1 N_{60} = 5.6 * 30 \cong 168\ kPa$

Modulus of Deformation

$E_u = 500\, c_u = 500 * 168 \cong 85000\, kPa$ (Bowles, 1996)

As stated before, since soil can be described as hard clay β' value can be taken as $\beta' = 0.6$.

Then $E'_s = \beta' E_u = 0.6 * 85000 = 51000$ kPa (Poulos and Small, 2000)

Likewise, the strength and deformation parameters for the 6 different soil type combinations mentioned earlier were calculated and summarized in the table below.

Table 3.5 The Parameters of Strength and Deformation for the Types of Soil Used in the Study

Soil Number	**PI (%)**	**SPT N_{60}**	**C_u (kPa)**	**E_u (kPa)**	**E'_s (kPa)**	**ϕ'(°)**	**c'(kPa)**
1	10	8	50	25000	10000	33	5
2	10	15	100	50000	25000	33	10
3	10	30	200	100000	60000	33	20
4	20	8	45	22500	9000	30	5
5	20	15	85	42500	21250	30	9
6	20	30	170	85000	51000	30	17

CHAPTER 4

RESULTS AND DISCUSSIONS

As mentioned earlier, the generation of the p-y curve was carried out with the finite element program considering various combinations of five key variables, namely three of geometry and two of soil properties.

In this section, it will be discussed how the p-y curve properties such as ultimate horizontal soil pressure (P_u) and initial slope (K_i) change under different soil and geometric conditions.

In the graphs presented in this section, the p-y data found from the finite element program are shown as scatter plots, and the high order polynomials that fit these data are shown as solid lines.

4.1 Changes in p-y Curve Properties Depending on Plasticity Index (PI)

In the study, PI = 10% and PI = 20% values were used as mentioned before. Figure 4.1 shows comparison of p-y curves for a case where all parameters are the same except the PI values.

When all analyses are examined, it is seen that general behavior with PI variation is similar.

It is thus observed that an increase in the value of PI results in a decrease in the value of ultimate horizontal soil pressure (P_u), but the value of initial slope (K_i) nearly remains constant.

In other words, while the value of PI increases internally, the internal friction angle, ϕ' and effective cohesion, c' decrease. Thus, it is expected that P_u (the ultimate lateral

earth pressure) of the p-y curve-will be reduced to provide a reduction in the horizontal load-carrying capacity of the pile.

In other words, strength parameters, such as the internal friction angle and effective cohesion, tend to decrease with increasing plasticity index (PI). Thus, reduction in the ultimate lateral earth pressure, Pu , of the p-y curve will be expected along with a decrease in the horizontal load-carrying capacity of the pile.

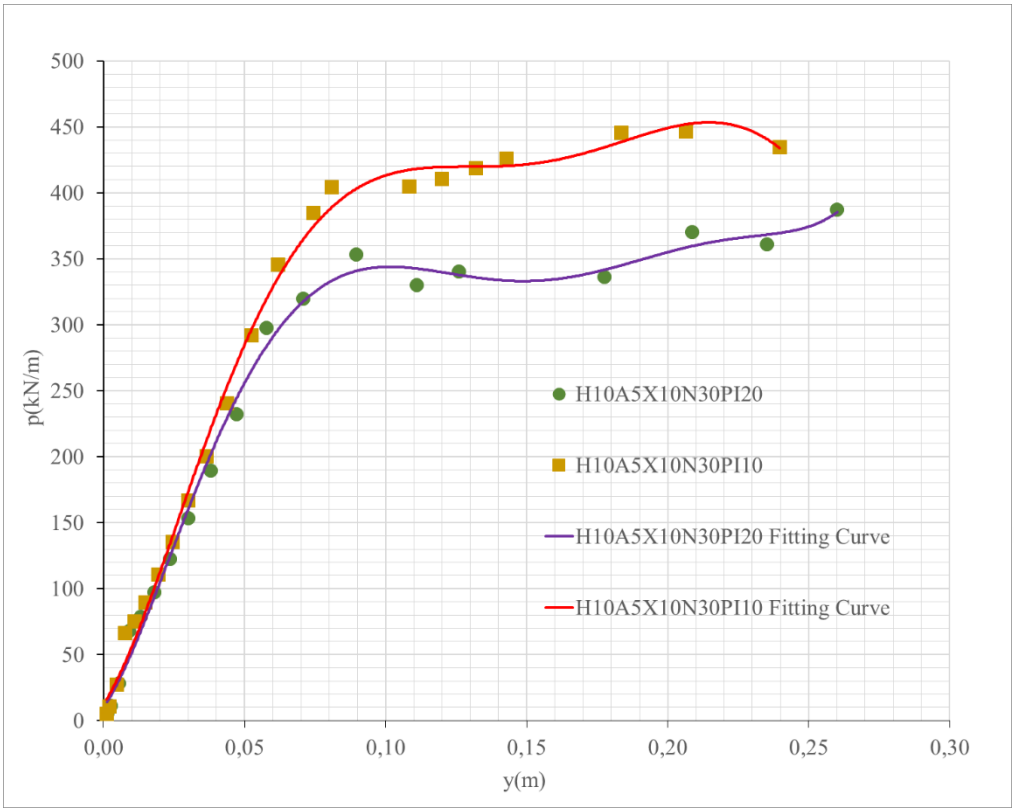

Figure 4.1 Comparison of p-y Curves with Changing PI Values

4.2 Changes in p-y Curve Properties Depending on SPT-N_{60} Values

In the study, 8, 15 and 30 values were used as SPT-N_{60} values, as previously mentioned. Figure 4.2 shows the p-y curve comparison for one case where all parameters are the same except the SPT-N_{60} values. In this figure, the smoothed p-y curves are also displayed by dashed lines.

When all analyses are examined, it is seen that the general behavior that develops with the change of SPT-N_{60} is the same.

Consequently, it was observed that the P_u and K_i values increase as the SPT-N_{60} value increases.

The effective cohesion and effective internal friction angle, which are among the strength parameters, decrease with increasing SPT-N_{60} value. Therefore, it is expected that the ultimate horizontal soil pressure value of the p-y curve and the horizontal carrying capacity of the pile increase with increasing SPT-N_{60} values.

In addition, the value of the drained deformation modulus (E'$_s$), one of the deformation parameters, also increases when the SPT-N_{60} value increases. This results in an increase in value of K_i and hence an increase in the horizontal stiffness of the pile.

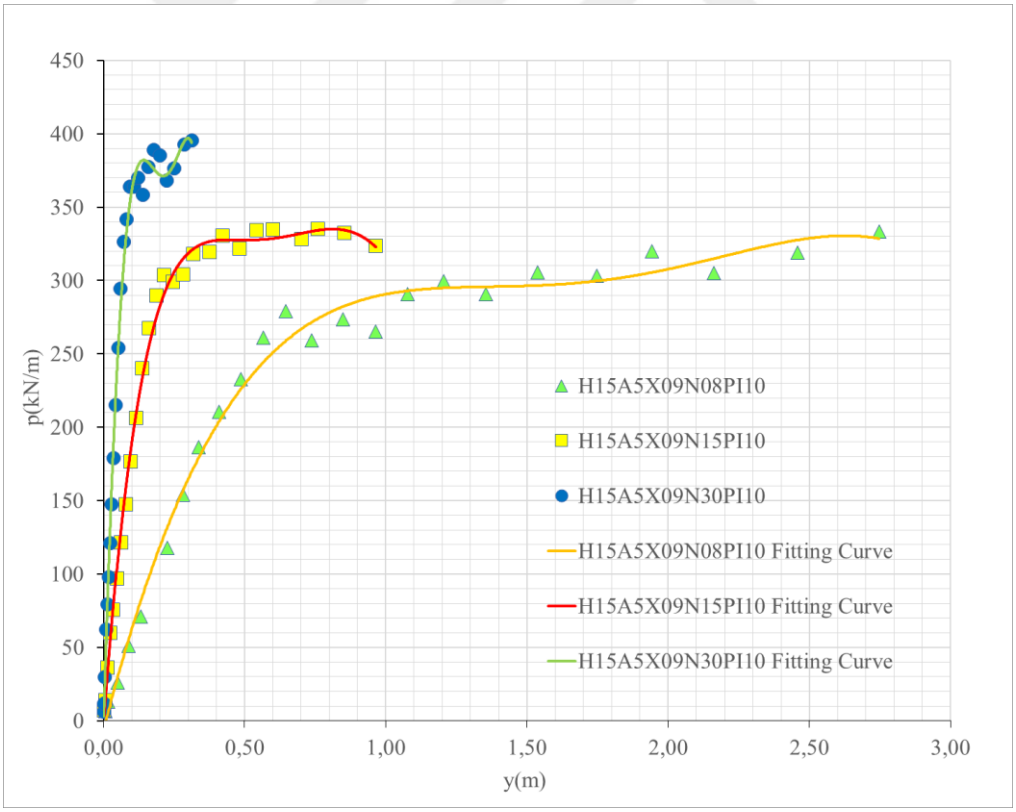

Figure 4.2 Comparison of p-y Curves with Changing SPT-N_{60} Values

4.3 Changes in p-y Curve Properties Depending on Slope Angle

From the analyses performed, it can be seen that piles at the toe of the slope and the crest behave quite differently. The piles which fall between these two positions exhibit a behavior somewhat similar to the piles at the crest or the toe of the slope. This will be elaborated in the next sections under the heading "Changes in p-y Curve Properties Depending on Distance to Crest".

In this study, the slope angle values of 5° and 15° were used as earlier mentioned. Whereas considering all analyses, the slope angle is observed to not affect the properties of the p-y curve in the piles positioned at the toe as seen in Figure 4.3. It is observed from Figure 4.4 that for the piles located at the crest, the ultimate value of lateral earth pressure decreases with the increase in slope angle and the initial slope remains almost the same.

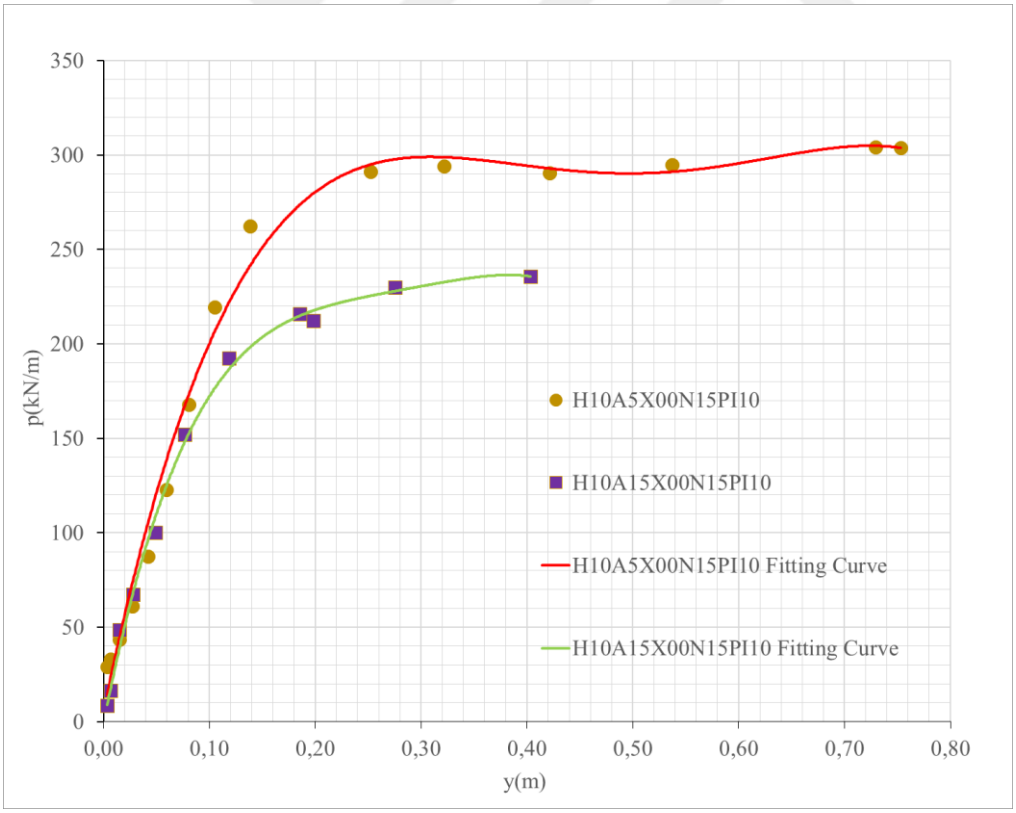

Figure 4.3 Comparison of p-y Curves with Changing Slope Angle for Piles on Crest

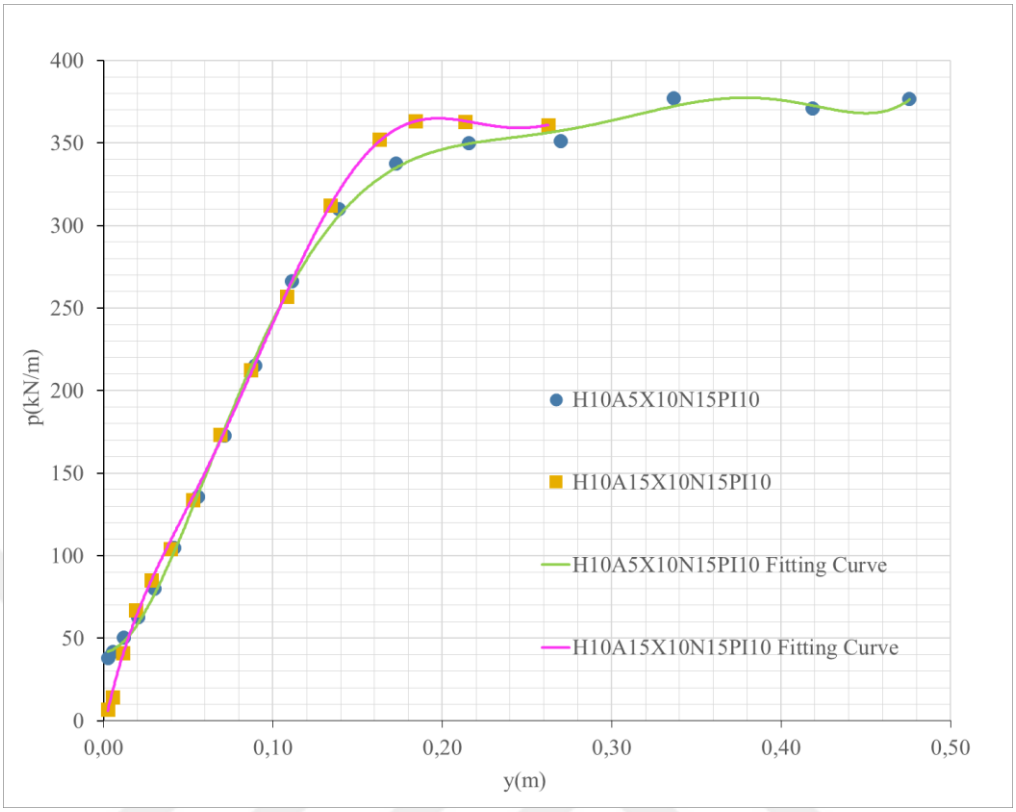

Figure 4.4 Comparison of p-y Curves with Changing Slope Angle for Piles on Toe

4.4 Changes in p-y Curve Properties Depending on Slope Height

In this study, the slope heights used are 10 meters and 15 meters. In analyses with a 10 meter slope height, 12 meter piles were used, while in those with a 15 meter slope height, 18 meter piles were used. During all analyses performed, slope height (H) does not affect the p-y curve properties of piles located at the toe. In the case of piles at the crest, with an increase in slope height, the value of P_u is inversely affected, whereas the initial slope (K_i) remains constant.

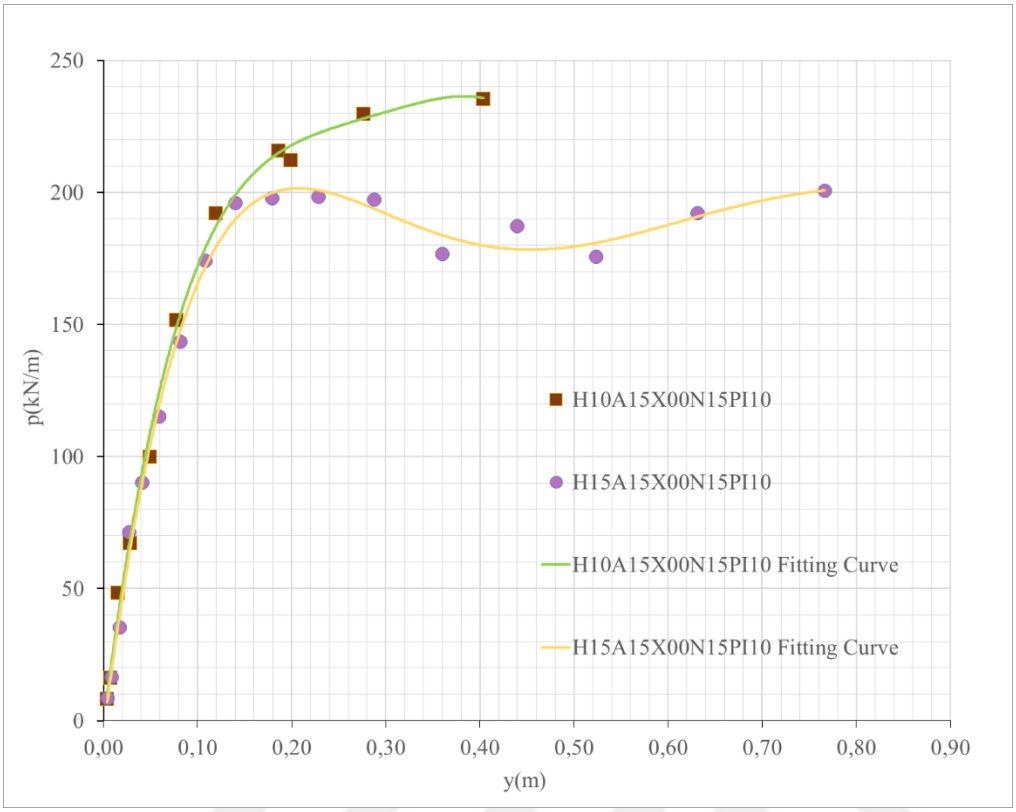

Figure 4.5 Comparison of p-y Curves with Changing Slope Height on the Crest

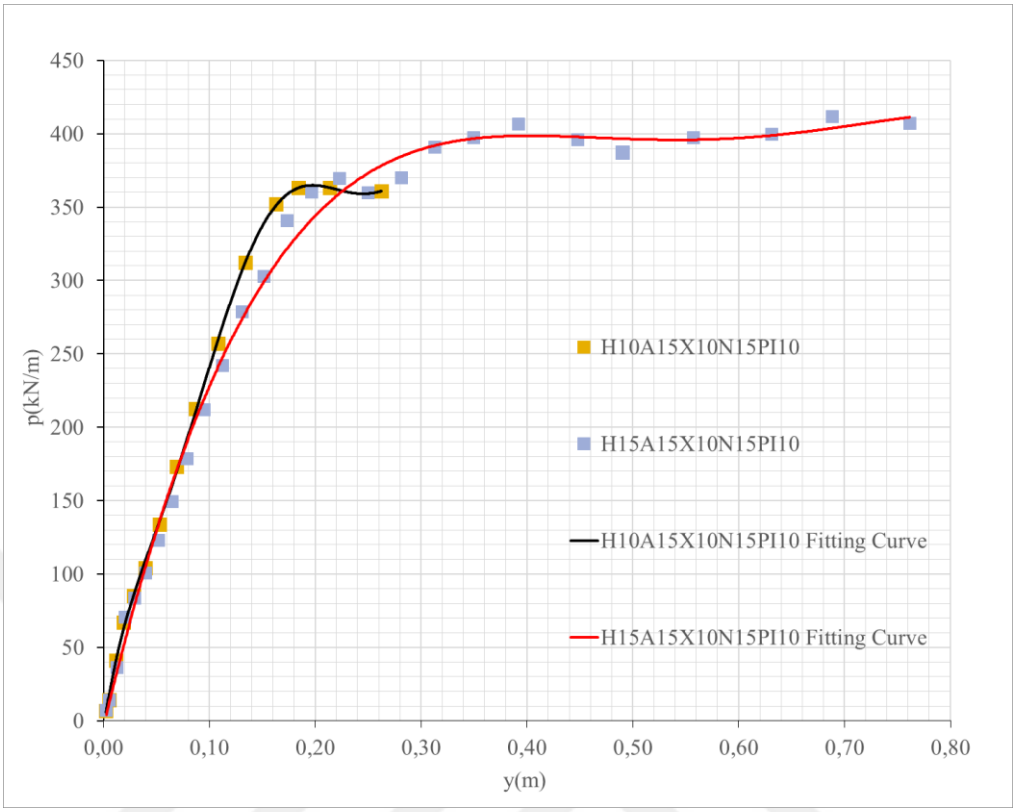

Figure 4.6 Comparison of p-y Curves with Changing Slope Height on the Toe

4.5 Changes in p-y Curve Properties Depending on Distance to Crest

The objective of the present section is to indicate under which conditions the piles on the slope would have behavior close to the piles at the crest of the slope and under which conditions piles of the slope would have similar behavior like that of the piles at the toe of the slope.

In general, it is noticed that the piles on the slope show the same characteristics as those of the pile at the crest in terms of lateral behavior, i.e. p-y curve characteristics, up until the pile to crest distance/ slope length ratio reaches 0.9, i.e. position X09. Whereas the behavior beyond this distance was conducted for a certain number of cases, a deeper study would be needed in order to establish the conditions by which similarity actually develops with the pile at the toe. Sample comparisons of p-y curves for piles at the crest, toe, and position X09 are provided in Figure 4.7.

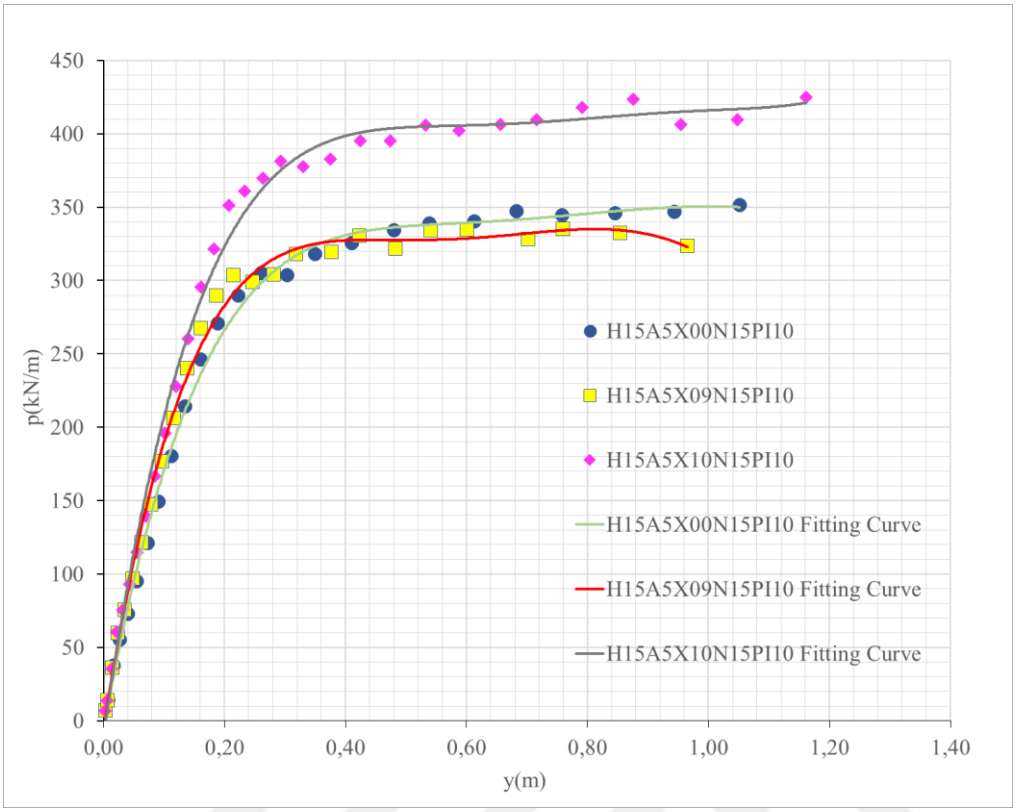

Figure 4.7 General Behavior of p-y Curves with Changing Pile Position

However, there are exceptions to this situation when soil parameters, pile length and slope angle are taken into consideration.

However, this trend was not witnessed in the case of a slope height of 15 meters with a slope angle of 15 degrees. From the comparison of the pile at location X09 with that at the crest, it can be observed that the ultimate lateral earth pressure, P_u was increased at location X09. For this, the piles at places represented by parameters X095 and X08 were also analyzed in order to assess the conditions that allow the pile at the slope to show similar characteristics with that at the crest or at the toe. The general trend that one obtains is that for a slope height of 15 meters and a slope angle of 15 degrees, the pile p-y curve behavior at location X08 is similar to that of a pile at the crest, beyond which the Pu value increases at a certain rate along the distance towards the base whereas the initial slope (K_i) remains constant. This is shown in Figure 4.8.

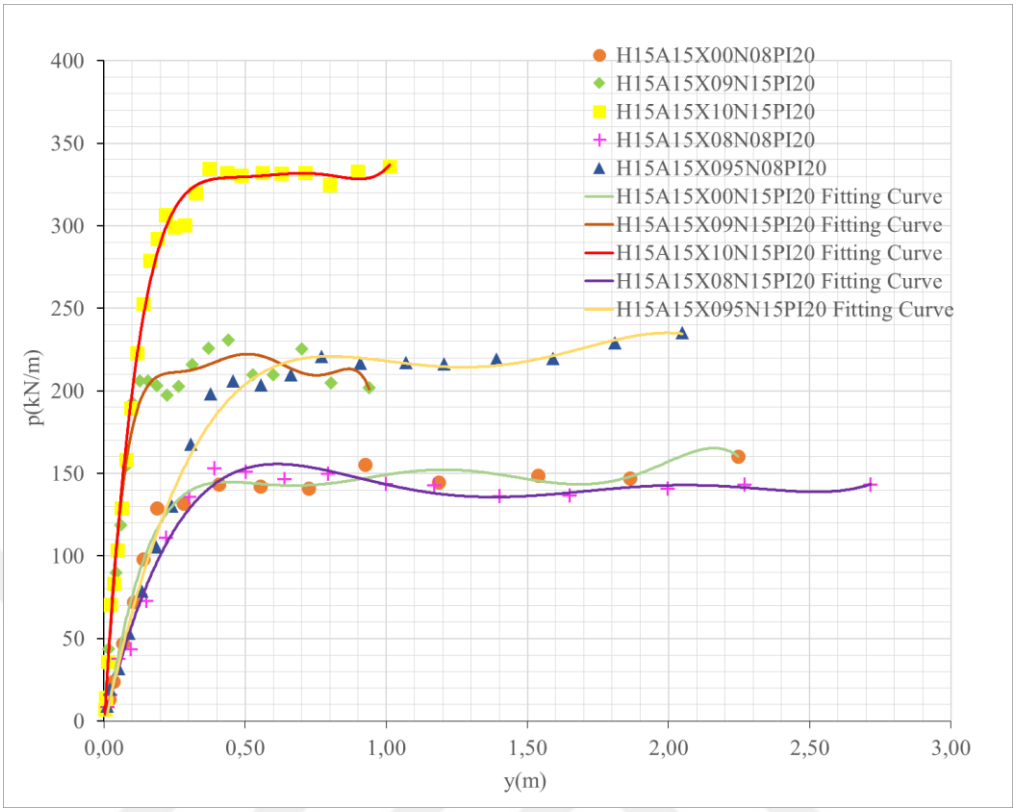

Figure 4.8 Behavior of p-y Curves with Changing Pile Position for the 15 Meters Height Slopes Having Slope Angle of 15 Degrees

In slopes with a slope height of 12 meters, the general behavior is that the ultimate lateral earth pressure (P_u) value increases as the distance from the crest increases. For this purpose, X08 and X095 distances were studied separately. A certain integrity was not achieved in the results and the following situations are summarized:

- In slopes with a slope height of 12 meters and an angle of 5 degrees, in N08PI10, N08PI20 and N15PI20 soil conditions, the p-y curve features up to the X09 position show the same behavior as the crest. The behavior is shown at Figure 4.9.
- In slopes with a slope height of 12 meters and an angle of 5 degrees, in N15PI10, N30PI10, and N30PI20 soil conditions, the ultimate lateral earth pressure (P_u) value increases as the distance from the crest increases. The behavior is shown at Figure 4.10.
- In slopes with a slope height of 12 meters and an angle of 15 degrees, in N08PI10 and N08PI20 and N15PI20 soil conditions, the ultimate lateral earth pressure (P_u) value increases as the distance from the crest increases. The behavior is shown at Figure 4.11.
- In slopes with a slope height of 12 meters and an angle of 15 degrees, under N15PI10, N30PI10, and N30PI20 soil conditions, the p-y curve properties up to the X08 position show the same behavior as the crest, while the piles located at positions from the X095 position to the toe show the same behavior as the toe. For other positions in between, the ultimate lateral earth pressure (P_u) value increases as the distance from the crest increases. The behavior is shown at Figure 4.12.

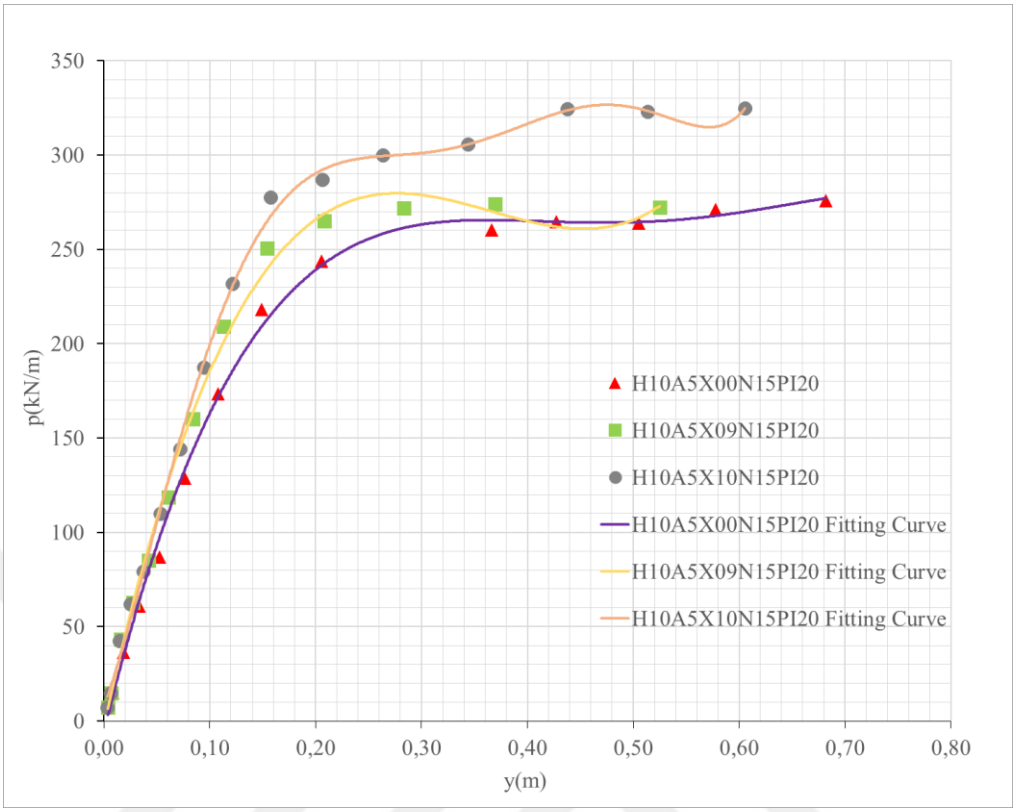

Figure 4.9 Behavior of p-y Curves with Changing Pile Position for the Slopes Having Slope Angle of 5 Degrees, and N08PI10, N08PI20 and N15PI20 Soil Conditions

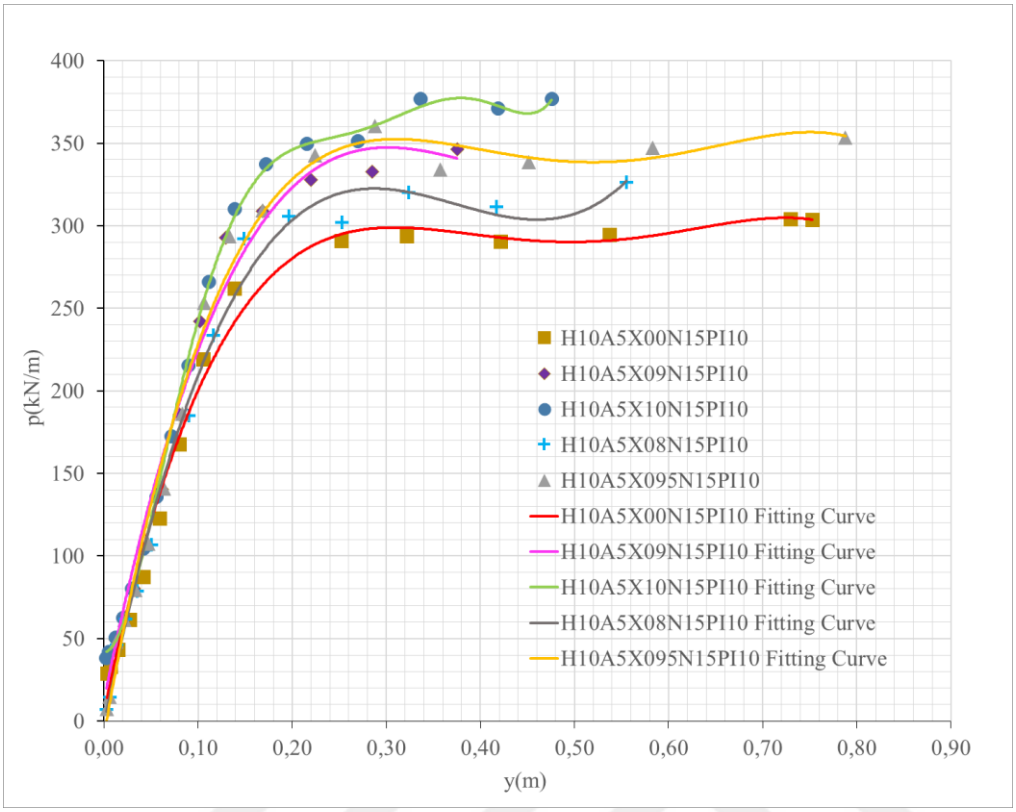

Figure 4.10 Behavior of p-y Curves with Changing Pile Position for the Slopes Having Slope Angle of 5 Degrees, and N15PI10, N30PI10, and N30PI20 Soil Conditions

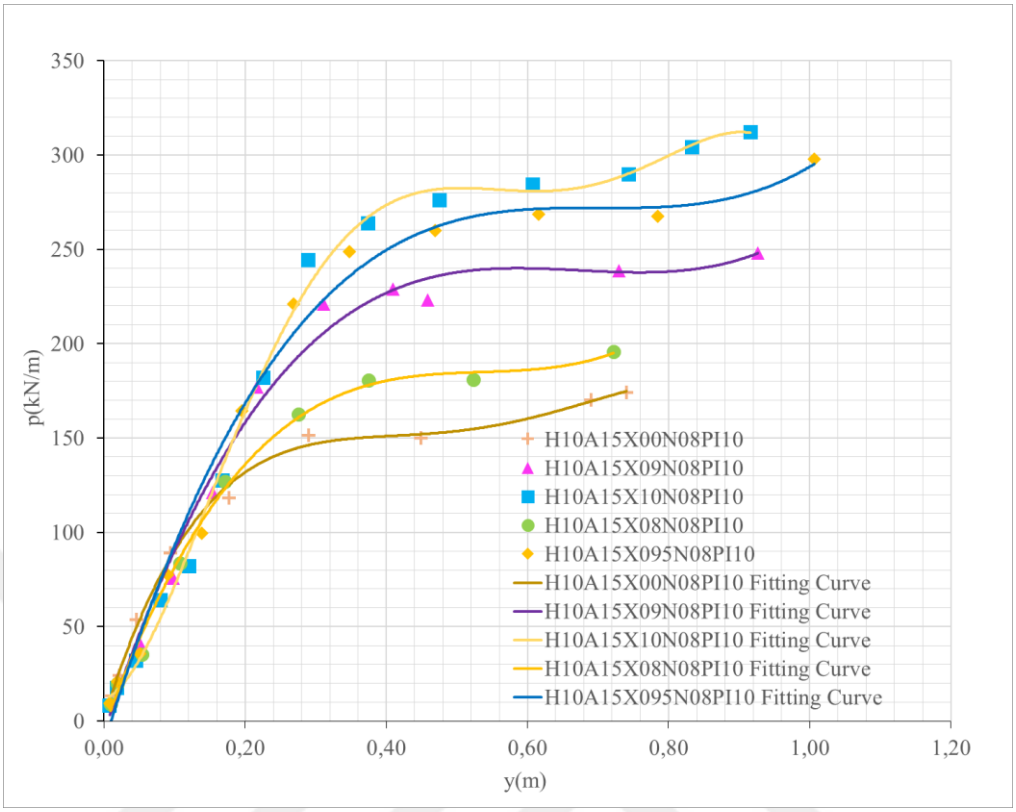

Figure 4.11 Behavior of p-y Curves with Changing Pile Position for The Slopes Having Slope Angle of 15 Degrees, and N08PI10, N08PI20 and N15PI20 Soil Conditions

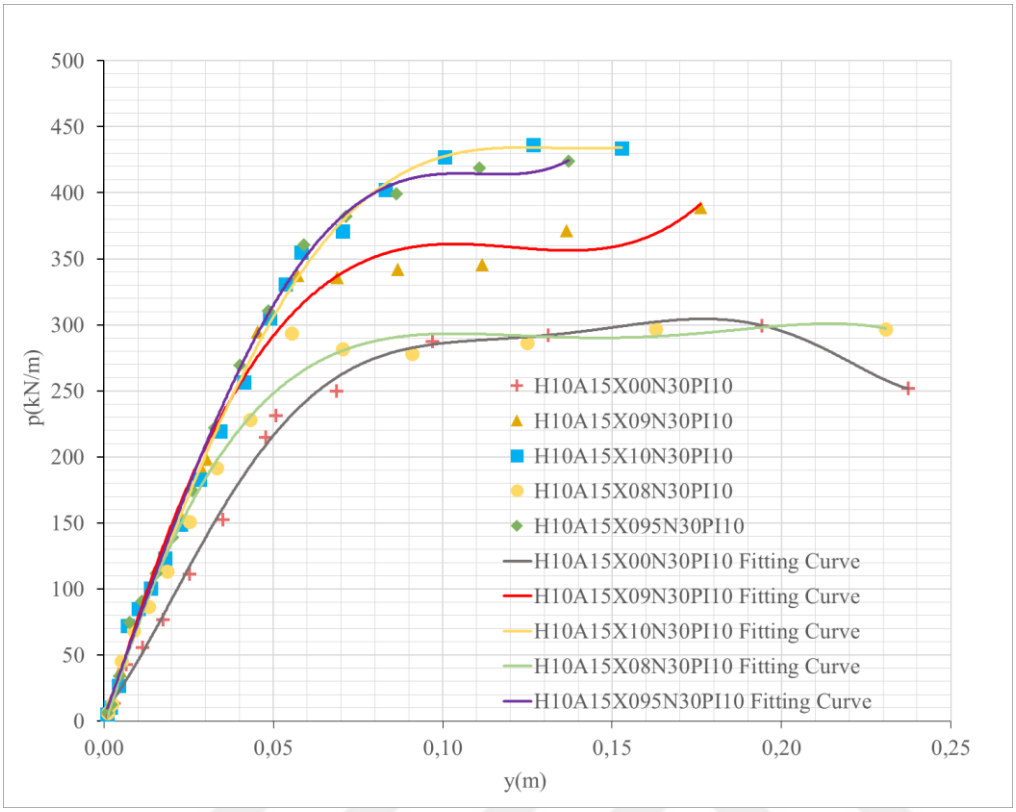

Figure 4.12 Behavior of p-y Curves with Changing Pile Position for the Slopes Having Slope Angle of 15 Degrees, and N15PI10, N30PI10, and N30PI20 Soil Conditions

CHAPTER 5

CONCLUSIONS AND RECOMMENDATIONS

This study presents the results of a parametric study carried out through the finite element analyses in order to investigate the influences of various parameters on the characteristics of p-y curves of piles in cohesive soils under drained conditions. Specifically, the influence of these parameters on the ultimate lateral earth pressure, P_u, and the initial slope, K_i, of the p-y curves is investigated.

These parameters were categorized into two groups: soil conditions and geometric conditions. Soil conditions include strength and deformation parameters of cohesive soil, such as effective cohesion, effective angle of friction, and drained deformation modulus, which are influenced by the plasticity index (PI) and SPT-N_{60} values. Geometric conditions refer to factors such as slope angle and slope height, which affect pile length.

The study examined in detail how the distance of piles on a slope from the crest affects the p-y curve properties, particularly, the ultimate lateral earth pressure (P_u) and the initial slope (K_i) values under various conditions. The focus is on how variations in this distance affect the behavior of p-y curves under different conditions.

FE analyses were utilized to generate p-y curves by subjecting the piles to loading until soil body collapse occurred.

Since the study concentrated on drained conditions, the groundwater table was not taken into account. Also, to maintain consistency, only the p-y values obtained at a depth of 3 meters were analyzed.

5.1 Comparison of p-y Curves from Finite Element Analysis and Literature-Based Models Generated with RSPile Software

The developed p-y curves by the finite element approach have been compared with the curves available in the literature to validate their accuracy. For this purpose, RSPile software was utilized to generate p-y curves for piles resting on flat ground, and the results from the finite element analyses were successfully validated against the RSPile-generated outcomes. This study is carried out especially for piles under level ground conditions and has been performed for the six different soil types described in Section 3.3.

Based on the soil types classified according to SPT-N_{60} and the plasticity index (PI) properties, the undrained shear strengths were considered to select the appropriate p-y curve model from the literature, as summarized in Table 5.1.

Table 5.1 p-y Curve Models Selected for the Six Different Soil Types

Soil Number	PI (%)	SPT N_{60}	C_u (kPa)	Selected p-y curve Model
1	10	8	50	Soft Clay- Soil Matlock (1970)
2	10	15	100	Dry Stiff Clay- Welch and Reese (1972)
3	10	30	200	Dry Stiff Clay- Welch and Reese (1972)
4	20	8	45	Soft Clay- Soil Matlock (1970)
5	20	15	85	Soft Clay- Soil Matlock (1970)
6	20	30	170	Dry Stiff Clay- Welch and Reese (1972)

The example model of the pile in RSPile software is given at Figure 5.1.

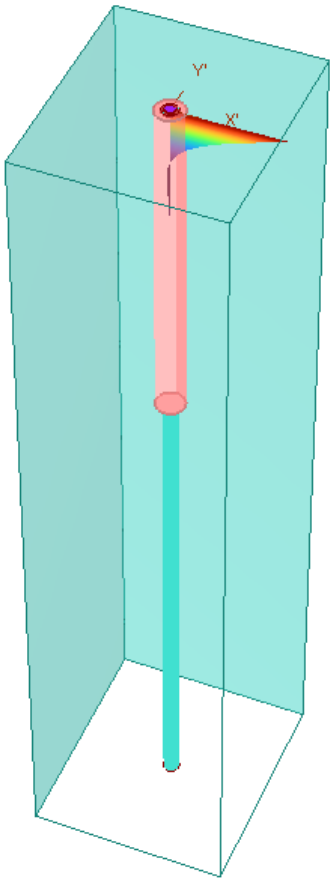

Figure 5.1 Conducted RSPile Model

The input parameters for the relevant p-y curve models include the undrained shear strength values and the strain factor (ε_{50}) of the soils as shown in Figure 5.2. Undrained shear strength values of the soils are given in Table 5.1. Strain factor (ε_{50}) values are selected by using the table recommended from Peck et al. (1974). The recommended values are given in Table 5.2.

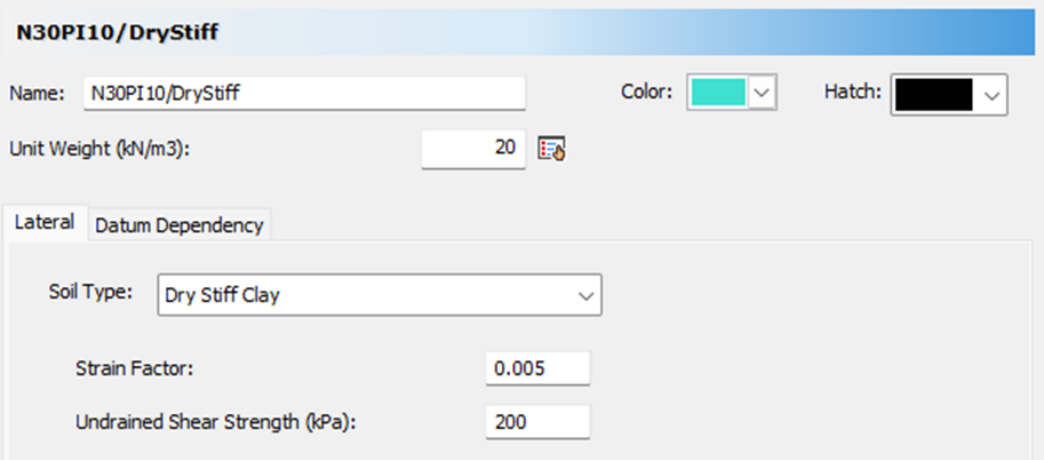

Figure 5.2 RSPile Soil Input Parameters

Table 5.2 Typical ε_{50} Values for Normally Consolidated Clays Peck Et Al. (1974)

Consistency of Clay	Average undrained shear strength (kPa)	ε_{50}
Soft	<48	0.020
Medium	48-96	0.010
Stiff	96-192	0.005

After the RSPile model was established on the level ground for each soil type, the p-y curve models available in the literature for each soil type were obtained using RSPile software and compared with the p-y curves obtained with Plaxis 2D finite element program.

Relevant comparisons are shown in figures from Figure 5.3 to Figure 5.8.

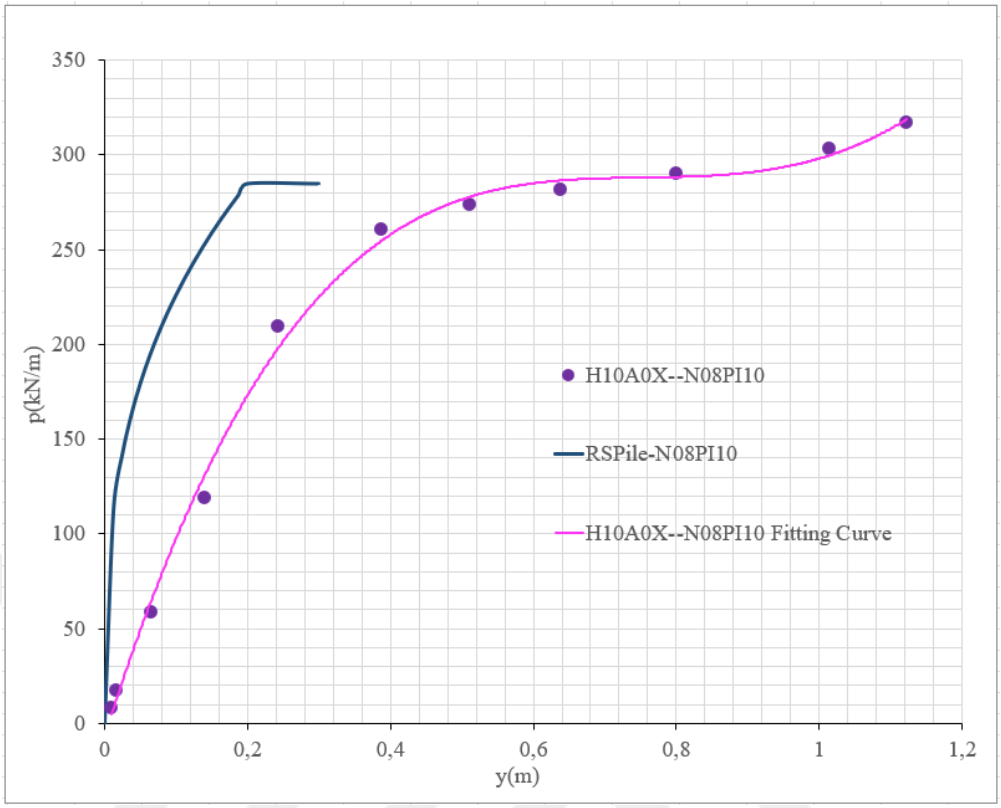

Figure 5.3 Comparison of p-y Curves from FE Analysis and Literature-Based Models Generated with RSPile Software - N08PI10

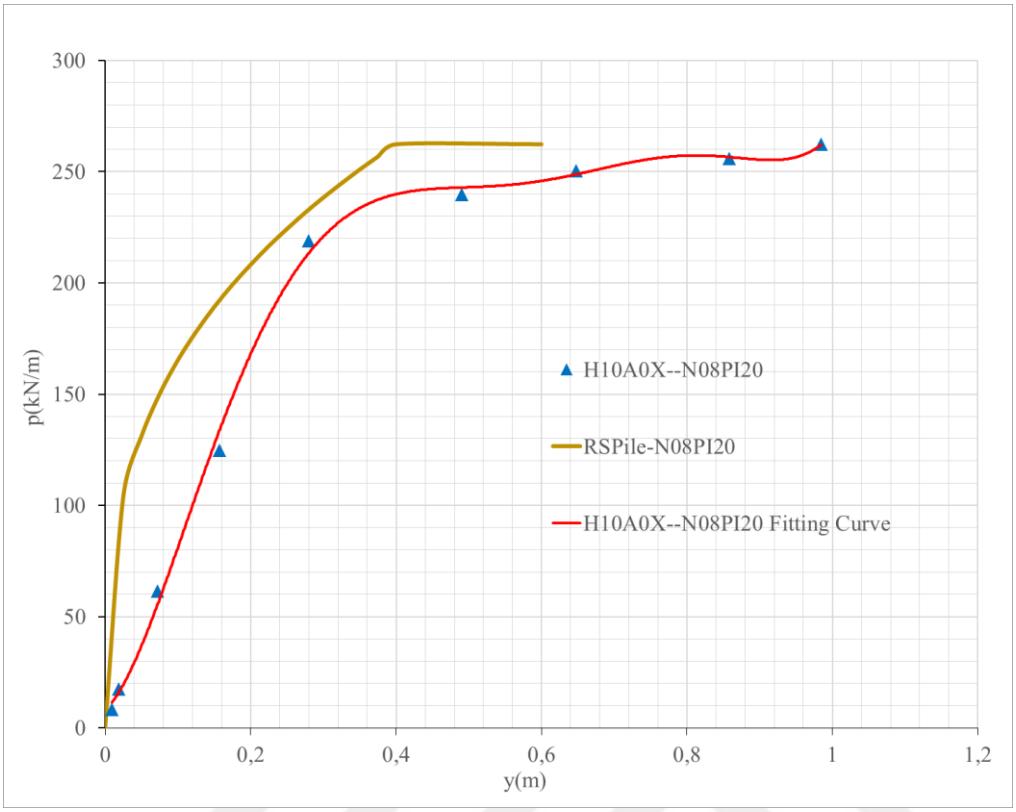

Figure 5.4 Comparison of p-y Curves from FE Analysis and Literature-Based Models Generated with RSPile Software - N08PI20

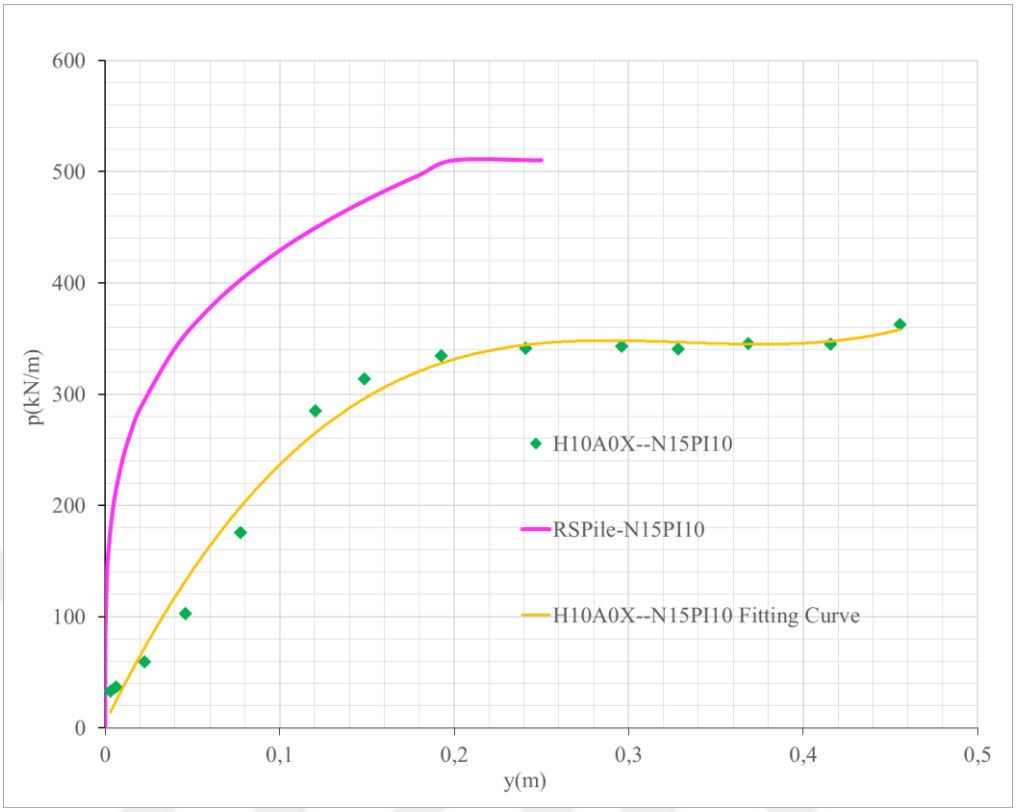

Figure 5.5 Comparison of p-y Curves from FE Analysis and Literature-Based Models Generated with RSPile Software - N15PI10

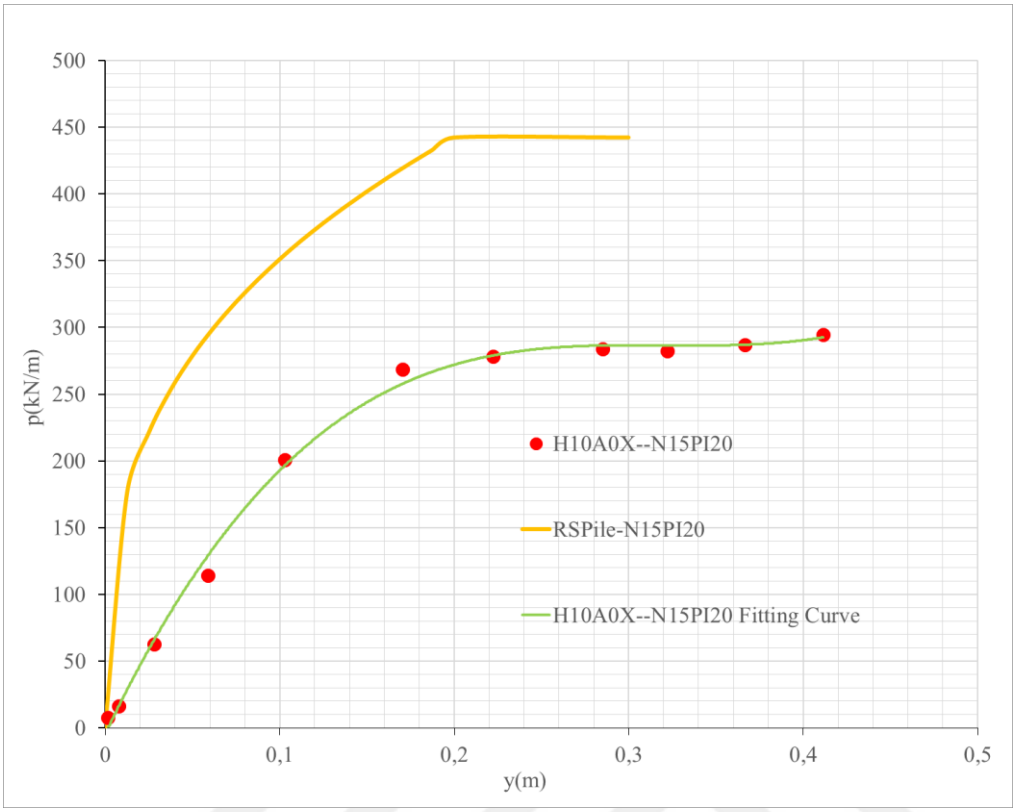

Figure 5.6 Comparison of p-y Curves from FE Analysis and Literature-Based Models Generated with RSPile Software - N15PI20

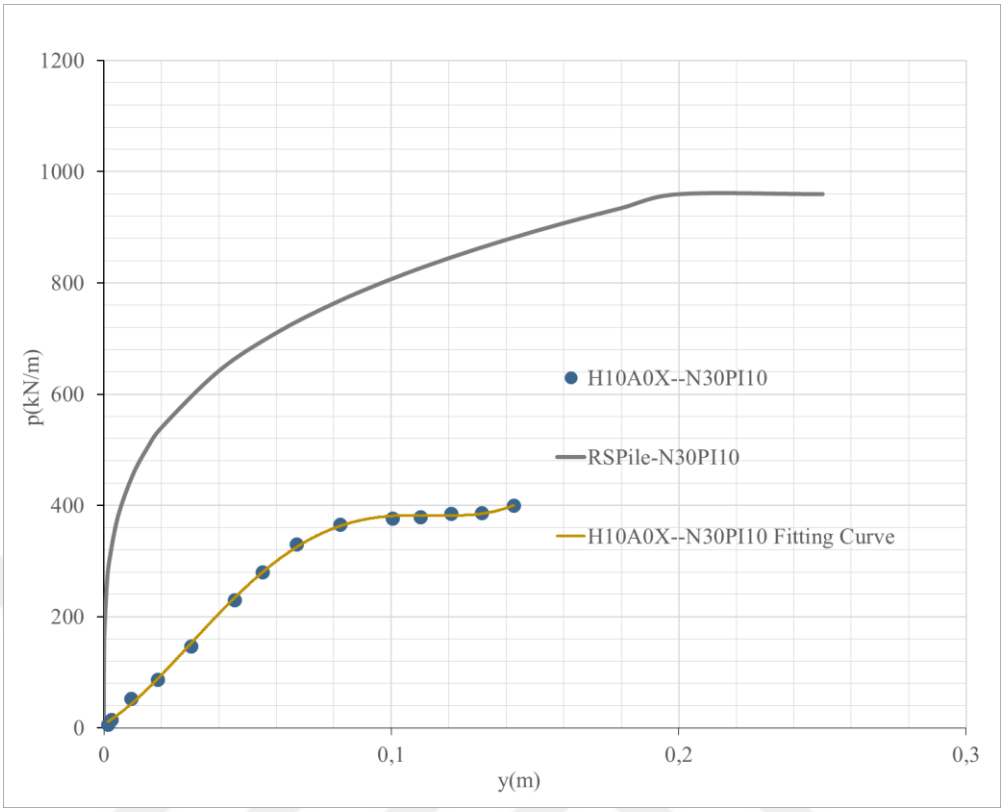

Figure 5.7 Comparison of p-y Curves from FE Analysis and Literature-Based Models Generated with RSPile Software - N30PI10

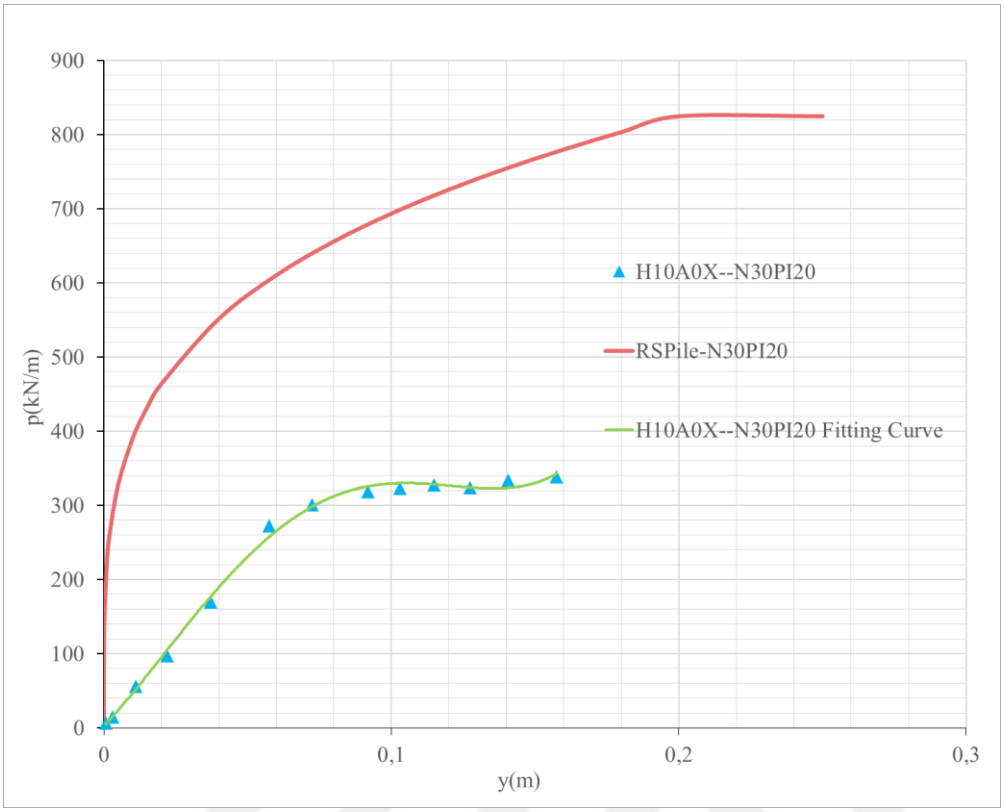

Figure 5.8 Comparison of p-y Curves from FE Analysis and Literature-Based Models Generated with RSPile Software - N30PI20

In all comparisons, the initial stiffness of the RSPile-generated p-y curves that are based on literature models is higher than those derived from finite element analyses for all soil types. This is, in fact, expected; since most p-y curve models, such as those from Matlock 1970 and Welch and Reese 1972, assume an infinite initial slope of the curve, minimum lateral displacements will be developed for low levels of load, according to Georgiadis & Georgiadis 2010.

Comparing the results of ultimate lateral earth pressure values (P_u) it is seen that the results are very close to each other for soils having SPT-N_{60} value of 8. Beyond this, with an increase in the SPT-N_{60} value, the P_u values obtained by RSPile software are higher than those obtained by finite element analysis. This difference can be explained by the different modeling approaches: in the finite element analysis, the clay is modeled with parameters defined for drained conditions, whereas the model obtained from the literature using RSPile uses undrained shear strength as a

parameter. The fact that these values were obtained with different correlations may have led to this observed difference.

For instance, for the same soil type with PI = 10%, increasing the SPT-N_{60} value from 8 to 15 and using the corresponding correlations given in Section 3.3 results in an increase in the effective cohesion from 5 kPa to 10 kPa and no change in the effective internal friction angle, as indicated in Table 3.5. In contrast, if the SPT-N_{60} value increases from 8 to 15 and the correlation given in Section 3.3.3 is adopted, then the undrained shear strength increases from 50 kPa to 100 kPa under undrained conditions.

Another reason for the difference is that, in the finite element analysis, each soil condition is specifically modeled according to the characteristics of the soil class being analyzed, resulting in a more tailored analysis. In contrast, the p-y curves obtained using RSPile rely on general formulations from the literature, which may not account for the unique properties of each soil type as accurately.

5.2 Comparison of p-y Curve Properties on Flat and Sloped Terrains

In this study, the development of p-y curves through finite element analysis was carried out for piles situated both on slopes and on flat terrain. Section 4.3 presented the effect of slope angle on the p-y curve characteristics for piles on slopes, while Section 4.4 focused on the effect of slope height on the p-y curve characteristics for piles on slopes. In this section, the variations in slope angle and slope height for piles on slopes will be compared with the p-y curve results obtained for piles on flat ground.

When the relevant comparisons were conducted for each ground condition, a consistent observation emerged across all cases: the p-y curve properties obtained on flat terrain were very similar to those of the piles located at the toe of the slope. In other words, almost no slope effect was observed on the piles positioned at the toe. Therefore, if the p-y curve properties on flat terrain are to be examined, the p-y

curve properties of the piles at the toe of the slope, as discussed in Section 4, can be referenced.

For example, Figure 5.9 presents the p-y curve properties developed at flat ground and those generated for piles at the toe and crest of the slope for different slope angles.

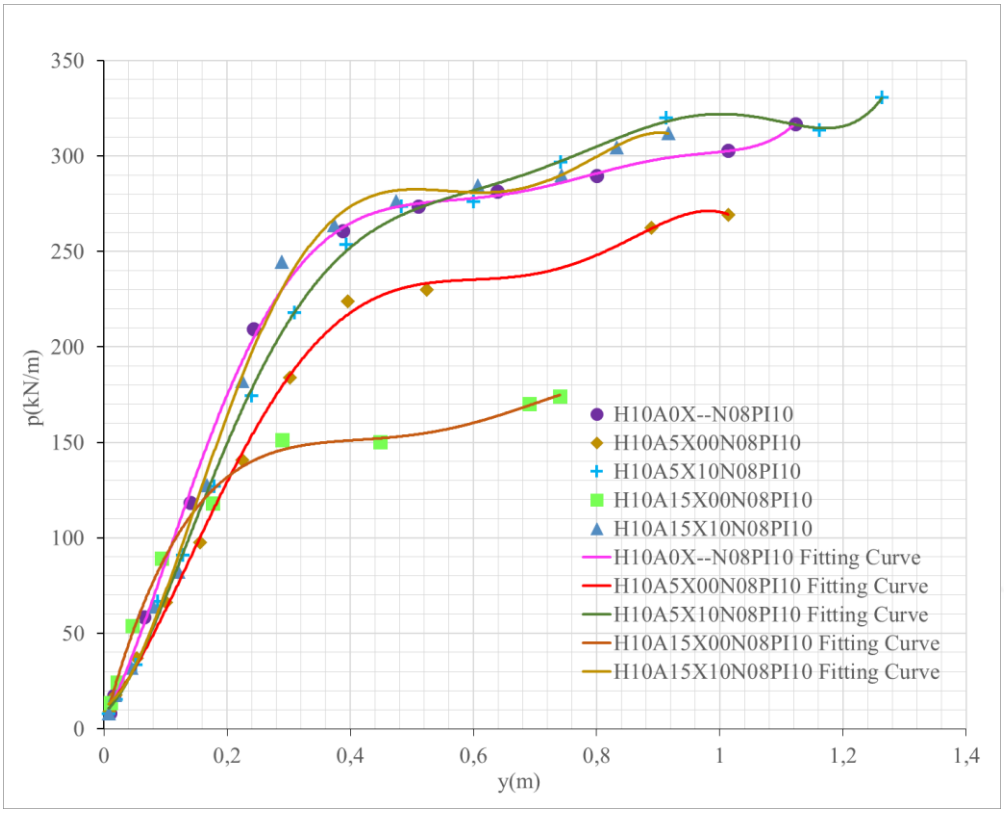

Figure 5.9 Comparison of p-y Curve Properties on Flat and Sloped Terrains Having N08PI10 Soil Conditions

5.3 Conclusions

There is limited literature on comprehensive investigations, taking into account all the soil and geometrical parameters under drained conditions for cohesive soils, in studies in which p-y curves are generated by means of finite element analysis. More importantly, most studies investigating the impact of slopes on p-y curves are focused on piles located at the top of the slope, and there is a lack of research directly

addressing the behavior of piles located on the slope. This lack of literature was an important motivation for the present study.

The main objective of the present study is to discuss how different parameters may affect properties of p-y curves for cohesive soils under drained conditions. One of the parameters, an important geometric aspect is the distance between pile located on the slope and the crest, which has been analyzed in a detailed way in order to understand its relationship with the characteristic of p-y curve. This focus is important because existing research has either been limited to piles placed directly at the crest or has analyzed the effect of distance from the crest only for piles installed on level ground. This study aims to fill that gap by specifically exploring the behavior of piles situated on slopes.

The following are the major conclusions of the parametric study for the clays in drained condition:

- Increase in the PI value led to a decrease in the ultimate lateral earth pressure (P_u), while the initial slope (K_i) remained relatively unchanged. Although the behavior varies with different soil and geometric conditions, the general trend observed is a 15% decrease in the ultimate lateral earth pressure (P_u) when the PI value increases from 10% to 20%.
- Results indicated that P_u (ultimate horizontal soil pressure) and K_i (initial slope) increased with increasing SPT-N_{60} value. Although there is some scatter because of the variety of soils and different geometrical conditions, it has been possible to identify a general trend: P_u increases of around 35% when the SPT-N_{60} varies from 8 to 15 and of around 25% when it increases from 15 to 30. Similarly, in cases where SPT-N_{60} increased from 8 to 15, the K_i values increased with an average of 3.2 times and from 15 to 30, the increase was about 2.5 times.
- When analyzing the impact of geometric parameters on p-y curves, it was observed that the behavior of piles at the slope crest differs significantly from those at the toe. It was found that the geometric characteristics of the slope

influence the p-y curve properties of piles located at the crest, while having little to no effect on those positioned at the toe. For piles located between the crest and toe, the effect of geometric parameters on the p-y curve depends on whether the behavior more closely resembles that of piles at the crest or those at the toe. This relationship is strongly tied to the distance of the piles from the crest, which will be further explained as relevant throughout the study.

- Across all analyses with varying parameters, it was found that increasing the slope angle from 5 degrees to 15 degrees resulted in an average reduction of 35% in the ultimate lateral earth pressure (P_u) for piles situated at the crest, although this effect varied depending on specific conditions. In contrast, the slope angle had minimal influence on the initial slope (K_i) of the p-y curve in these scenarios.
- In the study conducted by Muthukkumaran et al. (2008), the reduction factor formulation for ultimate lateral earth pressure in sandy soils, considering slope angles, is given in Formula 2.12. For 5 and 15 degrees of slope angle, respectively, the calculation of reduction factors for ultimate lateral earth pressure was done for a depth of soil 3 meters and a diameter of pile 1 meter as follows:

  For 5 degrees of slope angle:

$$R = 0.74 + 0.0378\left(\frac{3}{1}\right) - 0.6315 * 0.0873 = 0.7983$$

  For 15 degrees of slope angle:

$$R = 0.74 + 0.0378\left(\frac{3}{1}\right) - 0.6315 * 0.2618 = 0.6881$$

  Results have shown that, in the case of an increase in the slope angle from 5 degrees to 15 degrees, the value of ultimate lateral earth pressure, as obtained by Muthukkumaran et al. (2008), decreases about 11% under given conditions.

  Similarly, in the study conducted by Reese et al. (2006), the p-multiplier formulation for ultimate soil resistance in saturated clay as a function of slope angle is given in Formula 2.13. For 5 and 15 degrees of slope angle,

respectively, the calculation of reduction factors for ultimate lateral earth pressure was done as follows:

For 5 degrees of slope angle:

$$p - multiplier = \frac{1}{1 + \tan(5)} = 0.9196$$

For 15 degrees of slope angle:

$$p - multiplier = \frac{1}{1 + \tan(15)} = 0.7887$$

Results have shown that, in the case of an increase in the slope angle from 5 degrees to 15 degrees, the value of ultimate lateral earth pressure, as obtained by Reese et al. (2006), decreases about 13% under given conditions.

As obtained from the previous discussion, an average reduction of about 35% in ultimate lateral earth pressure for an increase in slope angle from 5 to 15 degrees was recorded for clayey soils under drained conditions in this study using a finite element program. In contrast, Muthukkumaran et al. (2008) showed an 11% reduction for sandy soils, while Reese et al. (2006) presented a 13% reduction for saturated clays. These findings indicate that the slope effect on the p-y curve is more pronounced in drained clayey soils compared to both sandy soils and saturated clays. While conducting this comparison, it is crucial to acknowledge the potential influence of varying p-y curve estimation methods and inherent differences in soil properties. These factors could introduce variability into the results and should be considered when interpreting the findings.

- The influence of the slope height on the p-y curve was varied throughout the analyses, with changing geometric and soil parameters, but in general, for an increase of the height from 10 to 15 meters, alongside an increase in pile length from 12 meters to 18 meters, the ultimate lateral earth pressure (P_u) remained the same or showed an average decrease of 14%. This variation in slope height did not have any significant effect on the initial slope of the p-y curve.

- According to the analysis in Section 4.5 about the distance to the crest parameter, the p-y curve characteristics for piles on the slope in different conditions showed different features. However, a generalized trend has been developed in which, when the ratio of the pile's distance to the crest over the slope length is up to 0.9, the p-y curve characteristics of the pile would likely follow the pattern of that of a pile positioned directly at the crest. Beyond this distance, though a few studies have been done, consensus has not been reached on the exact point beyond which the characteristics of the p-y curve of a pile on the slope would match those at the toe. Hence, this aspect needs further clarity from research.

5.4 Recommendations

In this study, the effect of the piles' distance from the crest on the p-y curve properties of piles located on slopes was investigated under varying geometric and soil parameters.

Future research could expand the variety of geometric and soil parameters considered in this study and develop a formulation that includes the distance from the crest as a variable parameter affecting the slope's influence on the p-y curve properties.

In the future studies that will be conducted to explore the slope effect on the properties of p-y curve, the factor of safety for the slope can be calculated by slope stability analysis. The effect of slope can then be represented as a function of these factor of safety values.

In this study, the effect of the distance of piles on a slope from the crest on p-y curve properties was investigated for clays under drained conditions. Future research could conduct a similar study for non-cohesive soils, such as sand, or for cohesive soils under undrained conditions.

In this study, slope effects on p-y curve properties were studied in only static conditions. Further studies could be performed with similar analysis by using either pseudo-static or dynamic earthquake analyses by taking seismic actions into consideration.

REFERENCES

Ashour, M., & Ardalan, H. (2012). Analysis of pile stabilized slopes based on soil–pile interaction. *Computers and Geotechnics*, *39*, 85–97. https://doi.org/10.1016/j.compgeo.2011.09.001

Bowles, J. E. (1996). Foundation Analysis and Design. 5th edition, The McGraw-Hill Companies, Inc., London.

Broms, B. B. (1964). Lateral resistance of piles in cohesive soils. *Journal of the Soil Mechanics and Foundations Division*, *90*(2), 27–63.

Chen, C. Y., & Martin, G. R. (2002). Soil–structure interaction for landslide stabilizing piles. *Computers and Geotechnics*, *29*(5), 363–386.

Chow, Y. K. (1996). Analysis Of Piles Used for Slope Stabilization. In *International Journal For Numerical And Analytical Methods In Geomechanics* (Vol. 20).

Dutta, S. C., & Roy, R. (2002). A critical review on idealization and modeling for interaction among soil–foundation–structure system. Computers & structures, 80(20-21), 1579-1594.

ExceLab 7.0 Calculus Add-in for Microsoft Excel available from ExcelWorks LLC, https://excel-works.com

Folić, B., & Folić, R. (2018). Comparative nonlinear analysis of a RC 2D frame soil-pile interaction. *Gradjevinski Materijali i Konstrukcije*, *61*(1), 63–89. https://doi.org/10.5937/grmk1801063f

Galli, A., & di Prisco, C. (2013). Displacement-based design procedure for slope-stabilizing piles. *Canadian Geotechnical Journal*, *50*(1), 41–53. https://doi.org/10.1139/cgj-2012-0104

Georgiadis, K., & Georgiadis, M. (2010). Undrained lateral pile response in sloping ground. *Journal of Geotechnical and Geoenvironmental Engineering*, *136*(11), 1489–1500.

Hassiotis, S., Chameau, J. L., & Gunaratne, M. (1997). Design method for stabilization of slopes with piles. *Journal of Geotechnical and Geoenvironmental Engineering*, *123*(4), 314–323.

He, Y., Hazarika, H., Yasufuku, N., Teng, J., Jiang, Z., & Han, Z. (2015). Estimation of lateral force acting on piles to stabilize landslides. *Natural Hazards*, *79*, 1981-2003.

Ito, T., & Matsui, T. (1975). Methods to estimate lateral force acting on stabilizing piles. *Soils and Foundations*, *15*(4), 43–59.

Jeong, S., Kim, B., Won, J., & Lee, J. (2003). Uncoupled analysis of stabilizing piles in weathered slopes. *Computers and Geotechnics*, *30*(8), 671–682. https://doi.org/10.1016/j.compgeo.2003.07.002

Kourkoulis, R., Gelagoti, F., Anastasopoulos, I., & Gazetas, G. (2012). Hybrid method for analysis and design of slope stabilizing piles. J*ournal of Geotechnical and Geoenvironmental Engineering*, *138*(1), 1-14.

Kourkoulis, R., Gelagoti, E., Anastasopoulos, I., & Gazetas, G. (2011). Stabilisation of seismically unstable slopes using piles: Parametric Analysis. *Santiago*, *10*, 13.

Lee, C. Y., Hull, T. S., & Poulos, H. G. (1995). Simplified pile-slope stability analysis. *Computers and Geotechnics*, *17*(1), 1-16.

Liang, R. Y., & Yamin, M. (2010). Three-dimensional finite element study of arching behavior in slope/drilled shafts system. *International Journal for Numerical and Analytical Methods in Geomechanics*, *34*(11), 1157-1168.

Liang, R., & Zeng, S. (2002). Numerical study of soil arching mechanism in drilled shafts for slope stabilization. *Soils and Foundations*, *42*(2), 83–92.

Lunne T., Robertson K. P., & Powell M. J. J. (1997). Cone Penetration Testing in geotechnical Practice. Blackie Academic and Professional.

Matlock, H. (1970). Correlation for design of laterally loaded piles in soft clay. *Offshore Technology Conference*, OTC-1204.

Meymand P. J. (1998): Shaking Table Scale Model Tests of Nonlinear Soil-Pile-Superstructure Interaction in Soft Clay. Thesis (Ph. D.) in Engineering-Civil Engineering. University of California, Berkeley.

Mezazigh, S., & Levacher, D. (1998). Laterally loaded piles in sand: slope effect on py reaction curves. *Canadian Geotechnical Journal*, *35*(3), 433-441.

Muthukkumaran, K., Sundaravadivelu, R., & Gandhi, S. R. (2008). Effect of slope on py curves due to surcharge load. *Soils and Foundations*, *48*(3), 353–361.

Nimityongskul, N., Kawamata, Y., Rayamajhi, D., & Ashford, S. A. (2018a). Full-scale tests on effects of slope on lateral capacity of piles installed in cohesive soils. *Journal of Geotechnical and Geoenvironmental Engineering*, *144*(1). https://doi.org/10.1061/(asce)gt.1943-5606.0001805

Peck, R.B., W.E. Hanson & T.H. Thorburn. (1974). Foundation engineering, 2nd edn. New York: Wiley.

Poulos, H. G. (1995). Design of reinforcing piles to increase slope stability. *Canadian Geotechnical Journal*, *32*(5), 808-818.

Poulos, H. G., & Small, J. C. (2000). Development of design charts for concrete pavements and industrial ground slabs. Chapter 2, Design Applications of Raft Foundations, Ed. J.A. Hemsley, Thomas Telford, 39-70.

Rahmani, A., Taiebat, M., Finn, W. D. L., & Ventura, C. E. (2018). Evaluation of py springs for nonlinear static and seismic soil-pile interaction analysis under lateral loading. *Soil Dynamics and Earthquake Engineering, 115*, 438–447.

Reese, L. C., Cox, W. R., & Koop, F. D. (1975). Field testing and analysis of laterally loaded piles om stiff clay. *Offshore Technology Conference*, OTC-2312.

Reese, L. C., Isenhower, W. M., and Wang, S. T. (2006). Analysis of design of shallow and deep foundations, Wiley, New York.

Reese, L.C., & Van Impe, W.F. (2011). Single Piles and Pile Groups Under Lateral Loading (2nd ed.). CRC Press.

Sharafi, H., Maleki, Y. S., & Fard, M. K. (2016). Three-dimensional finite difference modeling of static soil-pile interactions to calculate p-y curves in pile-supported slopes. *Arabian Journal of Geosciences, 9*, 1-16.

Terzaghi, K., & Peck, R. B. (1967). Soil Mechanics in Engineering Practice. John Wiley & Sons, Inc. New York.

Terzaghi, K., Peck, R. B., & Mesri, G. (1996). Soil Mechanics in Engineering Practice. 3rd edition, John Willey ve Sons, New York.

Viggiani, C. (1981). Ultimate lateral load on piles used to stabilize landslides. *Proc. 10th Int. Conf. on SMFE, 3*, 555–560.

Welch, R.C. & L.C. Reese. (1972). Laterally loaded behavior of drilled shafts. Research Report 35-65-89. Center for Highway Research. University of Texas, Austin.

Yamin, M., & Liang, R. Y. (2010). Limiting equilibrium method for slope/drilled shaft system. *International Journal for Numerical and Analytical Methods in Geomechanics, 34*(10), 1063-1075.

APPENDICES

A. Transition from Q (Shear Force)-z (Depth) Diagram to p (Lateral Load Per Unit Length)-z (Depth) Diagram Through Differentiation

In this study, p-y curves were obtained by differentiating Q-z curves (shear force-depth) obtained from finite element analyses to obtain p-z curves (lateral load per unit length-depth). Steps involved in this process are summarized below.

- Generating a p-y curve in essence requires adequate data on both p and y hence in the finite element program, the load applied to the pile was incremented until collapse of the soil body is achieved. Output taken from the program for every case of loading included vertical coordinate Y, shear force Q and lateral displacement y data.

The finite element analysis outputs from the initial and final loading steps for the H15A15X09N15PI10 case, selected as the sample loading analysis, along with the data used to construct the p-y diagram, are presented in figures from Figure A.1 to Figure A.8.

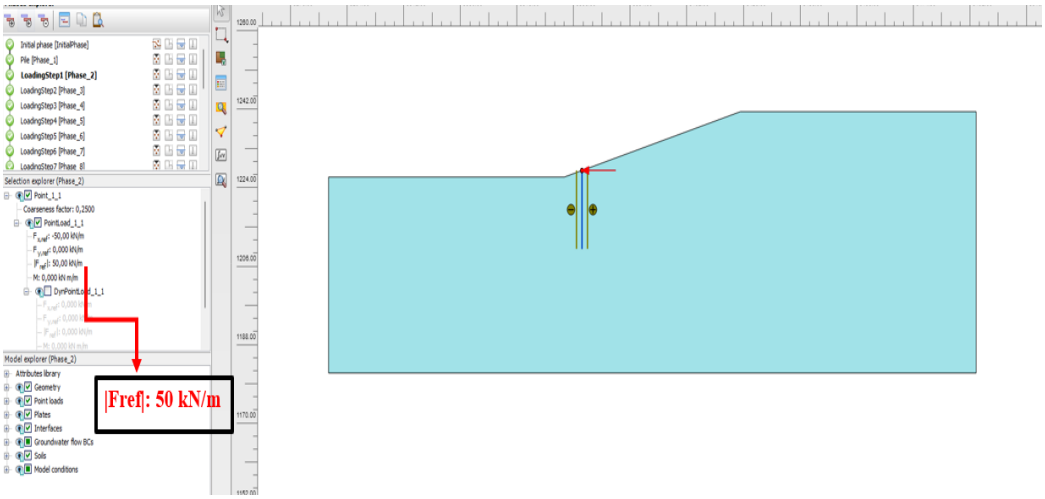

Figure A.1 The First Loading Step in the Example Analysis (H15A15X09N15PI10) to Obtain p-y Curve

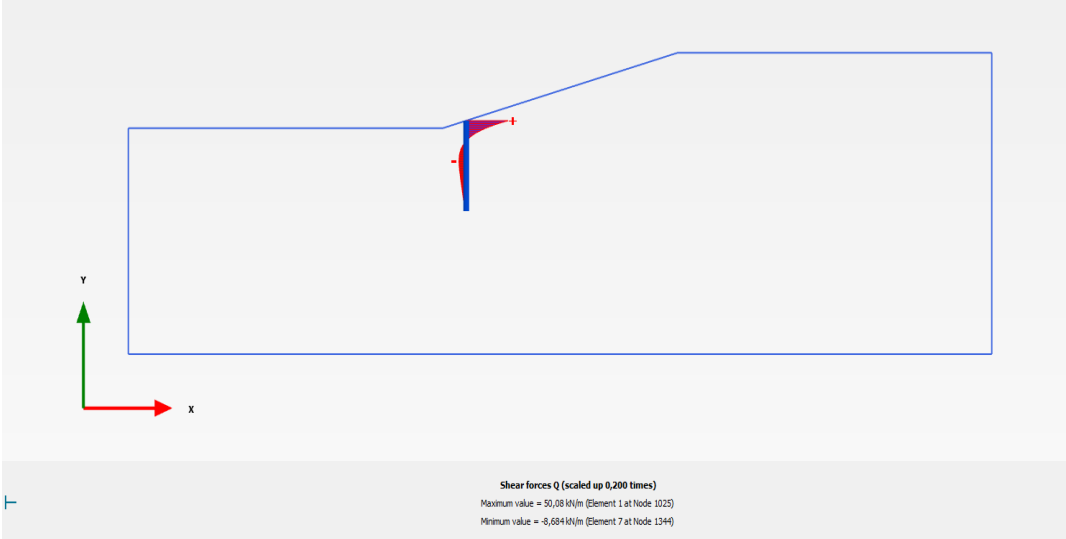

Figure A.2 Shear Force Distribution along the Pile for the First Loading Step

Structural element	Node	Local number	X [m]	Y [m]	N [kN/m]	N_{min} [kN/m]	N_{max} [kN/m]	Q [kN/m]	Q_{min} [kN/m]	Q_{max} [kN/m]	M [kN m/m]	M_{min} [kN m/m]	M_{max} [kN m/m]
Plate_1_1	1025	1	3368,743	1227,874	0,016	0,000	0,027	50,085	0,000	50,085	0,000	0,000	0,000
Element 1-1 (Plate)	1026	2	3368,743	1227,575	-0,869	-1,131	0,000	43,867	0,000	43,867	14,012	0,000	14,012
(Pile_D100_Single)	1027	3	3368,743	1227,277	-1,807	-2,314	0,000	38,099	0,000	38,099	26,239	0,000	26,239
	1028	4	3368,743	1226,978	-2,794	-3,515	0,000	32,788	0,000	32,788	36,814	0,000	36,814
	1039	5	3368,743	1226,680	-3,826	-4,729	0,000	27,940	0,000	27,940	45,866	0,000	45,866
Plate_1_1	1039	1	3368,743	1226,680	-3,820	-4,727	0,000	27,920	0,000	27,920	45,866	0,000	45,866
Element 1-2 (Plate)	1040	2	3368,743	1226,374	-4,908	-5,982	0,000	23,402	0,000	23,402	53,701	0,000	53,701
(Pile_D100_Single)	1041	3	3368,743	1226,068	-6,017	-7,237	0,000	19,287	0,000	19,287	60,220	0,000	60,220
	1042	4	3368,743	1225,762	-7,144	-8,490	0,000	15,570	0,000	15,570	65,541	0,000	65,541
	1053	5	3368,743	1225,456	-8,286	-9,740	0,000	12,247	0,000	12,247	69,784	0,000	69,784
Plate_1_1	1053	1	3368,743	1225,456	-8,282	-9,738	0,000	12,226	0,000	12,226	69,784	0,000	69,784
Element 1-3 (Plate)	1054	2	3368,743	1225,143	-9,459	-11,087	0,000	9,178	0,000	9,178	73,127	0,000	73,127
(Pile_D100_Single)	1055	3	3368,743	1224,830	-10,635	-12,262	0,000	6,447	0,000	6,447	75,566	0,000	75,566
	1056	4	3368,743	1224,517	-11,810	-13,501	0,000	4,027	0,000	4,027	77,199	0,000	77,199
	1083	5	3368,743	1224,203	-12,981	-14,723	0,000	1,911	0,000	1,911	78,121	0,000	78,121
Plate_1_1	1083	1	3368,743	1224,203	-12,978	-14,721	0,000	1,893	0,000	1,893	78,121	0,000	78,121
Element 1-4 (Plate)	1084	2	3368,743	1223,882	-14,167	-15,950	0,000	-0,002	-0,002	0,346	78,418	0,000	78,418
(Pile_D100_Single)	1085	3	3368,743	1223,562	-15,340	-17,153	0,000	-1,661	-1,661	0,070	78,145	0,000	78,145
	1086	4	3368,743	1223,241	-16,495	-18,329	0,000	-3,089	-3,089	0,000	77,377	0,000	77,377
	1167	5	3368,743	1222,920	-17,632	-19,478	0,000	-4,292	-4,292	0,000	76,187	0,000	76,187
Plate_1_1	1167	1	3368,743	1222,920	-17,630	-19,475	0,000	-4,307	-4,307	0,000	76,187	0,000	76,187
Element 1-5 (Plate)	1168	2	3368,743	1222,591	-18,770	-20,619	0,000	-5,345	-5,345	0,000	74,597	0,000	74,597
(Pile_D100_Single)	1169	3	3368,743	1222,263	-19,881	-21,726	0,000	-6,217	-6,217	0,000	72,692	0,000	72,692
	1170	4	3368,743	1221,934	-20,962	-22,797	0,000	-6,928	-6,928	0,000	70,527	0,000	70,527
	1197	5	3368,743	1221,605	-22,010	-23,831	0,000	-7,483	-7,483	0,000	68,156	0,000	68,156
Plate_1_1	1197	1	3368,743	1221,605	-22,009	-23,829	0,000	-7,494	-7,494	0,000	68,156	0,000	68,156
Element 1-6 (Plate)	1198	2	3368,743	1221,269	-23,046	-24,846	0,000	-7,934	-7,934	0,000	65,557	0,000	65,557
(Pile_D100_Single)	1199	3	3368,743	1220,932	-24,041	-25,816	0,000	-8,265	-8,265	0,000	62,827	0,000	62,827
	1200	4	3368,743	1220,596	-24,993	-26,739	0,000	-8,493	-8,493	0,000	60,003	0,000	60,003
	1343	5	3368,743	1220,259	-25,900	-27,614	0,000	-8,622	-8,622	0,000	57,121	0,000	57,121
Plate_1_1	1343	1	3368,743	1220,259	-25,898	-27,613	0,000	-8,630	-8,630	0,000	57,121	0,000	57,121
Element 1-7 (Plate)	1344	2	3368,743	1219,914	-26,777	-28,456	0,000	-8,684	-8,684	0,000	54,135	0,000	54,135
(Pile_D100_Single)	1345	3	3368,743	1219,569	-27,601	-29,241	0,000	-8,674	-8,674	0,000	51,140	0,000	51,140
	1346	4	3368,743	1219,225	-28,366	-29,966	0,000	-8,606	-8,606	0,000	48,159	0,000	48,159
	1393	5	3368,743	1218,880	-29,073	-30,630	0,000	-8,481	-8,481	0,000	45,213	0,000	45,213
Plate_1_1	1393	1	3368,743	1218,880	-29,071	-30,627	0,000	-8,487	-8,487	0,000	45,213	0,000	45,213

Figure A.3 Table of Forces for the First Loading Step

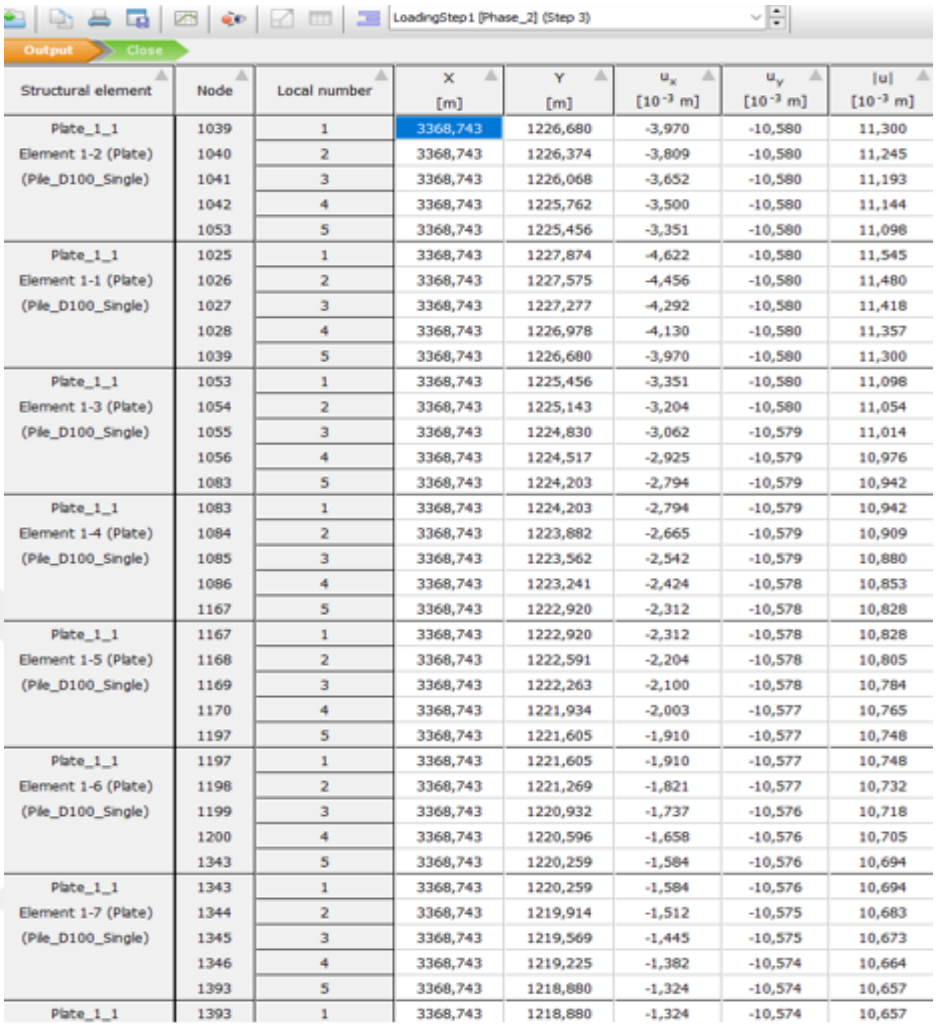

LoadingStep1 [Phase_2] (Step 3)

Output | Close

Structural element	Node	Local number	X [m]	Y [m]	u_x [10^{-3} m]	u_y [10^{-3} m]	|u| [10^{-3} m]
Plate_1_1	1039	1	3368,743	1226,680	-3,970	-10,580	11,300
Element 1-2 (Plate)	1040	2	3368,743	1226,374	-3,809	-10,580	11,245
(Pile_D100_Single)	1041	3	3368,743	1226,068	-3,652	-10,580	11,193
	1042	4	3368,743	1225,762	-3,500	-10,580	11,144
	1053	5	3368,743	1225,456	-3,351	-10,580	11,098
Plate_1_1	1025	1	3368,743	1227,874	-4,622	-10,580	11,545
Element 1-1 (Plate)	1026	2	3368,743	1227,575	-4,456	-10,580	11,480
(Pile_D100_Single)	1027	3	3368,743	1227,277	-4,292	-10,580	11,418
	1028	4	3368,743	1226,978	-4,130	-10,580	11,357
	1039	5	3368,743	1226,680	-3,970	-10,580	11,300
Plate_1_1	1053	1	3368,743	1225,456	-3,351	-10,580	11,098
Element 1-3 (Plate)	1054	2	3368,743	1225,143	-3,204	-10,580	11,054
(Pile_D100_Single)	1055	3	3368,743	1224,830	-3,062	-10,579	11,014
	1056	4	3368,743	1224,517	-2,925	-10,579	10,976
	1083	5	3368,743	1224,203	-2,794	-10,579	10,942
Plate_1_1	1083	1	3368,743	1224,203	-2,794	-10,579	10,942
Element 1-4 (Plate)	1084	2	3368,743	1223,882	-2,665	-10,579	10,909
(Pile_D100_Single)	1085	3	3368,743	1223,562	-2,542	-10,579	10,880
	1086	4	3368,743	1223,241	-2,424	-10,578	10,853
	1167	5	3368,743	1222,920	-2,312	-10,578	10,828
Plate_1_1	1167	1	3368,743	1222,920	-2,312	-10,578	10,828
Element 1-5 (Plate)	1168	2	3368,743	1222,591	-2,204	-10,578	10,805
(Pile_D100_Single)	1169	3	3368,743	1222,263	-2,100	-10,578	10,784
	1170	4	3368,743	1221,934	-2,003	-10,577	10,765
	1197	5	3368,743	1221,605	-1,910	-10,577	10,748
Plate_1_1	1197	1	3368,743	1221,605	-1,910	-10,577	10,748
Element 1-6 (Plate)	1198	2	3368,743	1221,269	-1,821	-10,577	10,732
(Pile_D100_Single)	1199	3	3368,743	1220,932	-1,737	-10,576	10,718
	1200	4	3368,743	1220,596	-1,658	-10,576	10,705
	1343	5	3368,743	1220,259	-1,584	-10,576	10,694
Plate_1_1	1343	1	3368,743	1220,259	-1,584	-10,576	10,694
Element 1-7 (Plate)	1344	2	3368,743	1219,914	-1,512	-10,575	10,683
(Pile_D100_Single)	1345	3	3368,743	1219,569	-1,445	-10,575	10,673
	1346	4	3368,743	1219,225	-1,382	-10,574	10,664
	1393	5	3368,743	1218,880	-1,324	-10,574	10,657
Plate_1_1	1393	1	3368,743	1218,880	-1,324	-10,574	10,657

Figure A.4 Table of Deformations for the First Loading Step

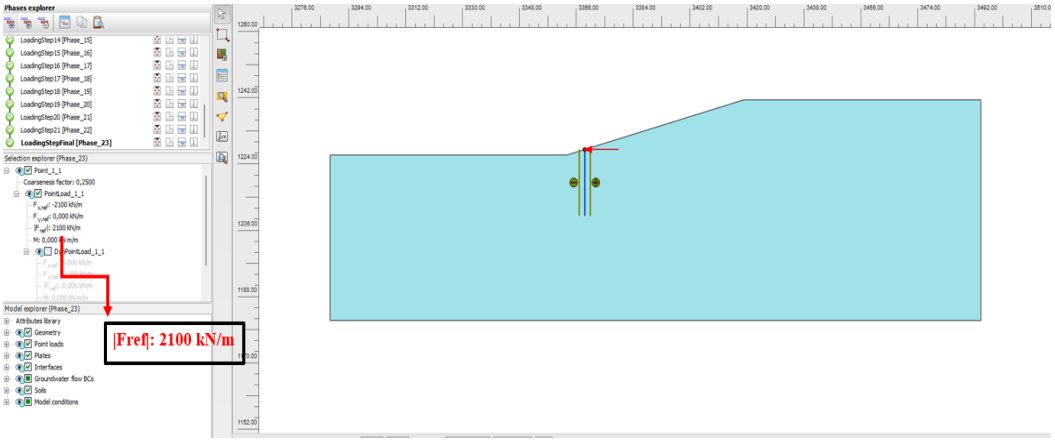

Figure A.5 The Last Loading Step in the Example Analysis (H15A15X09N15PI10) to Obtain p-y Curve

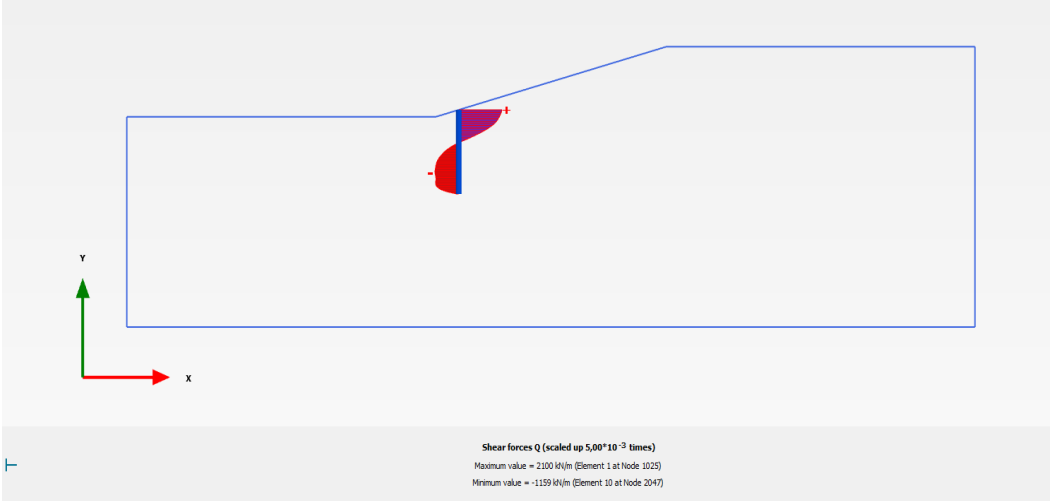

Figure A.6 Shear Force Distribution along the Pile for the Last Loading Step

LoadingStepFinal [Phase_23] (Step 360)

Output | Close

Structural element	Node	Local number	X [m]	Y [m]	N [kN/m]	N_{min} [kN/m]	N_{max} [kN/m]	Q [kN/m]	Q_{min} [kN/m]	Q_{max} [kN/m]	M [kN m/m]	M_{min} [kN m/m]	M_{max} [kN m/m]
Plate_1_1	1025	1	3368,743	1227,874	0,499	-0,676	0,914	2099,809	0,000	2099,809	0,000	0,000	0,000
Element 1-1 (Plate)	1026	2	3368,743	1227,575	3,015	-1,131	4,558	2084,294	0,000	2084,294	624,511	0,000	624,511
(Pile_D100_Single)	1027	3	3368,743	1227,277	6,605	-2,314	8,897	2066,074	0,000	2066,074	1244,398	0,000	1244,398
	1028	4	3368,743	1226,978	12,018	-3,515	15,102	2043,292	0,000	2043,292	1858,100	0,000	1858,100
	1039	5	3368,743	1226,680	20,003	-4,729	25,784	2014,093	0,000	2014,093	2463,884	0,000	2463,884
Plate_1_1	1039	1	3368,743	1226,680	17,932	-4,727	24,733	2019,254	0,000	2019,254	2463,884	0,000	2463,884
Element 1-2 (Plate)	1040	2	3368,743	1226,374	30,566	-5,982	35,495	1978,323	0,000	1978,323	3074,951	0,000	3074,951
(Pile_D100_Single)	1041	3	3368,743	1226,068	42,964	-7,237	48,924	1937,973	0,000	1937,973	3673,991	0,000	3673,991
	1042	4	3368,743	1225,762	55,858	-8,490	63,818	1896,390	0,000	1896,390	4260,440	0,000	4260,440
	1053	5	3368,743	1225,456	69,982	-9,740	81,991	1851,761	0,000	1851,761	4833,561	0,000	4833,561
Plate_1_1	1053	1	3368,743	1225,456	71,243	-9,738	81,491	1848,564	0,000	1848,564	4833,561	0,000	4833,561
Element 1-3 (Plate)	1054	2	3368,743	1225,143	90,421	-11,007	106,609	1791,241	0,000	1791,241	5404,259	0,000	5404,258
(Pile_D100_Single)	1055	3	3368,743	1224,830	117,837	-12,262	132,674	1713,280	0,000	1713,280	5953,425	0,000	5953,425
	1056	4	3368,743	1224,517	150,094	-13,501	161,697	1622,971	0,000	1622,971	6476,553	0,000	6476,553
	1083	5	3368,743	1224,203	183,793	-14,722	200,491	1528,603	0,000	1528,603	6969,918	0,000	6969,918
Plate_1_1	1083	1	3368,743	1224,203	185,875	-14,721	197,962	1521,510	0,000	1521,510	6969,918	0,000	6969,918
Element 1-4 (Plate)	1084	2	3368,743	1223,882	220,413	-15,950	233,652	1427,992	-3,381	1427,992	7443,846	0,000	7443,846
(Pile_D100_Single)	1085	3	3368,743	1223,562	262,858	-17,153	276,890	1310,123	-12,370	1310,123	7883,466	0,000	7883,466
	1086	4	3368,743	1223,241	309,071	-18,329	321,581	1176,026	-23,396	1176,026	8282,986	0,000	8282,986
	1167	5	3368,743	1222,920	354,915	-19,476	365,819	1033,822	-35,725	1033,822	8637,396	0,000	8637,396
Plate_1_1	1167	1	3368,743	1222,920	354,928	-19,475	365,096	1034,719	-35,863	1034,719	8637,396	0,000	8637,396
Element 1-5 (Plate)	1168	2	3368,743	1222,591	401,655	-20,619	408,270	887,240	-47,843	887,240	8953,275	0,000	8953,275
(Pile_D100_Single)	1169	3	3368,743	1222,263	444,936	-21,726	447,729	733,430	-60,803	733,430	9219,842	0,000	9219,842
	1170	4	3368,743	1221,934	485,553	-22,797	485,553	572,268	-74,243	572,268	9434,628	0,000	9434,628
	1197	5	3368,743	1221,605	524,289	-23,831	524,289	402,732	-101,940	402,732	9595,047	0,000	9595,047
Plate_1_1	1197	1	3368,743	1221,605	523,633	-23,829	523,633	406,380	-100,636	406,380	9595,047	0,000	9595,047
Element 1-6 (Plate)	1198	2	3368,743	1221,269	558,490	-24,846	558,490	229,310	-153,795	229,310	9702,029	0,000	9702,028
(Pile_D100_Single)	1199	3	3368,743	1220,932	589,322	-25,816	589,322	56,575	-212,660	56,575	9749,794	0,000	9749,794
	1200	4	3368,743	1220,596	615,567	-26,739	615,567	-107,160	-293,624	0,000	9741,133	0,000	9741,133
	1343	5	3368,743	1220,259	636,662	-27,614	636,662	-257,230	-368,169	0,000	9679,296	0,000	9679,296
Plate_1_1	1343	1	3368,743	1220,259	637,142	-27,613	637,142	-256,631	-367,886	0,000	9679,296	0,000	9679,296
Element 1-7 (Plate)	1344	2	3368,743	1219,914	654,295	-28,456	654,295	-389,158	-433,875	0,000	9567,569	0,000	9567,568
(Pile_D100_Single)	1345	3	3368,743	1219,569	667,846	-29,241	667,846	-507,251	-520,044	0,000	9412,619	0,000	9412,619
	1346	4	3368,743	1219,225	678,022	-29,966	678,022	-611,635	-611,635	0,000	9219,298	0,000	9219,298
	1393	5	3368,743	1218,880	685,049	-30,630	685,049	-703,033	-703,034	0,000	8992,369	0,000	8992,368
Plate_1_1	1393	1	3368,743	1218,880	685,181	-30,627	685,181	-703,801	-703,801	0,000	8992,369	0,000	8992,368

Figure A.7 Table of Forces for the Last Loading Step

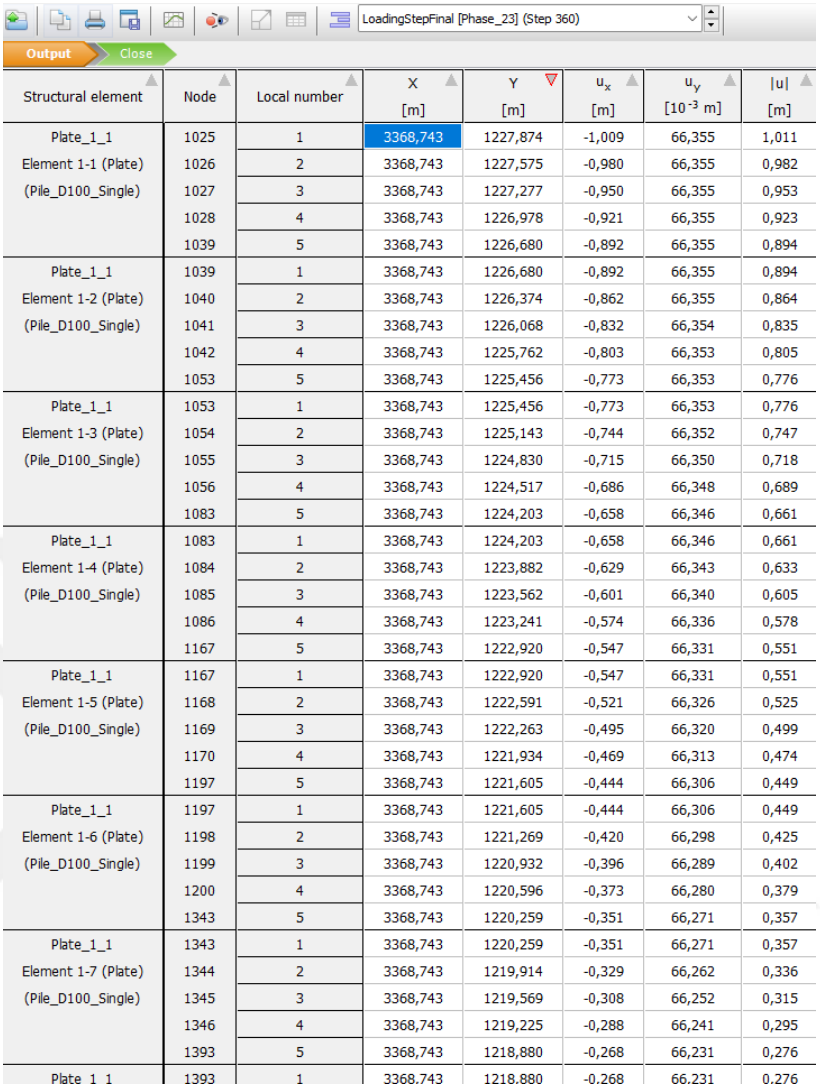

Structural element	Node	Local number	X [m]	Y [m]	u_x [m]	u_y [10^{-3} m]	|u| [m]
Plate_1_1	1025	1	3368,743	1227,874	-1,009	66,355	1,011
Element 1-1 (Plate)	1026	2	3368,743	1227,575	-0,980	66,355	0,982
(Pile_D100_Single)	1027	3	3368,743	1227,277	-0,950	66,355	0,953
	1028	4	3368,743	1226,978	-0,921	66,355	0,923
	1039	5	3368,743	1226,680	-0,892	66,355	0,894
Plate_1_1	1039	1	3368,743	1226,680	-0,892	66,355	0,894
Element 1-2 (Plate)	1040	2	3368,743	1226,374	-0,862	66,355	0,864
(Pile_D100_Single)	1041	3	3368,743	1226,068	-0,832	66,354	0,835
	1042	4	3368,743	1225,762	-0,803	66,353	0,805
	1053	5	3368,743	1225,456	-0,773	66,353	0,776
Plate_1_1	1053	1	3368,743	1225,456	-0,773	66,353	0,776
Element 1-3 (Plate)	1054	2	3368,743	1225,143	-0,744	66,352	0,747
(Pile_D100_Single)	1055	3	3368,743	1224,830	-0,715	66,350	0,718
	1056	4	3368,743	1224,517	-0,686	66,348	0,689
	1083	5	3368,743	1224,203	-0,658	66,346	0,661
Plate_1_1	1083	1	3368,743	1224,203	-0,658	66,346	0,661
Element 1-4 (Plate)	1084	2	3368,743	1223,882	-0,629	66,343	0,633
(Pile_D100_Single)	1085	3	3368,743	1223,562	-0,601	66,340	0,605
	1086	4	3368,743	1223,241	-0,574	66,336	0,578
	1167	5	3368,743	1222,920	-0,547	66,331	0,551
Plate_1_1	1167	1	3368,743	1222,920	-0,547	66,331	0,551
Element 1-5 (Plate)	1168	2	3368,743	1222,591	-0,521	66,326	0,525
(Pile_D100_Single)	1169	3	3368,743	1222,263	-0,495	66,320	0,499
	1170	4	3368,743	1221,934	-0,469	66,313	0,474
	1197	5	3368,743	1221,605	-0,444	66,306	0,449
Plate_1_1	1197	1	3368,743	1221,605	-0,444	66,306	0,449
Element 1-6 (Plate)	1198	2	3368,743	1221,269	-0,420	66,298	0,425
(Pile_D100_Single)	1199	3	3368,743	1220,932	-0,396	66,289	0,402
	1200	4	3368,743	1220,596	-0,373	66,280	0,379
	1343	5	3368,743	1220,259	-0,351	66,271	0,357
Plate_1_1	1343	1	3368,743	1220,259	-0,351	66,271	0,357
Element 1-7 (Plate)	1344	2	3368,743	1219,914	-0,329	66,262	0,336
(Pile_D100_Single)	1345	3	3368,743	1219,569	-0,308	66,252	0,315
	1346	4	3368,743	1219,225	-0,288	66,241	0,295
	1393	5	3368,743	1218,880	-0,268	66,231	0,276
Plate_1_1	1393	1	3368,743	1218,880	-0,268	66,231	0,276

Figure A.8 Table of Deformations for the Last Loading Step

- For each loading stage, data was obtained from finite element analysis outputs as shown in the previous step and all outputs were listed one below the other in the excel spreadsheet.

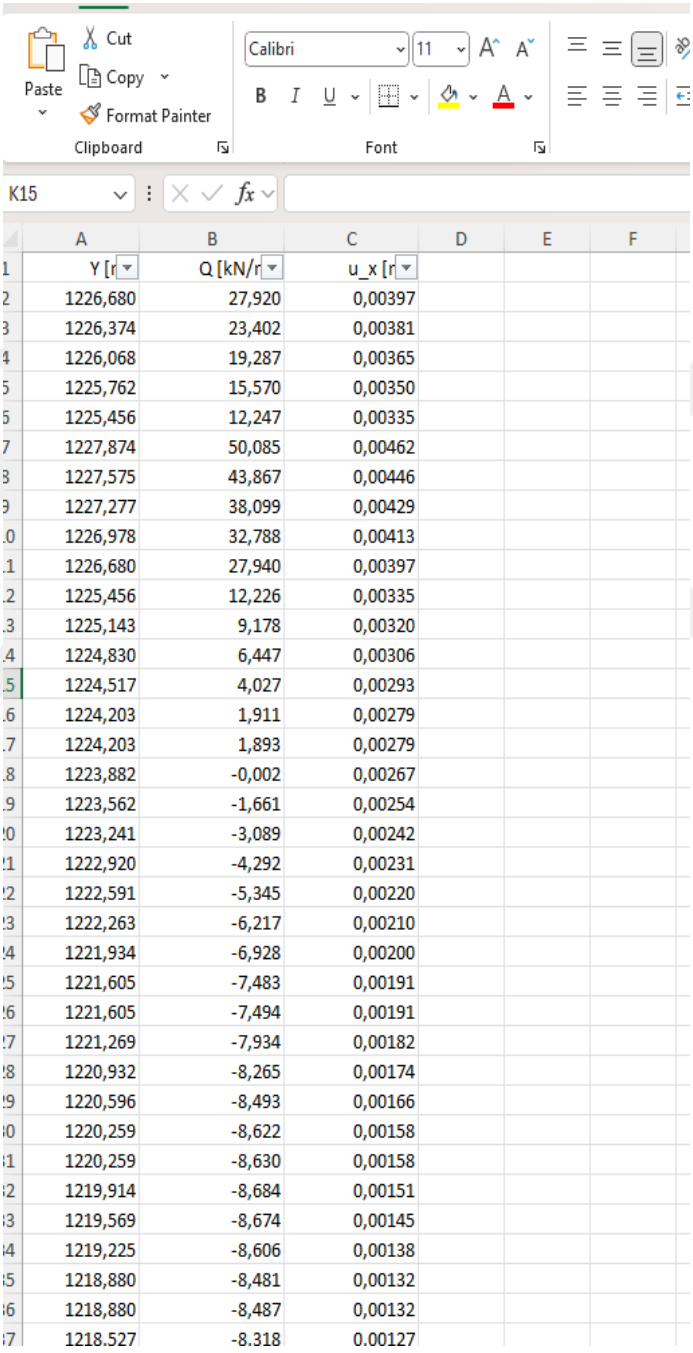

	A	B	C	D	E	F
1	Y [r	Q [kN/r	u_x [r			
2	1226,680	27,920	0,00397			
3	1226,374	23,402	0,00381			
4	1226,068	19,287	0,00365			
5	1225,762	15,570	0,00350			
6	1225,456	12,247	0,00335			
7	1227,874	50,085	0,00462			
8	1227,575	43,867	0,00446			
9	1227,277	38,099	0,00429			
10	1226,978	32,788	0,00413			
11	1226,680	27,940	0,00397			
12	1225,456	12,226	0,00335			
13	1225,143	9,178	0,00320			
14	1224,830	6,447	0,00306			
15	1224,517	4,027	0,00293			
16	1224,203	1,911	0,00279			
17	1224,203	1,893	0,00279			
18	1223,882	-0,002	0,00267			
19	1223,562	-1,661	0,00254			
20	1223,241	-3,089	0,00242			
21	1222,920	-4,292	0,00231			
22	1222,591	-5,345	0,00220			
23	1222,263	-6,217	0,00210			
24	1221,934	-6,928	0,00200			
25	1221,605	-7,483	0,00191			
26	1221,605	-7,494	0,00191			
27	1221,269	-7,934	0,00182			
28	1220,932	-8,265	0,00174			
29	1220,596	-8,493	0,00166			
30	1220,259	-8,622	0,00158			
31	1220,259	-8,630	0,00158			
32	1219,914	-8,684	0,00151			
33	1219,569	-8,674	0,00145			
34	1219,225	-8,606	0,00138			
35	1218,880	-8,481	0,00132			
36	1218,880	-8,487	0,00132			
37	1218.527	-8.318	0.00127			

Figure A.9 Finite Element Analysis Outputs from the Example Analysis (H15A15X09N15PI10)

- To calculate the lateral load per unit length (p) data, which is usually calculated using the vertical coordinate data Y, and shear force Q data, there was a need to establish a relation between Q vs. Y and then find its first derivative. For this purpose, ExceLab 7.0 calculus add-in for Excel was utilized during calculations. Lateral load per unit length, p, was derived for all depths at each loading condition using the add-in function DERIVXY(x, y, p). In this function, x represented the values of the vertical coordinate (Y) for all depths for a given loading condition, y were the values of shear force (Q) for all depths for the same loading condition, and p equated to the particular value of vertical coordinate (Y) for which the first derivative was required. This process was repeated for all the loading conditions such that p -values for every Q and Y value obtained from the finite element analysis were determined. Figures from Figure A.10 to Figure A.11 summarize this procedure:

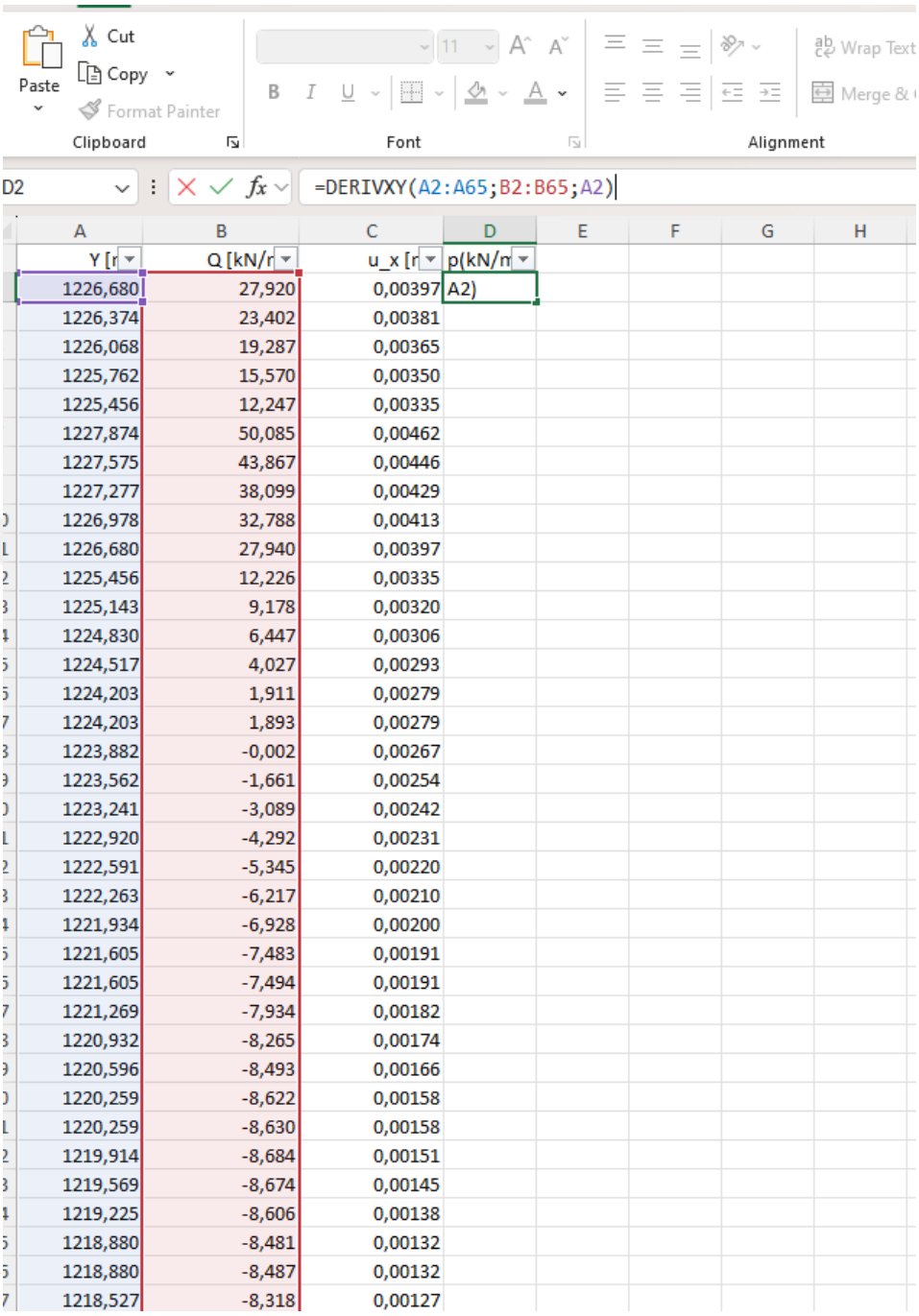

	A	B	C	D	E	F	G	H
	Y [r	Q [kN/r	u_x [r	p(kN/n				
	1226,680	27,920	0,00397	A2)				
	1226,374	23,402	0,00381					
	1226,068	19,287	0,00365					
	1225,762	15,570	0,00350					
	1225,456	12,247	0,00335					
	1227,874	50,085	0,00462					
	1227,575	43,867	0,00446					
	1227,277	38,099	0,00429					
	1226,978	32,788	0,00413					
	1226,680	27,940	0,00397					
	1225,456	12,226	0,00335					
	1225,143	9,178	0,00320					
	1224,830	6,447	0,00306					
	1224,517	4,027	0,00293					
	1224,203	1,911	0,00279					
	1224,203	1,893	0,00279					
	1223,882	-0,002	0,00267					
	1223,562	-1,661	0,00254					
	1223,241	-3,089	0,00242					
	1222,920	-4,292	0,00231					
	1222,591	-5,345	0,00220					
	1222,263	-6,217	0,00210					
	1221,934	-6,928	0,00200					
	1221,605	-7,483	0,00191					
	1221,605	-7,494	0,00191					
	1221,269	-7,934	0,00182					
	1220,932	-8,265	0,00174					
	1220,596	-8,493	0,00166					
	1220,259	-8,622	0,00158					
	1220,259	-8,630	0,00158					
	1219,914	-8,684	0,00151					
	1219,569	-8,674	0,00145					
	1219,225	-8,606	0,00138					
	1218,880	-8,481	0,00132					
	1218,880	-8,487	0,00132					
	1218,527	-8,318	0,00127					

Figure A.10 Excel add-in Formulation to Obtain p (Lateral Load Per Unit Length) Values

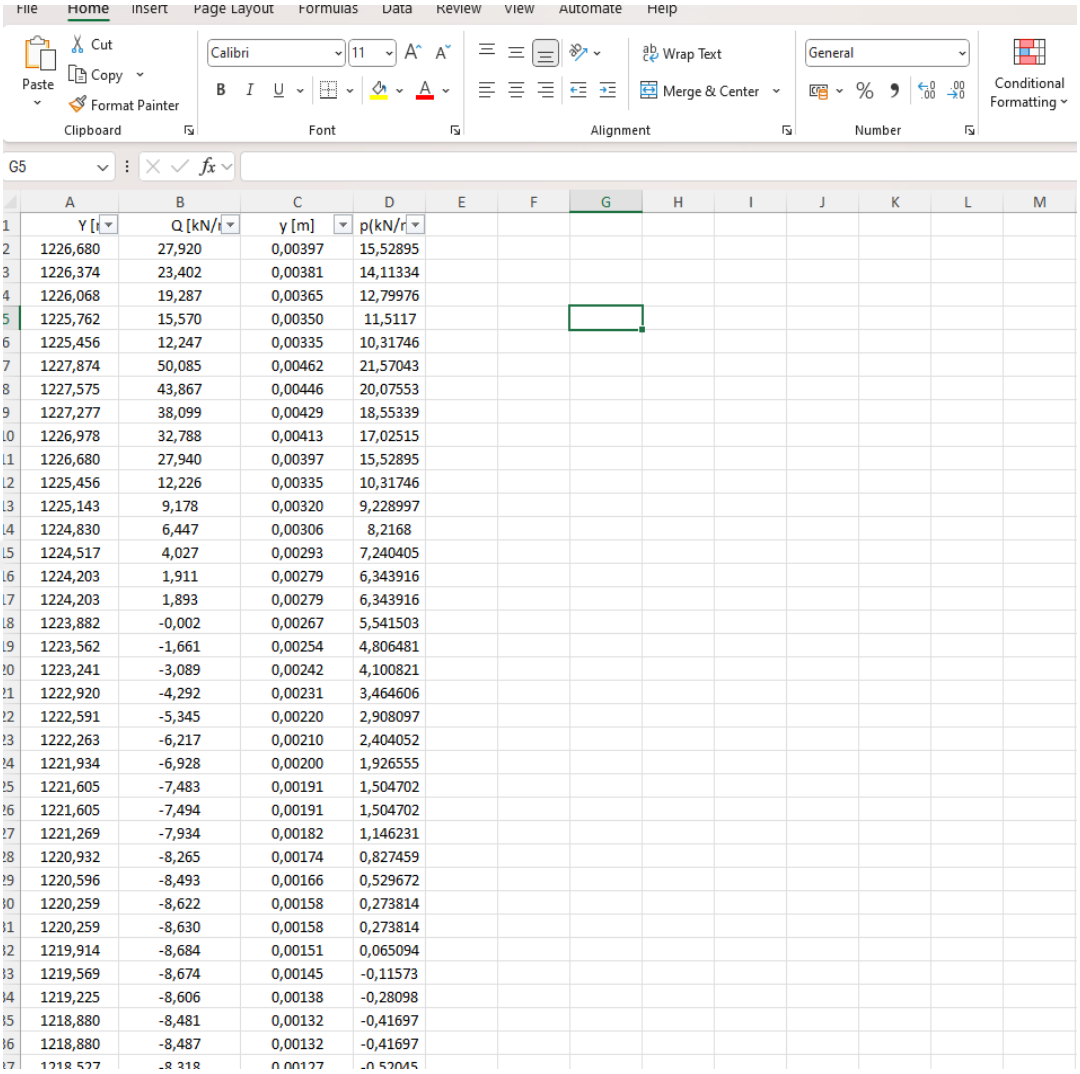

Y [	Q [kN/	y [m]	p(kN/r
1226,680	27,920	0,00397	15,52895
1226,374	23,402	0,00381	14,11334
1226,068	19,287	0,00365	12,79976
1225,762	15,570	0,00350	11,5117
1225,456	12,247	0,00335	10,31746
1227,874	50,085	0,00462	21,57043
1227,575	43,867	0,00446	20,07553
1227,277	38,099	0,00429	18,55339
1226,978	32,788	0,00413	17,02515
1226,680	27,940	0,00397	15,52895
1225,456	12,226	0,00335	10,31746
1225,143	9,178	0,00320	9,228997
1224,830	6,447	0,00306	8,2168
1224,517	4,027	0,00293	7,240405
1224,203	1,911	0,00279	6,343916
1224,203	1,893	0,00279	6,343916
1223,882	-0,002	0,00267	5,541503
1223,562	-1,661	0,00254	4,806481
1223,241	-3,089	0,00242	4,100821
1222,920	-4,292	0,00231	3,464606
1222,591	-5,345	0,00220	2,908097
1222,263	-6,217	0,00210	2,404052
1221,934	-6,928	0,00200	1,926555
1221,605	-7,483	0,00191	1,504702
1221,605	-7,494	0,00191	1,504702
1221,269	-7,934	0,00182	1,146231
1220,932	-8,265	0,00174	0,827459
1220,596	-8,493	0,00166	0,529672
1220,259	-8,622	0,00158	0,273814
1220,259	-8,630	0,00158	0,273814
1219,914	-8,684	0,00151	0,065094
1219,569	-8,674	0,00145	-0,11573
1219,225	-8,606	0,00138	-0,28098
1218,880	-8,481	0,00132	-0,41697
1218,880	-8,487	0,00132	-0,41697

Figure A.11 Obtained p-y Values for all Depths

- Finally, since the p-y curves examined in this study are at a depth of 3 meters in terms of consistency, the relevant pile vertical coordinate is filtered in Excel. p (lateral load per unit length) and y (lateral displacement) values are taken for each loading stage from the filtered results. Thus, the p-y curve is obtained. Final results are summarized in the figures from Figure A.12 to Figure A.13.

Y [r	Q [kN/r	y [m]	p(kN/r
1224,830	6,447	0,00306	8,2168
1224,830	11,463	0,00641	15,51972
1224,830	28,649	0,01405	44,36101
1224,830	78,191	0,02325	70,37373
1224,830	128,875	0,03479	88,65453
1224,830	185,706	0,04835	114,757
1224,830	250,379	0,06461	144,7015
1224,830	325,802	0,08257	181,9911
1224,830	419,998	0,10334	223,0513
1224,830	494,177	0,12382	243,4572
1224,830	588,508	0,14939	249,5311
1224,830	686,437	0,17602	247,0929
1224,830	786,020	0,20582	246,0602
1224,830	883,172	0,23838	241,789
1224,830	979,918	0,27392	242,6073
1224,830	1111,299	0,31547	252,9237
1224,830	1212,227	0,36118	277,8947
1224,830	1311,970	0,42394	287,8208
1224,830	1405,548	0,48088	291,0025
1224,830	1505,187	0,56041	267,4378
1224,830	1585,481	0,62050	269,0019
1224,830	1713,280	0,71484	271,427

Figure A.12 Obtained p-y Curve Values at the Depth of 3m in Example Analysis (H15A15X09N15PI10)

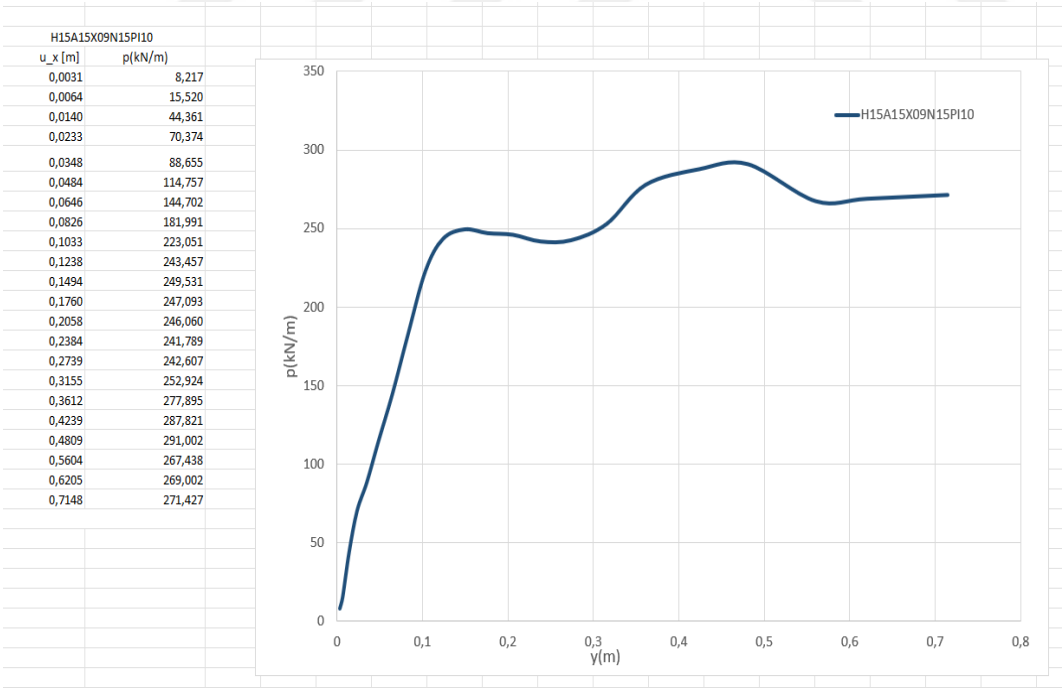

Figure A.13 Obtained p-y Curve at the Depth of 3m in the Example Analysis (H15A15X09N15PI10)

Alternatively, in the final loading stage, a cross-section was taken in front of the pile, as illustrated in Figure A.14, and the effective normal stress and lateral deformation values within this cross-section were analyzed.

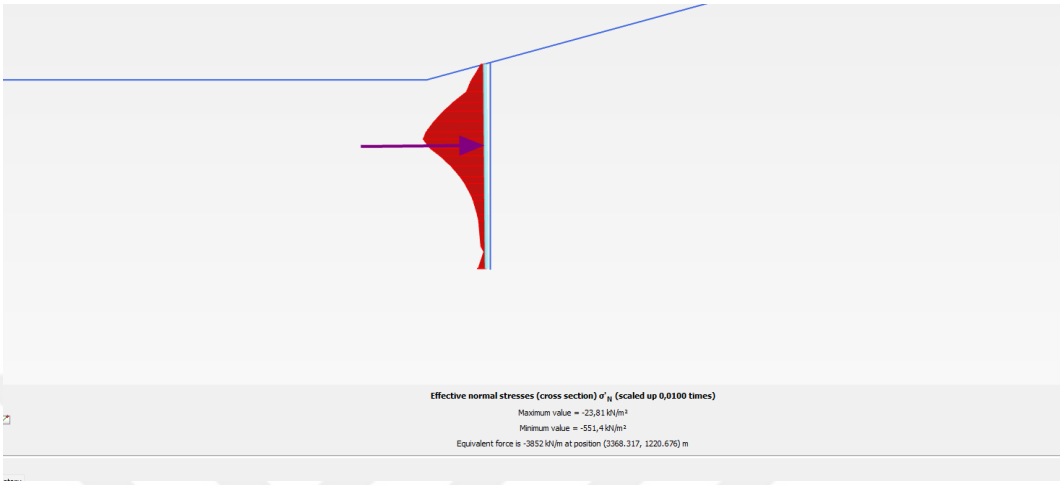

Figure A.14 Effective Normal Stress Distribution in the Cross-Section in Front of the Pile at the Final Loading Stage

For comparison, effective normal stress and lateral deformation outputs at a depth of 3 meters are shown in figure A.15 and figure A.16.

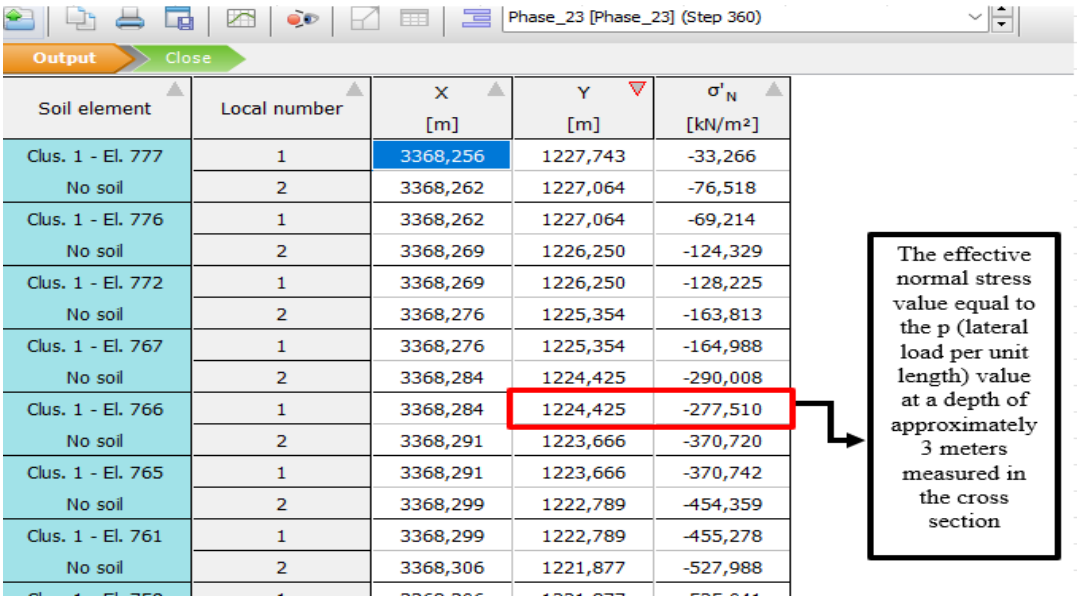

Soil element	Local number	X [m]	Y [m]	σ'N [kN/m²]
Clus. 1 - El. 777	1	3368,256	1227,743	-33,266
No soil	2	3368,262	1227,064	-76,518
Clus. 1 - El. 776	1	3368,262	1227,064	-69,214
No soil	2	3368,269	1226,250	-124,329
Clus. 1 - El. 772	1	3368,269	1226,250	-128,225
No soil	2	3368,276	1225,354	-163,813
Clus. 1 - El. 767	1	3368,276	1225,354	-164,988
No soil	2	3368,284	1224,425	-290,008
Clus. 1 - El. 766	1	3368,284	1224,425	-277,510
No soil	2	3368,291	1223,666	-370,720
Clus. 1 - El. 765	1	3368,291	1223,666	-370,742
No soil	2	3368,299	1222,789	-454,359
Clus. 1 - El. 761	1	3368,299	1222,789	-455,278
No soil	2	3368,306	1221,877	-527,988

The effective normal stress value equal to the p (lateral load per unit length) value at a depth of approximately 3 meters measured in the cross section

Figure A.15 The Effective Normal Stress Value at a Depth of Approximately 3 Meters Measured in The Cross Section

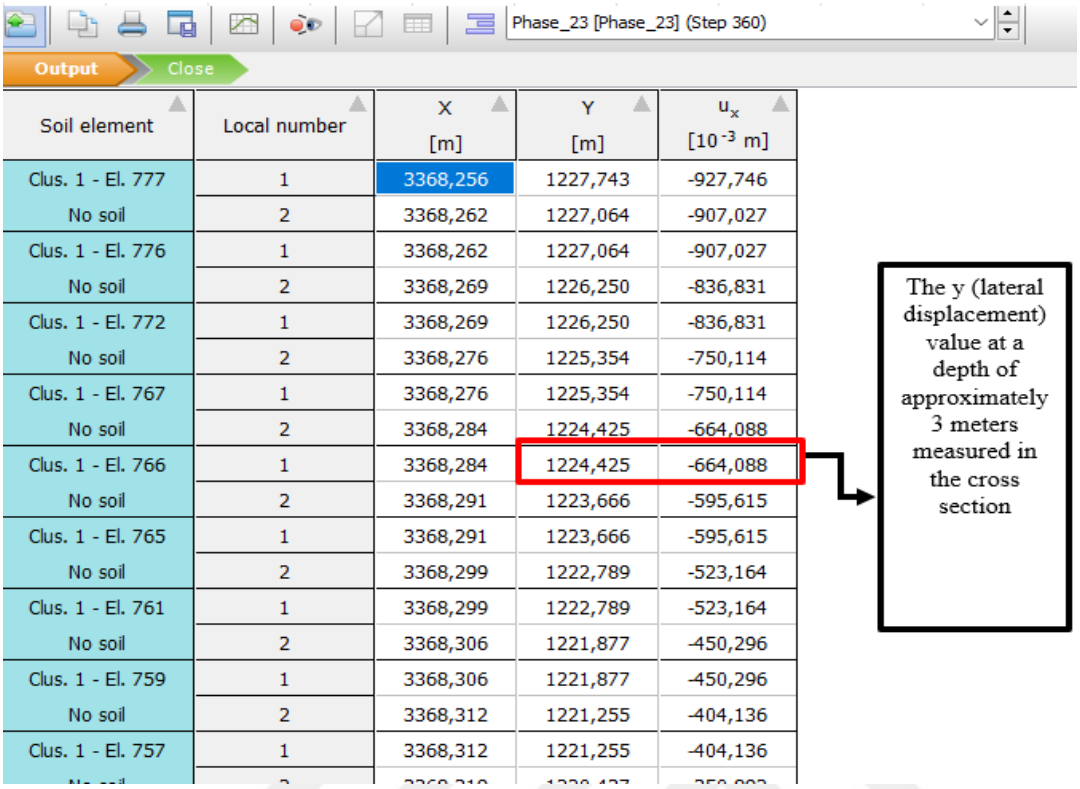

Figure A.16 The y (lateral displacement) Value at a Depth of Approximately 3 Meters Measured in the Cross Section

From the above figures, it is observed that at a depth of approximately 3 meters, the effective normal stress value on the cross-section is 277.5 kN/m². Now, assuming that the pile spacing is 1 meter, the value of p-lateral load per unit length, will also be 277.5 kN/m. At this depth, the y (lateral displacement) measured value is 0.664 m. The value of p was found to be 271.4 kN at 3 meters depth in Figure A.12, calculated using the p-y curve method that has been implemented in this study for the last load step, while y was found to be 0.715 m.

These findings illustrate that the p-y values determined from the two approaches are relatively consistent. Observed discrepancies can be explained by not being able to compare values at precisely the same depth due to limitations of mesh density in the finite element program. For this study, the p-y curve method derived from the differentiation of the Q (shear force)–z diagram was chosen, as it is more commonly used in the literature and provides greater computational efficiency.